



Adsorption layers of surfactant mixtures on non-polar solid particles and stability of dispersions

Inaugural-Dissertation

zur Erlangung des Doktorgrades
der Mathematisch-Naturwissenschaftlichen Fakultät
der Heinrich-Heine-Universität Düsseldorf

vorgelegt von

Meriem Jabnoun

aus Zarzis, Tunesien

Düsseldorf, December 2012

aus dem Institut für Physikalische Chemie
der Heinrich-Heine Universität Düsseldorf

Gedruckt mit der Genehmigung der
Mathematisch-Naturwissenschaftlichen Fakultät der
Heinrich-Heine-Universität Düsseldorf

Referent: Prof. Dr. Claus Seidel
Koreferent: Prof. Dr. Wolfgang von Rybinski

Tag der mündlichen Prüfung: 05.03.2013

*“All our knowledge begins with the senses, proceeds then to the understanding,
and ends with reason. There is nothing higher than reason”.*



Immanuel Kant (1724-1804)

To Holli, with love.

Acknowledgments

I would like to express my gratitude to the persons that did help me directly or indirectly for the completion of my doctoral thesis.

First of all, my sincere thanks go to Prof. Dr. Wolfgang von Rybinski for his supervision throughout the three years of PhD thesis in the field of colloid science.

I am especially thankful for his help when problems arose and where his great knowledge and experience in this field of colloid science among other fields did help me find solutions and continue my research work and for giving me the chance to present my results in various national and international conferences.

I am grateful to Prof. Dr. Claus Seidel for giving me the chance to conduct my thesis in cooperation with his institute and for the interesting group seminars I had the chance to attend and learn more about the field of fluorescence spectroscopy.

His expertise in the field of physical chemistry and his large network of scientists helped me also to get access to methods needed in this research study which were not directly available to me such as atomic force microscopy which was kindly made available by one of his former group members Prof. Dr. Philipp Österhelt.

The work made in the group of Prof. Dr. Österhelt helped me discover the molecular structures of the surfactants used at the graphite surface.

I am thankful for the great six months I had the chance to spend in his group among the institute of biophysics at the Heinrich-Heine University where I did learn more about atomic force microscopy.

I am also thankful for the various discussions that helped me adjust the experimental set-up needed for imaging surfactant solutions at the graphite surface and for his kind advice during imaging.

A special thank goes to the members of his group with whom I did directly work: Mario Schneider, Arpita Roychoudhury, Anna Bronder as well as the group of Dr. Luitgard Nagel-Steger and the group of Prof. Dr. Gerhard Steger and the other members of the institute, especially Mrs. Heidi Gruber.

I would like to thank the company Henkel AG&Co. KGaA for the financial support during my thesis and especially the group of Dr. Michael Dreja: Dr. Dreja himself, Dr. Peter Schmiedel, Dr. Paula Barreleiro, Dr. Thomas Gerke, Dipl-Ing. Heinz-Jürgen Völkel and all other colleagues at Henkel.

To my parents Mohamed and Regaya, thank you for being my parents, for your love and understanding. You gave me the chance to fulfill my dreams and go in search for myself. Thank you for your help and encouragement.

To my sisters Emna, Sarra, Saadia and Mounira and my brothers Belgacem and Khaled for their important support all over these years and for giving me precious nice moments outside science. I hope that you will find in this work the expression of my love and a small contribution to the scientific achievements inside the family.

I do not forget to thank my German family, the family Wiebel-Meier: Frederike, Frank, Georg and Robert, thank you for all the great moments I did share with you, the nice trips we did together, the evening readings that helped me improving my German. I felt part of the family and this made my life abroad a great experience and an enjoyable time.

You all made this PhD work an amazing time that helped me enrich my interest for science and especially colloid science but also go further with my personal fulfillment.

Choukran & merci à vous tous,

Meriem

Contents

Acknowledgments	3
Abstract	9
Zusammenfassung	13
Abbreviations	15
Introduction	17
1 Theoretical part	19
1.1 Solid-liquid dispersions	19
1.2 Surfactants as dispersing aids	21
1.3 Adsorption at the solid-liquid interface	23
1.3.1 Basic adsorption parameters and mechanisms	23
1.3.2 Adsorption isotherms	25
1.3.2.1 Henry isotherm	26
1.3.2.2 Langmuir isotherm	26
1.3.2.3 Other models	27
1.3.3 Thermodynamics of the adsorption process	27
1.3.3.1 Surfactant adsorption at interfaces using calorime- try	31
1.3.4 Surface structure	32
1.3.4.2 Surfactant adsorption at the solid-liquid inter- face using AFM	36
2 Materials and methods	41
2.1 Studied systems	41
2.1.1 Low-mass Surfactants	41
2.1.2 Adsorbents	43
2.1.2.1 Carbon black	43
2.1.2.2 Carbon black	44
2.1.3 Used Methods	45
2.1.3.1 Concentration measurement methods	45

2.1.3.2	UV-measurements of sodium dodecyl benzene sulfonate	45
2.1.3.3	Anionic surfactant titration	46
2.1.3.4	Nonionic surfactant titration	47
2.1.3.5	Isothermal Titration Calorimetry (ITC)	48
2.1.3.6	Atomic Force Microscopy (AFM)	49
3	Results	52
3.1	Adsorption isotherms	52
3.1.1	Adsorption isotherms for single surfactants	52
3.2	Adsorption isotherms for surfactant mixtures	58
3.3	Enthalpy effects during adsorption	65
3.3.1	Enthalpy effects during the adsorption of single surfactants at the carbon black-water interface	65
3.3.2	Enthalpy effects of adsorption for surfactant mixtures at the carbon black-water interface	69
3.3.2.1	Enthalpy effects of adsorption for SDS/C ₁₂₋₁₄ E ₇	69
3.3.2.2	Enthalpy effects of adsorption for SDS/C ₁₂₋₁₄ E ₇	71
3.3.2.3	Enthalpy effects of adsorption for SAS/C ₁₂₋₁₄ E ₇	72
3.3.3	Comparison with the results obtained on graphitized carbon black	74
3.4	Structure of the adsorbed layer using AFM	75
3.4.1	Structure of the adsorbed layer for the single surfactants at the graphite-water interface	75
3.4.1.1	AFM study of SDS adsorption at the graphite-water interface	75
3.4.1.2	AFM study of SDBS adsorption at the graphite-water interface	79
3.4.1.3	AFM study of SAS adsorption at the graphite-water interface	81
3.4.1.4	AFM study of C ₁₂₋₁₄ E ₇ adsorption at the graphite-water interface	83
3.4.2	Structure of the adsorbed layer for surfactant mixtures at the graphite-water interface	87

3.4.2.1	SDS/C ₁₂₋₁₄ E ₇ mixture	87
3.4.2.2	SDBS/C ₁₂₋₁₄ E ₇ mixture	88
3.4.2.3	SAS/C ₁₂₋₁₄ E ₇ 1:1 mixture	92
3.4.2.4	Summary of the results of the adsorbed layer	93
4	Discussion	95
4.1	Adsorption behavior of single surfactants and mixtures	95
4.1.1	Adsorbed amounts of single surface-active agents	96
4.1.1.1	Adsorption isotherms for the anionic surfactants	96
4.1.1.2	Adsorption isotherm for the nonionic surfactant	97
4.1.1.3	Correlation between the adsorption isotherms obtained experimentally and theoretical models	99
4.1.1.4	Langmuir model for anionic surfactant adsorp- tion at the carbon black-water interface	99
4.1.1.5	Langmuir model for the nonionic surfactant ad- sorption at the carbon black-water interface	102
4.1.1.6	Zhu model for anionic surfactant adsorption at the carbon black-water interface	103
4.1.2	Adsorbed amounts of surfactant mixtures at the carbon black-water interface	111
4.2	Enthalpy effects during adsorption for single surfactants and mixtures	115
4.3	Structure of the adsorbed layer using AFM	120
4.3.1	Structure observed for the single surfactants	120
4.3.2	Structure observed for the surfactant mixtures	126
4.3.3	Conclusion	127
5	Importance for the application	129
5.1	Study of dispersion stability	132
5.2	Dispersion stability using single surfactants	132
5.3	Dispersion stability using surfactant mixtures	134
6	Conclusion	137
7	Presentations in scientific conferences	139

Contents

References	141
List of Figures	153
List of Tables	155
Eklärung	157

Abstract

The adsorption mechanisms of surfactants at the solid-liquid interface are of high relevance for the modification of the interfacial properties in many applications. Especially the adsorption behavior of mixtures of different types of surfactants is of great importance as surfactant mixtures are preferably used in many products. Only few studies were reported for mixed surfactant systems at different surfaces.

In the present study, the adsorption process of the anionic surfactants sodium dodecyl sulfate (SDS), sodium secondary alkyl sulfonate (SAS) and sodium dodecyl benzene sulfonate (SDBS), the nonionic surfactant fatty alcohol ethoxylate (FAE) and their mixtures on non-polar surfaces (carbon black and graphite) was investigated using a combination of adsorption isotherms, calorimetry and atomic force microscopy (AFM) in order to propose a model for the adsorption of mixtures.

In addition to this, a comparison was done between the adsorption parameters and the stabilization behavior of solid particles by mixtures of different anionic surfactants having main structural differences and the nonionic surfactant. The combination of these three methods for the systematic study of mixed surfactant systems rather than single surfactants is the new approach of this study.

The first method used which is the study of the adsorption isotherms revealed differences between the adsorption isotherms of the single surfactants and the surfactant mixtures. The obtained adsorption isotherms at the carbon black-water interface for the anionic surfactants were quite similar especially for SDBS and SAS and could be described using the Langmuir model whereas for the nonionic surfactant FAE, the adsorbed amounts were higher than the values given by the Langmuir model especially at low concentrations. This result was related to a stronger interaction between the nonionic surfactant and the carbon black surface than for the anionic surfactants and a strong interaction of the molecules of the nonionic surfactant in the adsorbed layer. Differences were also observed between the adsorbed amounts of the mixed systems depending on the structure of the anionic surfactant used by mea-

surings independently the concentration of both surfactants in the mixture. Higher adsorbed amounts were observed for the mixture of the nonionic surfactant with the linear anionic surfactant SDS compared to the other anionic surfactants SDBS and SAS. The concentration ratio of the anionic and the nonionic surfactant in the adsorbed layer was shifted to the nonionic surfactant in the case of SDS especially at higher bulk concentrations. In contrast to this, the concentration ratio in the adsorbed layer was shifted toward the anionic surfactant for SDBS. This represents the most important result gained from the study of the adsorption behavior of surfactant mixtures which is the correlation between the structure of the alkyl chain of the anionic surfactant and the amount of nonionic surfactant adsorbed. Obviously, the linear alkyl chain anionic surfactant SDS can be displaced by the more strongly adsorbing and aggregating nonionic surfactant forming a mixed adsorption layer. For the branched alkyl chain surfactant SDBS and in less extent also for SAS, this substitution by the nonionic surfactant is not possible to the same extent and the strong interaction of the anionic surfactant towards the carbon black surface leads to a preferred adsorption of this surfactant in the mixture.

For the further understanding of the mechanisms involved in the adsorption process of the mixtures, isothermal titration calorimetry was chosen. This technique was used to measure the molar enthalpies of adsorption and revealed differences between the enthalpies of adsorption for the single surfactants as well as differences between the enthalpies of adsorption for the studied mixed systems. The anionic surfactants exhibited lower enthalpy values compared to the nonionic surfactant which has been correlated to the presence of the charged head group for the anionic surfactants (mutual repulsion between the charged head groups for the anionic surfactants in the adsorbed layer resulted in the decrease of the total enthalpy of adsorption).

Another important aspect was also revealed by the enthalpies of adsorption which is the effect of the chain length of the surfactant. Higher enthalpy values are observed including data from literature for the single surfactants having longer alkyl chains which gives a strong indication for a horizontal arrangement of the surfactants at the carbon black surface. At higher concentrations, the differential molar adsorption enthalpy decreases and comes close to the enthalpy of micelle formation. This indicates that the mutual interaction of the

adsorbed surfactant molecules becomes more important than the interaction with the surface. This suggests that micellar-like aggregates are formed for the studied surfactants and mixtures at the surface at higher concentrations. An additional interesting result shows that the enthalpy of adsorption in the mixture is governed by the nonionic surfactant as the adsorption enthalpies measured for the mixtures were comparable to the one measured for the single nonionic surfactant.

AFM measurements of the mixed surfactant systems on flat graphite surfaces gave an insight directly into the structure of the adsorption layer and confirmed the results of the adsorption experiments with carbon black. They show semi-cylindrical structures except for the single surfactant system of SDBS. For mixtures of SDBS with the nonionic surfactant, structures of the adsorbed layer on the graphite surface can be seen, however. The periodicity of the structures corresponds to the length of two tail-to-tail oriented surfactants on the surface and differs only slightly for the mixtures, which suggests a homogeneous mixed adsorption layer. For mixtures of SDBS with the nonionic surfactant, semi-cylindrical structures of the adsorbed layer on the graphite surface can be seen in contrast to SDBS alone. This supports the results of the adsorption isotherms on carbon black with a specific effect of SDBS. The comparison of the structures in the adsorption layer with the phase behavior in bulk solution shows that only SDBS did not form semi-cylindrical structures on the surface. In addition to that, SDBS forms no hexagonal phase of cylindrical aggregates in the bulk solution. Obviously, there is a correlation between structures of surfactants on surfaces and their behavior in a liquid.

The stability of solid particles in solution is important for many applications and a direct correlation of the results of the adsorption measurements with the stability of the dispersions was possible. The effect of the dodecyl benzene sulfonate (SDBS) in the mixture was different from the other anionic surfactants: SDBS stabilizes the dispersion in the mixture of surfactants at lower concentrations than the other anionic surfactants and the nonionic surfactant alone.

Zusammenfassung

Der Adsorptionsmechanismus von Tensiden an Phasengrenzen zwischen festen und flüssigen Medien ist von großer Bedeutung für die Modifikation der Grenzflächeneigenschaften in einer Vielzahl von Anwendungsgebieten. Dabei ist das Adsorptionsverhalten unterschiedlicher Tensidmischungen von besonderer Wichtigkeit, da diese in verschiedensten Anwendungsfeldern zum Einsatz kommen. Bislang sind nur wenige Studien durchgeführt worden, die sich mit gemischten Tensidsystemen an verschiedenartigen Oberflächen befassen.

In der hier vorliegenden Arbeit wurden die Adsorptionsprozesse der anionischen Tenside Sodium-Dodecyl-Sulfat (SDS), des Natriumsalzes eines Sekundären Alkyl-Sulfonats (SAS) und Sodium-Dodecyl-Benzyl-Sulfonat (SDBS) sowie des nichtionischen Tensids Fett-Alkohol-Ethoxylat (FAE) als auch deren Mischungen an nicht-polaren Oberflächen (Carbon Black, Graphit) untersucht.

Ziel der Arbeit war es, ein Modell zur Adsorption von Tensidmischungen vorzuschlagen, das unter Verwendung von Adsorptionsisothermen, kalorimetrischen Messungen und Untersuchungen mittels Rasterkraftmikroskopie (AFM) abgeleitet wurde.

Zudem wurden die erhaltenen Adsorptionsparameter und die daraus resultierenden Stabilisierungseffekte auf Feststoffpartikel in Mischungen verschiedener anionischer Tenside, die deutliche Unterschiede in ihrer Struktur aufweisen, mit denen des nichtionischen Tensids verglichen.

Erstmalig werden in dieser Arbeit die drei vorgenannten Methoden zur systematischen Untersuchung gemischter Tensidsysteme miteinander verknüpft, und nicht nur zur Untersuchung einzelner Tenside herangezogen.

Die Ergebnisse des kombinierten Einsatzes der angewendeten Verfahren lassen auf einen starken Einfluss der Struktur des anionischen Tensids auf das Adsorptionsverhalten der Mischungen schließen.

Abbreviations

Latin abbreviations

a	Activity
a _s	Specific surface area of adsorbent
Å	Angström (10 ⁻¹⁰ m)
BET	Specific surface area of solid according to Brunauer, Emmett and Teller
c	Concentration
°C	Degree Celcius
CMC	Critical micelle concentration
C _m E _n	Alkylethoxylate
c _p	Heat capacity at constant pressure
E	Nernst potential
F	Faraday constant
FAE	Fatty alcohol ethoxylate
g	Gramm
g	Gas
h	Hour
H	Molar enthalpy of reaction
h _i	Partial molar enthalpy
HLB	Hydrophilic/lipophilic balance
J	Joule
K	Adsorption coefficient
°K	Kelvin
l	Liter
LAM	Lamellar phase
liq	Liquid
L1	Micellar phase
m	Mass
M	Molecular weight
max	Maximum
M _h	Molecular weight of the hydrophilic part
min	Minimum

mol	Mole number
N	Newton
N	Avogadro constant
nm	Nanometer (10^{-9} m)
P	Pressure
Q	Heat effect
RT	Room temperature (295°K, 25°C)
R	Gas constant
r	Radius
SAS	Sodium secondary alkyl sulfonate
SDBS	Sodium dodecyl benzene sulfonate
SDS	Sodium dodecyl sulfate
s	Second
T	Temperature
t	Time
v	Volum
w%	Weight percent

Greek Abbreviations

α	Angle
γ	Interfacial tension
Δ	Difference
∂	Differential
Γ	Adsorbed amount
μ	Micro (10^{-6})
σ	Surface tension
Θ	Degree of coverage
ν	Stoichiometric coefficient
ξ	Extent of reaction

Introduction

Dispersions are present everywhere in our surrounding with all its fields as well as in our bodies. This wide presence of dispersions and their use in many industrial processes are important reasons for the development of the so-called dispersion science [1].

Dispersion science has risen-up in the last half century from series of qualitative descriptions of complex phenomena to a science based on theories that provided a high reliability of dispersion science as a tool for a better understanding of complex phenomena involving dispersions.

One important aspect treated by dispersion science is the study of dispersion stability which is also the fundamental objective of this work.

In fact, dispersions and especially solid-liquid dispersions are heterogeneous systems which are not thermodynamically stable. Therefore the use of surface-active agents such as polymers and ions is common for dispersion stabilization due to their interfacial properties.

However, the mechanism of stability of dispersions using low-molar mass surface-active agents is not completely understood especially for complex systems despite many studies reported in the literature.

The objective of this work is to give a better understanding of physical-chemical phenomena for the stability of dispersions using mixtures of low-molar mass surface-active agents.

This specific target is important as mixed systems find a broader use in applications than single systems.

Objectives and motivation of this work

The aim of this work is to investigate the physical-chemical phenomena involved for the stabilization of dispersions of hydrophobic solid particles in aqueous medium using mixtures of low-molar mass surface-active agents.

In a first place, the quantitative measurement of the adsorbed amounts for the studied surface active agents using depletion measurement methods gives information about the adsorption isotherms for these systems.

The correlation between the experimental results and theoretical models gives important information about the adsorption layer.

Further study of the thermodynamics of the adsorption process and mainly the enthalpy of adsorption using isothermal titration calorimetry enables the correlation of the adsorbed amounts with the enthalpy values which provides further structural information about the adsorbed layer.

These results are then correlated with the atomic force micrographs for the studied systems which show a self-assembly of the used surface-active agents at the hydrophobic solid particle/aqueous medium interface.

In this thesis an introduction to dispersion science gives an overview of the main theoretical aspects related to dispersion stability and mainly solid/liquid dispersions.

This part aims at bringing a theoretical background for the study of dispersion stability which is the basis for the interpretation of the experimental results.

The following chapter is dedicated to the systems studied and the experimental techniques used with emphasis on isothermal titration calorimetry and atomic force microscopy.

The results of the experimental study for the single surfactants as well as for the surfactant mixtures are then presented followed by the chapter discussion which includes the main findings as revealed by the adsorption isotherms, the calorimetry study and the atomic force microscopy.

The concluding chapter is concerned with the importance of the results obtained in this thesis for industrial applications and mainly the stabilization of hydrophobic solid particles in aqueous medium.

1 Theoretical part

Since the beginning of the 20th century, many research studies have been dedicated to the understanding of the parameters related to the stabilization of solid-liquid dispersions.

This big interest for dispersion stability and especially the stability of solid-liquid dispersions is due to their importance in a wide range of applications such as flotation, detergency, cosmetics etc.

Despite the big number of scientific publications in this field, the basic understanding of dispersion stability especially through the adsorption of surfactants and especially surfactant mixtures at the solid/liquid interface is not yet fully understood.

This specific aspect of dispersion stability is the main topic of this research study.

The present chapter will be divided into three sections.

The first section is a general introduction to dispersion and flocculation, here the main theoretical aspects related to dispersions will be treated.

In the second section “Surfactants as dispersing aids”, a short introduction to surfactant science will be given. The correlation between surfactant properties and their function as dispersing aids will be developed.

The last section will be dedicated to the quantitative (adsorption isotherms), thermodynamic (calorimetry) and the structural aspects related to the adsorption process at the solid/liquid interface (studied using atomic force microscopy among other techniques).

1.1 Solid-liquid dispersions

Dispersions [2] are defined as a system of a dispersed phase and a dispersing medium .

Ostwald [3] proposed a classification based on the state of aggregation of the dispersed phase and the dispersion medium.

Solid-liquid dispersions are therefore dispersions where the dispersing medium is a liquid generally water and the dispersed phase is a solid.

According to Tadros [4], solid-liquid dispersions can be obtained either by breaking down a solid phase into fine particles of small diameter and mixing those in a liquid (mainly water) or they could be obtained by crystallization or polymerization of materials from their molecular level.

These systems are also known as suspensions. Solid-liquid dispersions from both aqueous and non-aqueous type are encountered in many applications.

In fact, products and processes in the chemical and related industries are involving solid-liquid dispersions for example paints, pigments, printing inks, paper coatings, cosmetics, ceramics, detergents, food, pharmaceutical formulations and many others.

For solid-liquid dispersions, the particle size range is one of the most important criteria of classification.

Tadros [4], among others, made an estimation of this range and set the particle size limit at 1 nm (10 Å) which represents the smallest aggregate for which it is meaningful to distinguish between “surface” and “interior” molecules.

The upper limit is defined as 1000 nm (1µm) which is the upper size where molecules that are in or close to the surface make significant contributions to the energy that differ from those made by molecules in the interior.

A detailed description of the most important criteria for the classification of colloidal dispersions has been done by Voyutsky [5] among which are the degree of dispersion, the state of the dispersed phase and that of the dispersion medium, the interaction between the dispersed phase and the dispersion medium, and the interaction between the particles.

Dobiás and von Rybinski [1] described solid-liquid dispersions as being heterogeneous systems characterized by the presence of interfaces between the particles and the dispersed medium which are responsible for the instability of these dispersions against aggregation causing sedimentation, flocculation or coalescence.

Two major mechanisms exist for the stabilization of dispersions [1]:

- Electrostatic stabilization
- Steric stabilization

For aqueous systems, the use of surfactants for the stabilization of solid/liquid dispersions is widely spread and concerns various industrial processes.

The adsorption of surfactants at surfaces or interfaces has a direct impact on their physical-chemical properties which is mainly due to the structure of these surfactants.

The properties of these substances which are responsible for their wide use as dispersing aids will be treated in the next section.

1.2 Surfactants as dispersing aids

Surfactants are amphiphilic compounds that adsorb at interfaces such as liquid/liquid, solid/liquid and gas/liquid systems.

This is due to the fact that these compounds combine in their structure a non polar part which is mainly a hydrocarbon chain containing 8 to 18 carbon atoms and a polar part, as the head-group which can be either from a nonionic, an ionic (cationic or anionic) or a zwitterionic nature.

A commonly used schematic representation of a low-mass surfactant molecule is given in figure 1.1.

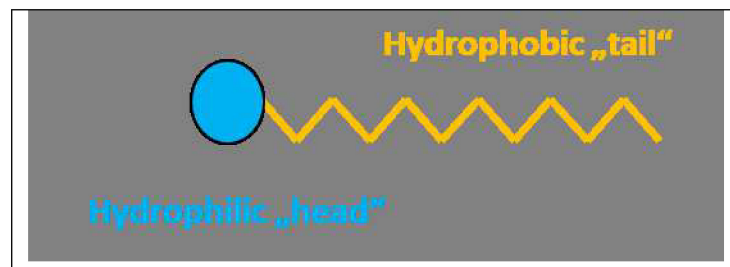


Figure 1.1: Schematic representation of a low-mass surfactant [4]

As already stated above, according to the nature of the hydrophilic head-group of the surfactant, one distinguishes between ionic (i.e. anionic, cationic or amphoteric) and nonionic surfactants.

Anionic surfactants and especially the one containing carboxylates, sulfates, sulfonates and phosphates as polar groups are widely used in application such as detergents and cosmetic formulations.

In terms of their use in industrial applications and according to market studies done in this field [6], nonionic surfactants are comparatively less used than anionic surfactants but do present the same importance for application. The


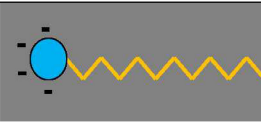
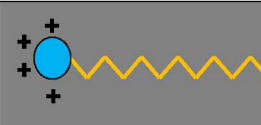
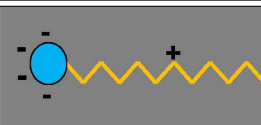
commonly used nonionic surfactants do present repeating ethylene oxide units or carbohydrates in the hydrophilic part of the molecule.

Cationic surfactants, mostly quaternary ammonium compounds, are less used and are rather incorporated in specific applications such as corrosion inhibitors or fabric softeners.

Amphoteric or zwitterionic surfactants contain both cationic and anionic groups. They are preferably used in personal care products as they generally induce lower skin irritation [6].

Table 1.1 gives some examples of surfactants:

Table 1.1: Classification of surfactants based on the charge of the head-group

Type of surfactant	Illustration	Example
Nonionic		PE
Anionic		SDS
Cationic		CTAB
Zwitterionic (Amphoteric)		Betaines

PE = Alkylpolyglycoether

SDS = Sodium Dodecyl Sulfate

CTAB = Cetyltrimethylammonium Bromide

Another classification is also used and is based on the chemical composition of the hydrophobic part of the surfactants (fluorinated surfactants for example).

In fact, and as already stated above, the structure of a surfactant consists of two parts: a hydrophobic or non polar part (tail) and a hydrophilic, polar part (head-group).

Due to this amphiphilic character, surfactants can adsorb for instance at solid-liquid interfaces, resulting in a better stabilization of the solid particles in the liquid medium as schematically presented in figure 1.2 for a hydrophobic solid surface.

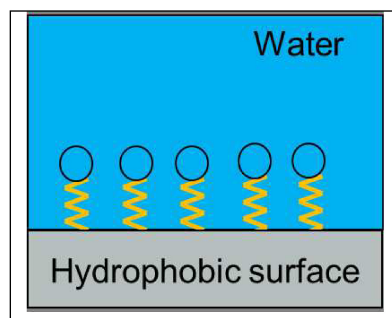


Figure 1.2: Schematic representation of the adsorption of surfactants at the solid/liquid interface [1]

For low molar-mass surfactants, the structure is not only restricted to one hydrophobic tail binding covalently to a hydrophilic head-group but can be extended to two surfactant molecules bonded together by a spacer which corresponds to the so-called gemini surfactants.

1.3 Adsorption at the solid-liquid interface

1.3.1 Basic adsorption parameters and mechanisms

Surface-active agents are mainly characterized by their aggregation in solution and at interfaces.

The aggregation in solution results in micelle formation and the aggregation at interfaces on the other hand results in surfactant films.

In the presence of solids, the aggregation of surfactants takes place at the solid-liquid interface.

Different parameters play an important role in the adsorption at the solid-liquid interface, among which are:

1. Solvent type :
 - Aqueous or non-aqueous systems
 - Presence or absence of electrolytes
 - Solubility of adsorbates
2. Surface properties of the solid phase:
 - Specific surface also known as BET surface [7]: BET stands for the initials of the names Brunauer, Emmett and Teller who developed the so-called BET theory. The BET theory is the basis for the determination of the specific surface area of a material through the adsorption of a known gas concentration at its surface
 - Porosity
 - Polarity
 - Solvent spreading
3. Surfactant properties:
 - Type (anionic, cationic, nonionic and zwitterionic)
 - Hydrophilic/Lipophilic Balance: the so-called HLB is the method which was first introduced by Griffin [8] and which measures the degree to which a surfactant is hydrophilic or lipophilic.

HLB according to Griffin is given by the following equation :

$$HLB = 20 \frac{M_h}{M} \quad (1.1)$$

M_h represents the molecular weight of the hydrophilic portion of the molecule and M is the molecular weight of the entire molecule

– for $HLB < 10$ the surfactant is water insoluble

- for $\text{HLB} > 10$ the surfactant is water soluble
- Chain length

Depending on the nature of the surfactant and according to M. J. Rosen [9], the adsorption of surfactants at the solid-liquid interface is driven by one of the following mechanisms:

1. Ionic exchange: adsorption of an ionic surfactant instead of the substrate counter-ion
2. Ion-pairing: adsorption of surfactant ions on free counter-ion sites
3. H-Binding
4. Adsorption through polarization of π -electrons: interaction of aromatic groups of the adsorbates and cations of the substrate
5. Adsorption through van der Waals dispersion forces
6. Adsorption through alternating hydrophobic interactions: this mechanism takes place through strong attractive forces between the hydrophobic tail of the surfactant and the solid surface

The adsorption of surfactants at the solid-liquid interface has been intensively studied which constituted a base for the development of the so-called adsorption models related to the adsorption isotherms, these models were described among others by von Rybinski et al in their book “Solid-liquid dispersions” [1] which is one of the references used in this chapter.

1.3.2 Adsorption isotherms

An adsorption isotherm is defined as the relationship between the activity of the adsorbing substance in the interface layer (a_i) and in the liquid phase or volume phase (a_v) at a constant temperature.

For a_i or c_i (for diluted solutions) either the adsorption density (surface concentration) Γ (mol/m^2) or the degree of coverage $\Theta = \Gamma/\Gamma_{\text{max}}$ (where Γ_{max} = saturation value for monolayer adsorption) is used.

Most of these adsorption isotherms are originally related to the adsorption of gases at the solid surface and have been used also for the study of the adsorption of liquid phases but with limited ranges of applicability.

1.3.2.1 Henry isotherm The Henry isotherm is applied only for very diluted solutions and is derived from the Henry-Dalton solubility law for gases formulated in 1803.

The Henry equation :

$$\Theta = Kc \quad (1.2)$$

With:

- Θ = degree of coverage
- K = adsorption coefficient
- c = concentration of the dilute phase

The Henry law can only be applied to ideal systems.

1.3.2.2 Langmuir isotherm This well known isotherm is based on the following considerations:

- Maximum adsorption gives a monomolecular adsorption layer
- Energetically equivalent adsorption sites
- No lateral interactions in the adsorbed layer

The Langmuir adsorption isotherm is described using the following equation:

$$\Gamma = \frac{\Gamma_{max} Kc}{(1 + Kc)} \quad (1.3)$$

With:

- Γ_{max} = maximum adsorbed amount per unit area (mol/m²)
- K = Langmuir constant (m³/mol)
- c = solute concentration (mol/m³)

1.3.2.3 Other models Other models used the Langmuir adsorption isotherm and developed it by taking into account important aspects during adsorption which were neglected in the Langmuir isotherm [1] such as:

- The exchange processes (Zuchovikij isotherm)
- Lateral interactions (Frumkin isotherm);
- Multilayer formation (BET isotherm).

1.3.3 Thermodynamics of the adsorption process

Each chemical reaction is accompanied by changes of the free energy.

These changes can be expressed by the reaction enthalpy in the case of a reaction at constant pressure or by the reaction energy in the case of a reaction at constant volume.

For reactions at constant pressure, the reaction enthalpy is the sum of the heat effect (dQ), the electrostatic effect (dW_{elec}) and the mechanical effect (dW_{mech}) [10].

$$dH = dQ + dW_{elec} + dW_{mech} \quad (1.4)$$

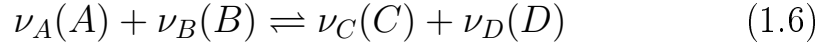
The variation of the enthalpy of a reaction at a temperature T , a pressure P and for n_i compounds can be expressed as follows:

$$dH = \left(\frac{\partial H}{\partial T} \right)_{P, n_i} dT + \left(\frac{\partial H}{\partial P} \right)_{T, n_i} dP + \sum_i \left(\frac{\partial H}{\partial n_i} \right)_{T, P, n_{j \neq i}} dn_i \quad (1.5)$$

with:

- $\left(\frac{\partial H}{\partial T} \right)_{P, n_i} = c_P$ = heat capacity at constant P
- $\left(\frac{\partial H}{\partial n_i} \right)_{T, P, n_j} = h_i$ = partial molar enthalpy at constant T and P

For the following chemical reaction of ν_A moles of the reactant A with ν_B moles of the reactant B giving ν_C moles of the product C and ν_D moles of the product D :



The molarity of the reactants and the products of the reaction can be expressed as follows:

$$-\frac{dn_A}{\nu_A} = -\frac{dn_B}{\nu_B} = \frac{dn_C}{\nu_C} = \frac{dn_D}{\nu_D} = d\xi \quad (1.7)$$

with:

- ν_i = stoichiometric coefficient of the compound i
- ξ = extent of reaction

The reaction enthalpy can be then written as follows:

$$dH = \sum H_i dn_i = \sum \nu_i H_i d\xi = \Delta H_R d\xi \quad (1.8)$$

with ΔH_R = reaction enthalpy

The above equations for a reaction at constant pressure give:

$$dH = dQ + dW_{elec} + dW_{mech} = c_p dT + \Delta H_R d\xi \quad (1.9)$$

For a reaction at constant temperature and pressure, equation 1.9 can be written as follows:

$$dH = \Delta H_R d\xi = \sum_i \left(\frac{\partial H}{\partial n_i} \right)_{T, p, n_{j \neq i}} dn_i \quad (1.10)$$

This means that the variation of the reaction enthalpy at constant temperature and pressure is directly proportional to the concentration or the molarity of the species involved in the reaction.

Calorimetric measurements are based on this fundamental principle. In fact, a calorimeter measures the heat of reaction as a function of the concentration at constant temperature and pressure.

The heat effect in the case of the adsorption of a surfactant at the solid/liquid interface is called enthalpy of adsorption and is given by the following equation [11]:

$$\Delta H_{ads} = \frac{Q_m - Q_{dil}}{m_s a_s} \quad (1.11)$$

With:

- Q_m = heat effect measured
- Q_{dil} = dilution heat during adsorption
- m_s = mass of adsorbent
- a_s = specific surface area of adsorbent

The term enthalpy of displacement is used rather than enthalpy of adsorption because the generated heat effect during adsorption of surfactants at the solid/liquid interface includes at least the adsorption of the surfactant molecules and the desorption of the solvent molecules from the adsorbent.

Calorimetry is the method of choice for the determination of the enthalpies of displacement during the adsorption of surfactants at the solid/liquid interface as well as the determination of the thermodynamic parameters related to micelle formation [12].

In fact, Paula et al [13] used titration calorimetry to measure the critical micelle concentration (CMC) and the heat of demicellization (ΔH_{demic}) of different surfactants, among them SDS.

From these data the thermodynamic parameters ΔG_{demic} (free energy of demicellization) and ΔS_{demic} (entropy of demicellization) were calculated.

These were the first published results on the use of titration calorimetry for the determination of the micellization parameters of surfactants.

During titration calorimetry, determined amounts of a highly concentrated surfactant solution (at least 20 times higher than the CMC of the studied surfactant) are injected in a cell containing a determined amount of water.

The heat of reaction generated by the addition of the surfactant solution is monitored during the entire experiment.

For the first injections, the final concentrations in the sample cell are below the CMC.

Here, the enthalpic effects are due to the demicellization process (dilution of micelles) as well as the dilution of the corresponding monomers.

When a sharp increase in the curve is observed, this means that the CMC in the sample cell has been reached.

If more micellar solution is added, the micelles are no longer dissolved and the heat registered is the heat of micelle dilution, which corresponds to the second concentration range in the titration curve.

The CMC value is given by the first derivative of the curve.

ΔH_{demic} is equal to the enthalpy difference between the two “lines” at the CMC.

Paula et al’s paper has shown that it is possible to measure CMC and ΔH_{demic} in one experiment as presented in figure 1.3:

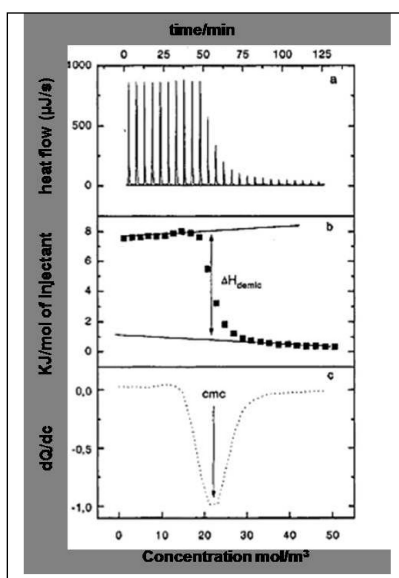


Figure 1.3: Calorimetric determination of CMC and ΔH_{demic} for Octyl Glucoside according to Paula et al [13]

In figure 1.3, the results of the titration of 10 μL aliquots of Octyl Glucoside micelles ($270 \cdot 10^{-3} \text{ mol/m}^3$) are given. Curve (a) represents the heat flow as a function of time; curve (b) gives the reaction enthalpy versus the total concentration in the sample cell (this curve is obtained by integrating the peaks

of curve (a)) and curve (c) which represents the first derivative of curve (b). The CMC is defined as the concentration where curve (c) has a minimum.

1.3.3.1 Surfactant adsorption at interfaces using calorimetry As already stated above, calorimetry is a powerful tool for monitoring the thermodynamics of surfactant adsorption at interfaces. These measurements are often used to predict adsorption mechanisms and as such deduce the possible structure of the adsorbed surfactant at the interface. This is done by comparing the adsorption calorimetry results (mainly the partial molar enthalpy of adsorption) with the amounts adsorbed and the micellization enthalpy in solution. Results published for both hydrophilic [14, 15, 16] and hydrophobic surfaces [17, 18] show similar features for different surfactants. In fact, the adsorption was exothermic at very low surface coverages and weakly exothermic (or even endothermic) when saturation is reached. The first step (strongly exothermic adsorption) is considered to be energy driven and is mainly dominated by the surfactant interaction towards the surface due to the low surface coverage. The second step (weakly exothermic or even endothermic) is considered entropy driven where the intermolecular interactions are supposed to play a major role. In this step, it is assumed that surfactant aggregates start forming at interfaces at certain surface coverage. This assumption is based on the comparison of these values and bulk micellization which is mainly endothermic or weakly exothermic for most surfactants [9].

Király et al [16] found out that the molar adsorption enthalpy of C_8E_4 and C_8G_1 for high surface coverage of hydrophilic silica are similar to corresponding micellization enthalpies of the studied surfactants. These studies and especially the work done by Király and Findenegg [18] presented strong evidence for aggregate formation at interfaces without excluding the possibility of monolayer and bilayer formation at surface saturation. In fact, both authors compared the enthalpy assuming half-micelles aggregation at the graphite surface and the enthalpy values assuming a horizontal-to-vertical reorientation of surfactants [18] towards the surface. Their experimental results correlated at best with the half-aggregates at surfaces.

These assumptions were further investigated using techniques that study di-

rectly surface structures. An overview of these techniques is presented in the next section.

1.3.4 Surface structure

The way amphiphilic molecules or polymers do organize at solid surfaces is an important aspect for the stabilization of colloidal dispersions. Atomic force microscopy (AFM) and scanning tunneling microscopy (STM) are techniques which can be used for the direct study of surface structures. This review on the principle of AFM and STM is mainly based on the review done by Scales [19].

STM) and AFM are techniques which enable imaging of molecular structures at solid interfaces. The images provided are three-dimensional with an atomic resolution. A schematic diagram of a scanning tunneling microscope is given in figure 1.4 [20]:

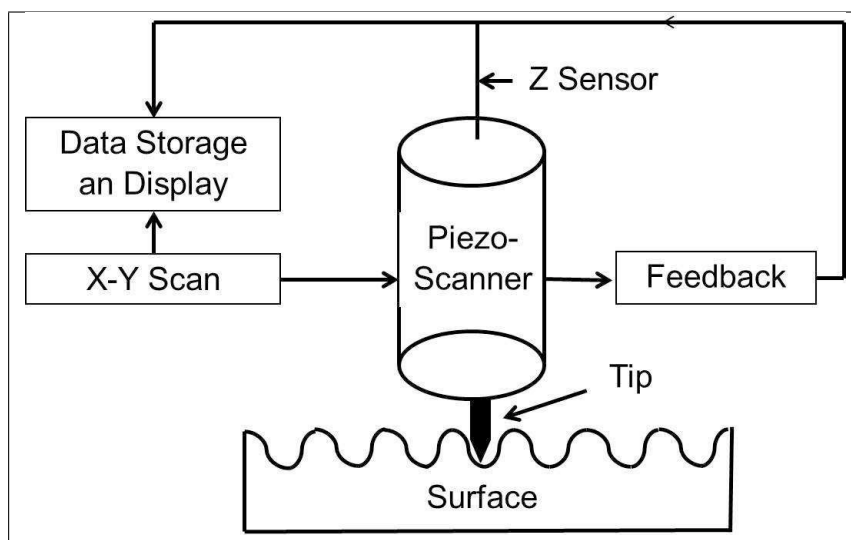


Figure 1.4: Schematic diagram of a scanning tunneling microscope

The principle can be described as follows: a sharp metallic tip attached to a cylindrical piezoelectric tube is brought approximately 1 nm close to the surface of a conducting material. By applying a voltage, electrons begin to tunnel

between the tip and the surface. By varying the voltage across the piezoelectric tube the tip begins to scan over the surface in the x and y direction. The generated tunneling current is then measured and recorded. As the tip approaches a high or low spot on the surface, the tunneling current increases or decreases in response to the change in distance between the tip and the surface. An electronic feedback loop adjusts the vertical position of the tip in order to maintain a constant current. By plotting the tip height z versus the lateral position x and y , a three dimensional image of the scanned surface is produced. The STM basic concept records the voltages as a function of position creating a three dimensional image. In AFM measurements the metallic STM tip is replaced by a tip made of diamond or silicon nitride (Si_3N_4) mounted onto a cantilever spring. When the tip starts rastering the surface, the vertical movements of the tip are detected using a laser beam which is positioned on the back of the spring. The signal from the detector is collected by an electronic feedback loop which adjusts the position of the sample (by raising or lowering it) in order to maintain a constant force. The schematic diagram of an atomic force microscope is presented in figure 1.5 [20]:

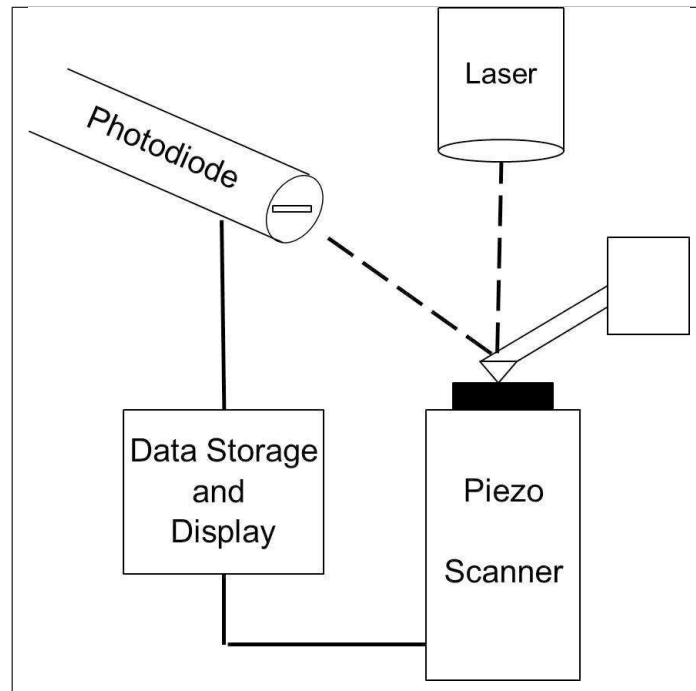


Figure 1.5: Schematic diagram of an atomic force microscope

The first atomic force microscope appeared in 1986 as a further development of scanning tunneling microscopy done by Binnig, Rohrer, Gerber and Weibel at IBM in Zurich (Switzerland); Binnig and Rohrer won the Nobel Price of Physics 1986 for this invention. The further development done by Binnig, Quate and Gerber as collaboration between IBM and Stanford University resulted in the development of the AFM in 1986 [21]. AFM can be applied to both conductive and non-conductive surfaces and in gaseous or liquid environments which gives this technique a special status among surface characterization techniques. In this section, the explanation of the main principles of AFM measurements are based on the chapter “Atomic Force Microscope Studies of Membrane Surfaces” from Richard Bowen [22]. In AFM, the tips used are only a couple of microns long and are less than 10 nm in diameter. The cantilevers used are mainly 100-200 μm long. When the tip is scanning the surface of a sample, the forces generated between the tip and the surface cause the cantilever to bend. A detection system (such as a photodiode) intercepts this deflection, measures it allowing the connected computer to generate a topographical image of the surface. A piezo-element is used to control the displacement of the sample attached to its surface in the x, y and z direction. Piezo-elements are generally manufactured from crystalline elements that are referred to as non-centro symmetric which means that the crystalline structures move when applying an electric field producing dimensional changes in the material. This property enables the use of these materials as precise electromechanical displacement elements. The piezo-electric material is expanded and contracted using a DC voltage typically in the range -500 to +500 volts. Typical piezo-elements are perovskite materials such as lead-zirconium-titanate. A V-shaped cantilever usually from silicon or silicon nitride attached to a substrate of similar material is used (depending from the model used, there could be more than 5 tips mounted on a cantilever and can be simultaneously used for each experiment). At the end of each cantilever, there is a tip as shown in figure 1.6.



Figure 1.6: AFM cantilever tip

A laser and an optical path consisting of a lens, prism, mirror, cantilever and a position-sensitive photo-diode detector are needed. The laser is focused onto the back of the tip of the cantilever. The light beam is then reflected from the cantilever to a mirror and finally on the position-sensitive photo-diode detector. The detector enables the measurement of the cantilever's movements. An electronic feedback loop responds to the changes in the cantilever deflection by adjusting the tip-sample separation to a set point. This mode is the most common mode of imaging known as contact mode or constant force mode when the cantilever deflection remains constant as the surface is rastered relative to the tip.

When imaging membranes and surfaces, different modes can be used. The below section introduces the main imaging modes used:

- Contact mode:

Contact mode is the most straightforward mode in AFM imaging. As already described, the cantilever tip is held close to the sample surface which is rastered underneath it, the change in the topography results in a change in tip-sample interaction. Contact mode can be operated in two ways:

- Constant height mode in which the cantilever is held in a fixed position with respect to the piezo-element so that each change in the cantilever deflection is used to generate a topographic image of the surface.

The advantage of this mode is that it enables high scan speeds allowing real time images.

- Constant force mode where a feedback loop keeps the total force between

the cantilever tip and the sample constant; this mode is the preferred mode as the total force exerted by the tip on the sample is controllable.

The disadvantage of this mode is that the response time of the feedback circuit and the movement of the scanner limits the effective scanning speed.

- Non-contact mode:

The cantilever vibrates near the surface of the sample (5-10 nm away from the surface) which is the force distance region where Van der Waals forces are predominant. An applied force serves to change the vibrational amplitude and resonant frequency of a vibrating cantilever. Thus, as the sample is rastered under the vibrating cantilever tip the topography gives a change in the tip-sample interaction.

The principle advantage of this mode is that during imaging of the surface, no contact exists between the tip and the sample which is of high importance when imaging soft surfaces.

- Tapping mode:

This mode, also known as intermittent mode, is getting more and more importance in the last years and constitutes a “hybrid” mode of contact mode and non-contact mode. In fact, as in non-contact mode the cantilever is vibrating and held at a tip-sample distance close to the region of contact imaging so that there is no permanent contact with the surface. The image is produced by monitoring the changes in the cantilever oscillation amplitude as the tip to sample distance changes with surface topography. In this mode, lateral forces are reduced which does not damage the surface, but the disadvantage of this mode is mainly on the slightly slower scan speed compared to contact mode.

1.3.4.2 Surfactant adsorption at the solid-liquid interface using AFM

The adsorption of surfactants at the solid/liquid interface has been widely studied. As already discussed in the section dedicated to adsorption isotherms

and the thermodynamics of the adsorption process, most of these studies focus on the adsorption isotherms of the studied systems as well as their calorimetric behavior. For hydrophobic surfaces, the adsorbed surfactants molecules are supposed to form hemi-cylinders at the solid surface according to Király et al [18]. The lack of suitable imaging tools has hindered direct visualization of the adsorbed surfactant aggregates. Due to the mentioned development of the AFM technique in 1986, it was possible to study the adsorption of surfactants on flat surfaces directly. This section presents the main results of two studies on surfactant adsorption on hydrophobic surfaces using AFM. The first research study published using AFM for the imaging of surfactant aggregates at the solid surface was from Manne et al (1994) [23] who studied the adsorption of hexadecyltrimethylammonium bromide ($C_{16}TAB$) on HOPG. HOPG stands for Highly Ordered (or Oriented) Pyrolytic Graphite. It is used as a probe for the calibration of scanning tunneling microscopes and has been the adsorbent of choice in studies on surfactant adsorption using AFM. The AFM images of the surfactant at the graphite surface show parallel stripes that were interpreted as hemi-cylinders structures of the surfactant at the graphite surface, these structures appeared in a periodic fashion as shown in 1.7:

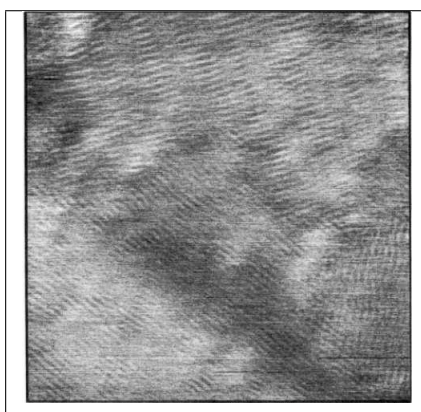


Figure 1.7: Contact mode image (240x240 nm) of the adsorbate structure of 0.8 mol/m^3 $C_{16}TAB$ on graphite [23]

The key for imaging was the use of a specific force that was insufficient to displace the surfactant but had a sufficient gradient to discriminate surface structures.

This publication was the starting point of a series of studies done by differ-

ent groups in order to image adsorbed surfactants at different solid surfaces (mainly mica, silica and graphite). In 1995, Ducker et al [24] studied the adsorption of sodium dodecyl sulfate (SDS) at the graphite surface using a pyrolytic graphite of the so-called monochromator grade ZYH (supplied by the company SPI). Several structures were observed in the concentration range from 2.1 to 81 mol/m³ (the used SDS has a CMC value of 8.1 mol/m³). By increasing SDS concentration between 2.1 and 81 mol/m³, the morphology of the observed structures remained apparently unchanged, but the distance between aggregates did decrease. Ducker et al also measured a period of 5.1 nm for the highest SDS concentration which means an aggregate section of about 3 nm². Greenwood et al [25] data at the same concentration indicates that the surfactant occupies 0.42 nm²/molecule. This means at least 7 molecules in the cross section which is not consistent with the hydrocarbon chains lying parallel to the surface. These results indicate that the hemi-cylindrical structure is more probable. Ducker et al published in the same paper [24] the results of the effect of salt on imaging using NaCl at high concentration (0.16 mol/m³). It was observed that the addition of salt made the structures appear at lower concentrations of SDS which is rather expected as the CMC value of SDS is very dependent on ionic strength. This morphology registered at the graphite surface is correlated to the own structure of the graphite surface.

Graphite interacts primarily with surfactant tail groups via hydrophobic and van der Waals interactions, the alkyl chains are oriented along the three symmetry axes of graphite following the zigzag line connecting nearest-neighbor carbon atoms [26, 27]. This characteristic is illustrated by the universality of the morphology presented which has been observed for a variety of surfactants with 12 or more carbon atoms presenting a hexagonal phase in their phase diagram: those are ionic, [23, 24, 28, 29, 30] non ionic [31, 32, 33] and zwitterionic [34] surfactants.

Surfactants that do not form half-cylindrical aggregates include univalent double-tailed surfactants that form lamellar and bi-continuous bulk phases, for which cylindrical curvatures are not favored, and surfactants with 10 or fewer carbon atoms in the tail group which form flat vertical monolayers on graphite, because the tail falls short of a critical length required for orientation by the graphite surface [32]. Similar results have been reported at the cleavage plane

of MoS₂ despite the differences in lattice symmetry, spacing, and surface chemistry between this surface and graphite.

2 Materials and methods

In this chapter, the studied systems (the surfactants used as well as the adsorbents) are introduced in terms of their structures and main properties.

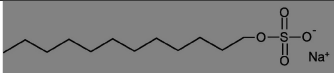
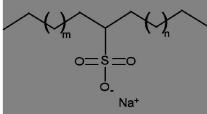
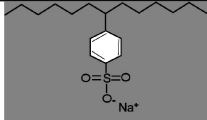
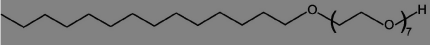
In addition to that, the methods used for the determination of the adsorption isotherms, the enthalpy of adsorption and the structure of the adsorbed layers for the single surfactants and the surfactant mixtures are described.

2.1 Studied systems

2.1.1 Low-mass Surfactants

In this study, anionic and nonionic low-mass surface active agents have been used as adsorbates. This choice is due to the relevance of both groups in different fields of application. Three anionic amphiphiles have been used. All three present major structural differences: different ionic head groups (sulfate and sulfonate groups) and different hydrophobic parts (a linear alkyl chain, a branched alkyl chain and a branched alkyl chain with an aromatic ring). The structures as well as the compositions of the used surfactants are given in the table below:

Table 2.1: Used surfactants

Surfactant	Structure	Composition
SDS		C ₁₂ = 99%
SAS		C ₁₃ -C ₁₅ = 59% ; C ₁₆ -C ₁₇ = 39%
SDBS		96% (isomer mixture)
C ₁₂₋₁₄ E ₇		C ₁₂ = 48% C ₁₄ = 17% ≥ C ₁₆ = 11%

- Sodium dodecyl sulfate (SDS) : linear alkyl chain

SDS belongs to the group of alkyl sulfates that are mainly produced from natural fatty alcohols (derived from palm oil, palm kernel oil, coconut oil) or from oxo-alcohols of petrochemical origin [35]. Alkyl sulfates having a natural origin are, however, more used. The SDS used in this study was supplied by the company Roth and has a 99% purity grade; the structure of SDS is given in table 2.1.

- Sodium dodecyl benzene sulfonate (SDBS) : branched alkyl chain with a phenyl ring

SDBS, as most alkyl sulfonates, has a high solubility and very good detergency performance. As a result, they have found a broad use in detergent formulations. The used SDBS quality supplied by Sasol has a 96% purity and a structure as given in table 2.1.

- Secondary alkyl sulfonate (SAS) : branched alkyl chain

Secondary alkyl sulfonates are produced by photochemical sulfoxidation or sulfochlorination of suitable C_{12} - C_{18} paraffins [36],[37],[38],[39]. SAS was supplied by Clariant under the trade name Hostapur SAS 93. The alkyl chain is at 59% C_{13} - C_{15} and at 39% C_{16} - C_{17} .

- Fatty alcohol ethoxylate (FAE):

The nonionic surfactant used is a fatty alcohol ethoxylate. Alkyl heptaglycol ether ($C_{12-14}E_7$) was supplied by BASF SE (Cognis) under the trade name Dehydol LT7. Dehydol LT7 is actually a $C_{12-18}E_7$ with a high percentage of $C_{12-14}E_7$ as given in table 2.1. That is why this surfactant will be referred to in this thesis as $C_{12-14}E_7$. This group of surface-active agents presents an important characteristic which is the possible adjustment of its hydrophilic moiety by gradual addition of ethylene oxide for a better solubility or interfacial activity of the molecule.

2.1.2 Adsorbents

2.1.2.1 Carbon black The adsorbent used has a large surface area that facilitates adsorption studies of surface-active agents in solutions due to a strong decrease in solution concentration during adsorption. This makes carbon black the adsorbent of choice in this study. In fact, the carbon black used is a furnace black (Printex L from Evonik) with a surface area of $150 \text{ m}^2/\text{g}$ and a pH value at the surface of 9. The value of the surface area was measured at the institute of physical-chemistry through a Brunauer-Emmett-Teller (BET) analysis where the adsorption of Nitrogen (whose cross-sectional surface area is known) at the carbon black surface is measured [40]. Figure 2.1 shows a SEM (Scanning Electron Microscopy) micrograph of a carbon black dispersion done in this study . Figure 2.2 shows the porous structure of the used carbon black.

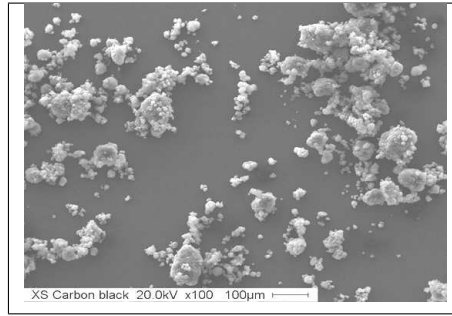


Figure 2.1: SEM micrograph of the carbon black dispersion (20kV x 100)



Figure 2.2: SEM micrograph of the carbon black dispersion (20kV x 5000)

2.1.2.1 Carbon black Figure 2.3 presents the graphite plates used in this study. Graphite is one of the allotropes of carbon, whose molecular structure consists of layers of carbon atoms arranged in a hexagonal lattice. All layers are bound through van der Waals interactions.



Figure 2.3: HOPG plates

Graphite exists in two crystallographic forms: a hexagonal form (alpha) and rhombohedral form (beta). The difference in the spacing of the layers of hexagonal-linked carbon atoms in graphite gives rise to hexagonal and rhombohedral crystallographic forms.

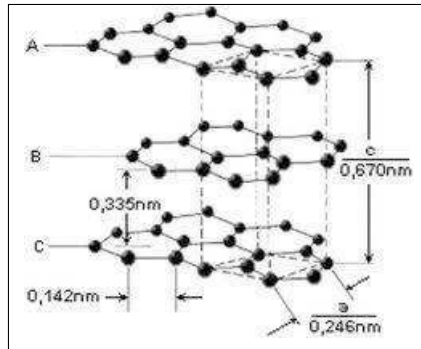


Figure 2.4: HOPG crystallographic structure [41]

HOPG is used as a probe for the calibration of scanning tunneling microscopes and is, in this thesis, the adsorbent of choice for the AFM study. The quality used is supplied by SPI under the trade name ZYH and each plate has the following dimensions : 12x12x2 mm.

2.1.3 Used Methods

2.1.3.1 Concentration measurement methods In a solid-liquid dispersion, the adsorbed amounts of amphiphiles is measured by monitoring the decrease of surfactant concentration in solution. Knowing the surface area of the solid adsorbent, the following formula is used to calculate the corresponding adsorbed amount (Γ):

$$\Gamma = \frac{(c_i - c_{eq})}{mA} V \quad (2.1)$$

With :

- c_i = initial surfactant concentration (mol/l)
- c_{eq} = equilibrium concentration (mol/l)
- m = mass of adsorbent (g)
- A = surface area of adsorbent (m^2/g)
- V = solution volume (l)

During concentration measurements, the decrease of surfactant concentration in the bulk solution due to its adsorption at a solid interface of known surface area is recorded. The resulting diagram represents the adsorbed amount of surfactant (Γ) per unit area of the substrate (carbon black) as a function of the equilibrium concentration and is known as adsorption isotherm. The rapid increase towards plateau values observed in most adsorption isotherms occurs before and around the critical micelle concentration value (CMC) of the used surfactant.

2.1.3.2 UV-measurements of sodium dodecyl benzene sulfonate The UV spectra were recorded using a Cary 1 UV-Vis spectrophotometer equipped with a temperature-controller (Julabo F-10). Quartz cells with a path length of 1 cm were used for the determination of absorption values. This method has been used for the determination of the equilibrium concentration of the anionic surfactant SDBS which presents a phenyl group in its structure that can be detected at a wavelength of 262 nm. All absorption values were measured at

this value (262 nm). A calibration curve has been measured first in order to correlate directly the absorption values with the concentration of the anionic surfactant after adsorption.

2.1.3.3 Anionic surfactant titration It is the field of electrochemistry in which a potential is measured under the conditions of no-current flow. The measured potential is an indirect measurement of the solution concentration. The potential that develops in the electrochemical cell is the result of the free energy change under equilibrium conditions.

$$\Delta G = -nFE \quad (2.2)$$

with:

- n = mole number
- F = Faraday constant
- E = Nernst Potential

In the electrochemical cell, the potential difference between the cathode (C) and the anode (A) is the potential of the cell and is given by:

$$E = E_C - E_A \quad (2.3)$$

Under standard state conditions:

$$E = E^0 - \frac{RT}{n_i F} \ln(K_{eq}) \quad (2.4)$$

$$E = E^0 - \frac{RT}{n_i F} \ln(a_i) \quad (2.5)$$

With:

- E^0 = standard potential
- R = gas constant
- T = temperature
- n_i = mole number of (i)
- a_i = activity of (i)
- K_{eq} = equilibrium constant

For the determination of the SDS concentrations, a titration with a cationic surfactant DDMICL (1, 3 Didecyl-2-methylimidazolium Chloride) has been performed. A surfactant selective electrode was used for the detection of the turbidity point which is characterized by an increase of the potential value. This correlates the potential measured with the SDS concentration.

2.1.3.4 Nonionic surfactant titration The titration is done using a fluor-based titrant (Tetrakis (4-fluorophenyl) borate) for the complexation of the nonionic surfactant as described by Tsubouchi et al [42]. Nonionic surfactants can form complexes with metal ions such as potassium and barium. The formed complex cation does react with anions and this reaction has been the basis for various spectrophotometric methods as well as precipitation titration for the determination of the nonionic surfactant concentration [42]. However, the presence of anionic surfactants makes titration difficult as the formed complex cation of the nonionic surfactant is known for forming ion pairs with the anionic surfactants present in solution. The so-called two-phase titration technique has been used in this study for the determination of the nonionic surfactant concentration in the presence of an anionic surfactant. During titration, the excess of the titrant results in a color change of the cationic dye, Victoria blue B, which can be detected using UV-Spectroscopy which enables the determination of the nonionic surfactant concentration in solution.

2.1.3.5 Isothermal Titration Calorimetry (ITC) Adsorption isotherms can be complemented by measurements of the heat of adsorption. There are different methods for the monitoring of the heat of reactions. The one used in this study is a titration calorimetry method using an isothermal heat flow microcalorimeter (TAM 2277 (Thermal Activity Monitor) from Lund, Sweden (Waters)). This Microcalorimeter allows the monitoring of heat quantities in μJ and nJ -ranges (figure 2.5 and 2.1.3.5). A twin detector, supplied with a sample cell and a reference cell, was used.

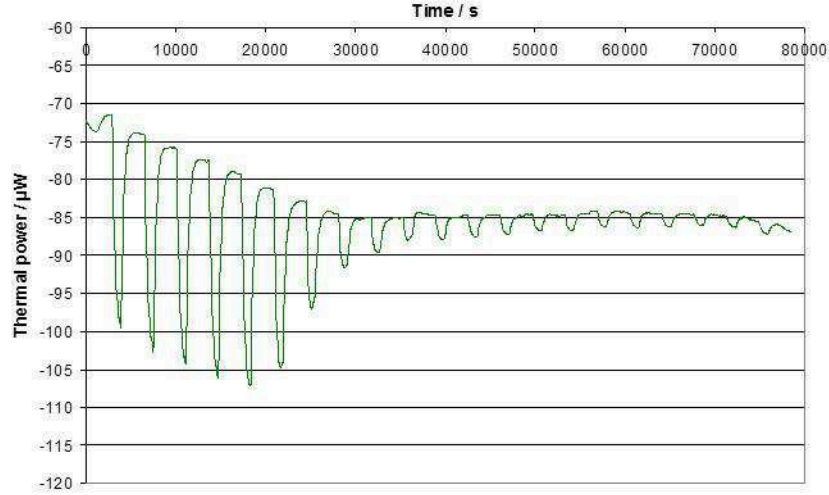


Figure 2.5: TAM 2277

The measurements of the adsorption enthalpies were performed at $298.15 \pm 2 \cdot 10^{-4}$ K. High concentration solutions of surfactants (30g/l) were filled in a Hamilton Microlab Syringe that was disposed in a dosing unit controlled by the Digitam Software. Good baseline stability with a noise of less than $\pm 0.1 \mu\text{W}$ was achieved during all experiments. This technique enables the monitoring of the heat of adsorption throughout the adsorption isotherm. This is done by measuring the heat generated by the injection of a certain concentration of the surfactant solution into the sample cell which contains the carbon black dispersed in water under continuous stirring. The sample cell is contained within the microcalorimeter chamber. During the experiment, a constant temperature is achieved by a feedback loop that controls the power

supply to a heating coil [43]. The energy required to maintain the temperature of the sample cell at a constant value is monitored which gives the plot of the heat flow as a function of time. The generated heat is given by the area under the peaks as given in figure 2.6.

Figure 2.6: Plot of the heat flow as a function of time



Knowing that the process is isothermal, the area under the peaks gives the heat of adsorption also known as heat of displacement. The enthalpy of adsorption (ΔH_{ads}) is obtained by dividing the heat of adsorption by the adsorbed amount (Γ) following this equation [11]:

$$\Delta_{ads}H = \frac{Q_{ads}}{\Gamma} \quad (2.6)$$

With:

- Q_{ads} = heat of adsorption
- Γ = adsorbed amount

2.1.3.6 Atomic Force Microscopy (AFM) Atomic force microscopy is an imaging technique allowing the topographical study of membrane surfaces. A full description of the method is given in the section “Theoretical part”. The used AFM set-up is supplied by the company MFD-3D™.

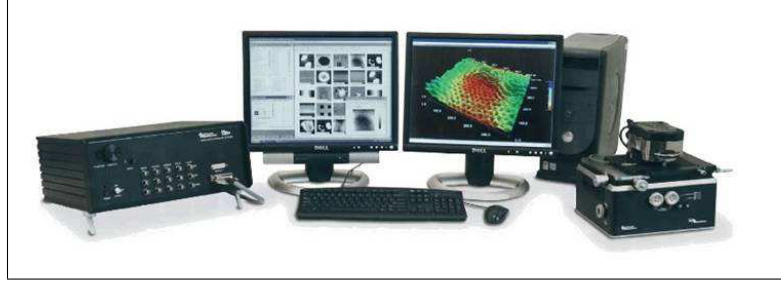


Figure 2.7: Used AFM set-up

The used cantilevers are supplied by Olympus and have the following reference:

Table 2.2: AFM Cantilever specification

Reference	Material	Length (μm)	Width (nm)	Spring constant (N/m)
OMCL-TR400PSA	$\text{Si}_3\text{N}_4/\text{Au-Cr}$ coating	200	400	0.07

The used Si_3N_4 cantilevers are coated with gold and chrome for a better reflection of the laser. This cantilever type is especially designed for imaging soft films. Prior to each experiment, a new cantilever having the same specifications as mentioned in table 2.2 was used and the graphite plate was freshly cleaved using adhesive tape. The specific experimental challenge in this thesis is that the AFM measurements are all done in solution. This is done by using a Petri dish into which the graphite fixed on a metal plate is kept immobile by a magnet fixed on the bottom of the Petri dish. 3 ml surfactant solution were needed in each experiment in order to cover the graphite surface enabling favorable imaging conditions. The cantilever tip was held in solution during the entire experiment. The used mode for all the experiments performed in this thesis is the so-called contact mode [23, 28, 29]. The setpoint was adjusted in order to raster the surfactant layer rather than the graphite layer. This is done by adjusting the setpoint to a value within the repulsive part (region 2 in figure 2.8) before film rupture.

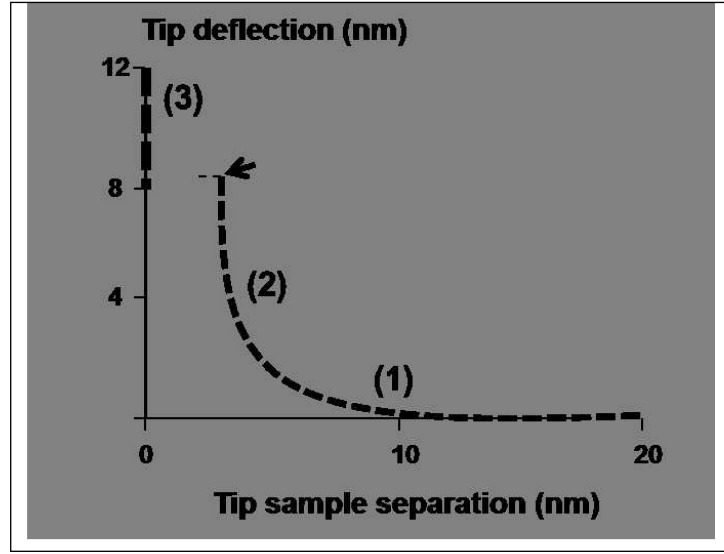


Figure 2.8: AFM force curve [44]

The force curve in figure 2.8 represents the variation of the cantilever deflection as a function of the separation between the tip and the sample. This is done by holding the scanner constant in all directions except z .

- (1): represents the region of electrostatic forces
- (2): represents the region immediately prior to film rupture
- (3): this is the region where the tip has ruptured the surfactant film and is in contact with the underlying substrate.

In order to increase the quality of the micrographs during scanning, an acoustic control parameter is added: the used AFM set-up is equipped with an electroacoustic transducer that produces a sound in response to the scanner signal and enables the selection of the scanner position which corresponds to the soft-contact mode.

3 Results

3.1 Adsorption isotherms

In this section, the results of the adsorption isotherms will be presented first for the single surfactants at the carbon black-water interface and compared to the behavior of these surfactants in the mixture.

3.1.1 Adsorption isotherms for single surfactants

Figure 3.1 illustrates the adsorption isotherm performed at a pH value of 10 and $T = 298$ K for the anionic surfactant sodium dodecyl sulfate (SDS) at the carbon black-water interface.

For the other studied systems the sodium dodecyl benzene sulfonate (SDBS), the secondary alkane sulfonate (SAS) and the nonionic surfactant ($C_{12-14}E_7$), the adsorption isotherms are given in figure 3.2 in comparison to SDS.

The shape of the adsorption isotherms for SDS, SDBS and SAS at the carbon black-water interface is typical for the adsorption isotherms obtained for long chain anionic surfactants on hydrophobic surfaces [45]. The adsorption isotherm for the nonionic surfactant presents a different shape with a higher increase of the adsorbed amounts at low concentrations. These isotherms are often correlated with the aggregation at the liquid-air interface and the surface tension and the aggregation of the surfactant in the bulk phase which are characterized by the CMC (as presented in table 3.1). The surface tension concentration curve and the CMC value for each surfactant are determined from surface tension measurements as presented in figure 3.3.

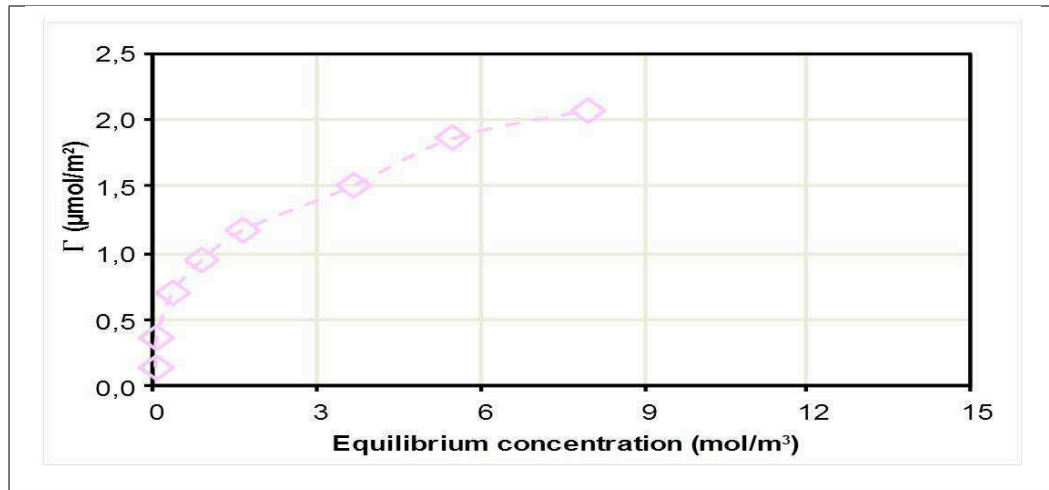


Figure 3.1: Adsorption isotherm for the anionic surfactant SDS at the carbon black-water interface

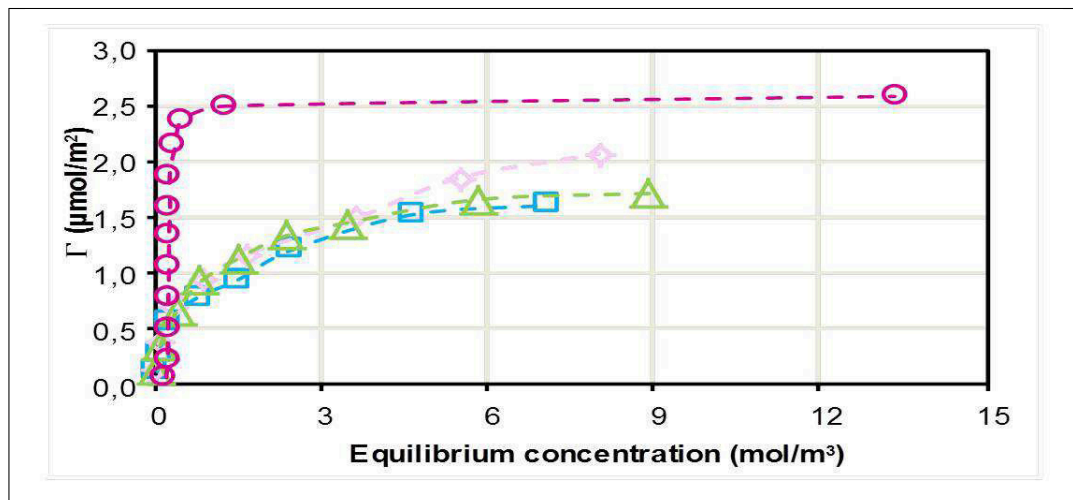


Figure 3.2: Adsorption isotherms for the single surfactants at the carbon black-water interface

○ C₁₂₋₁₄E₇ ◇ SDS □ SDBS △ SAS

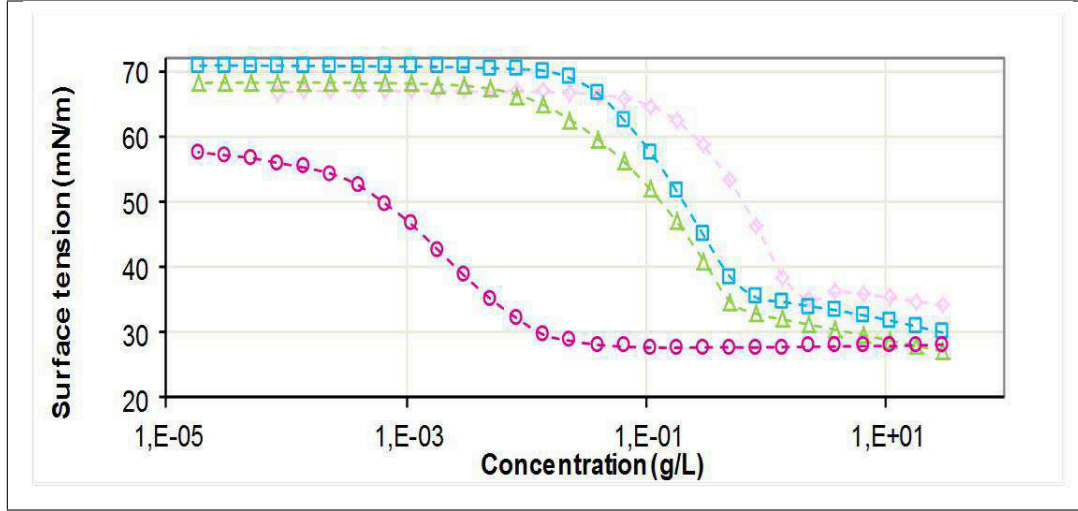


Figure 3.3: Surface tension curves and CMC for the single surfactants

○ $C_{12-14}E_7$ ◇ SDS □ SDBS △ SAS

The surfactant concentration values (x-axis) are given in figure 3.3 in g/l rather than in mol/m^3 as the case in figure 3.1 and 3.2 as well as in table 3.1 because this is the common practice in application.

Table 3.1: CMC values at $T = 298 \text{ K}$, $\text{pH} = 10$ for the single surfactants

Surfactant	CMC value (mol/m^3)
SDS	6.84
SDBS	1.67
SAS	1.44
$C_{12-14}E_7$	0.03

The adsorption isotherms for the anionic surfactants and the nonionic surfactant at the carbon black/water interface are presented together with the corresponding CMC values in figure 3.4.

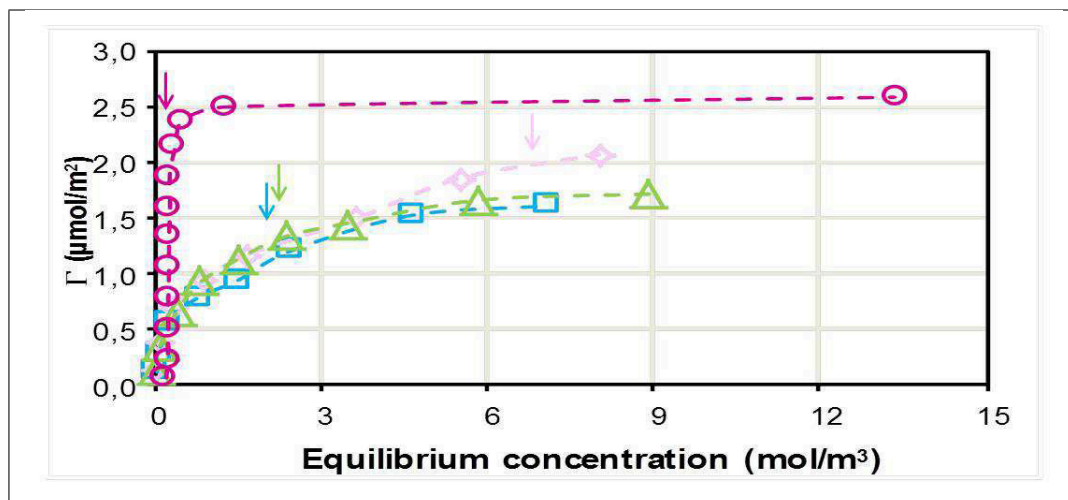


Figure 3.4: CMC values (\downarrow) and adsorption isotherms for the single surfactants at the carbon black/water interface at $T = 298$ K, $pH = 10$

○ $C_{12-14}E_7$ ◇ SDS □ SDBS △ SAS

For the anionic surfactants, all three plots show already at low equilibrium concentrations an increase of the adsorbed amounts (Γ) of these surfactants at the hydrophobic surface. This increase of the adsorbed amounts is then followed by a nearly plateau region where the surface excess values (Γ) remain quite constant. This takes place at concentrations above the CMC of the corresponding surfactant in solution. For the anionic surfactants, SDS presents higher plateau values than the ones observed for SDBS and SAS. This adsorption isotherm for SDS is in good agreement with the one reported by Zettlemoyer et al. as well as Day et al. at the Graphon surface [46, 47, 48]. The higher values for SDS for the beginning of the plateau region further confirm the dependence of plateau values on the CMC value of the corresponding surfactant which in the case of SDS is higher than for the other anionic surfactants SDBS and SAS. The higher adsorbed amounts observed for SDS compared to SDBS and SAS show the role played by the hydrophobic part of the molecule during the adsorption process as this represents the main structural difference for the interaction with hydrophobic surfaces between the studied anionic surfactants. The CMC value for the nonionic surfactant $C_{12-14}E_7$ of 0.03 mol/m^3 explains the steep increase towards plateau values that takes place at very small concentrations. In fact, for the nonionic surfactant, the sudden increase is observed at very low

concentrations almost 100 times smaller than for the anionic surfactants SDS, SDBS or SAS which again correlates with the dependence of this increase on the CMC value of the corresponding surfactant. In fact, higher CMC values result in higher plateau values as observed for the anionic surfactants and a low CMC value results in a steep increase at low equilibrium concentration as observed for the nonionic surfactant. The increase towards plateau values for the adsorption isotherms taking place in the CMC region has been related to the formation of a vertical monolayer for hydrophobic surfaces and a vertical bilayer for hydrophilic surfaces [49, 50, 51, 52]. The area per molecule provides important information on the degree of packing and the possible orientation of the alkyl chain for each surfactant towards the hydrophobic carbon black surface. Knowing the values of Γ_{\max} (maximum adsorbed amount) for each single surfactant, it is possible to directly calculate the limiting area per molecule at the interface (a_S) for each studied surfactant. The parameter a_S is defined by:

$$a_S = \frac{10^{18}}{N\Gamma_{\max}} \quad (3.1)$$

Where:

- a_S : limiting area per molecule (nm^2)
- N : Avogadro constant ($6.023 \cdot 10^{23}$ molecules/mol)
- Γ_{\max} : Maximum surface excess concentration (mol/m^2)

The table below presents the limiting areas per molecule for each surfactant calculated using the above equation 3.1 as well as the limiting areas per molecule calculated assuming a vertical and a horizontal orientation of the alkyl chain towards the surface. The CMC values are also indicated for each surfactant.

Table 3.2: Limiting areas per molecule for the single surfactants

Surfactant	$\Gamma_{\max}(\text{mol/m}^2)$	Area per molecule a_s (nm^2)	$a_s(\text{h.o})$ (nm^2)	$a_s(\text{v.o})$ (nm^2)	CMC (mol/m^3)
C ₁₂₋₁₄ E ₇	$2.5 \cdot 10^{-6}$	0.66	1.05	0.20	0.03
SDS	$2.0 \cdot 10^{-6}$	0.83	1.05	0.20	6.84
SDBS	$1.7 \cdot 10^{-6}$	0.97	1.05	0.20	1.67
SAS	$1.6 \cdot 10^{-6}$	1.03	1.05	0.20	1.44

Where:

- h.o: horizontal orientation
- v.o: vertical orientation

The values calculated for the horizontal and the vertical orientation of the alkyl chain towards the surface (as presented in figure 3.5) are derived from the Langmuir film measurements [53].

NB: Assumption of a vertical and a horizontal orientation of the alkyl chain of the surfactants towards the carbon black surface.

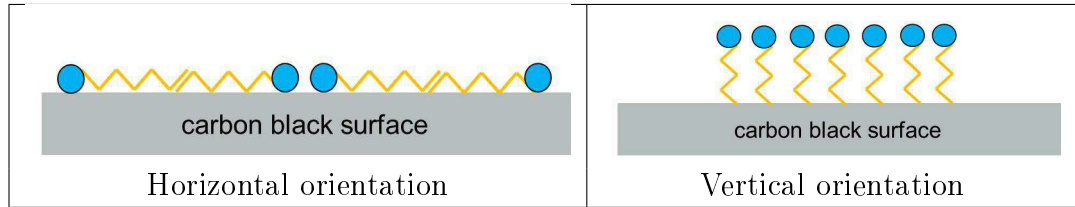


Figure 3.5: Schematic presentation of a vertical and a horizontal orientation of the alkyl chain on hydrophobic surfaces

The surface excess values for the nonionic surfactant are higher than for the anionic surfactants which results in an area per molecule for the nonionic surfactant smaller than that for the anionic surfactants. The areas per molecule already show that the experimental values indicate a horizontal orientation at the carbon black surface as even with higher concentrations no close packed layer with vertical orientation is reached. Moreover, multilayer structures with a horizontal arrangement can be assumed in parts of the surface due to the values between vertical and horizontal arrangement.

3.2 Adsorption isotherms for surfactant mixtures

The main focus of this study is the investigation of the adsorption behavior of mixtures of anionic and nonionic surfactants at the carbon black surface compared to the single surfactants. Having studied the behavior of each single anionic surfactant at the carbon black surface (refer to figure 3.6), it is possible to correlate the adsorption isotherms for mixtures with those already determined for each single surfactant in order to infer possible synergies. The adsorption isotherms for mixtures were determined using the same experimental procedure as for single systems (see 1.1 for further details). It is important to mention that the concentrations of both surfactants in the mixture were determined independently.

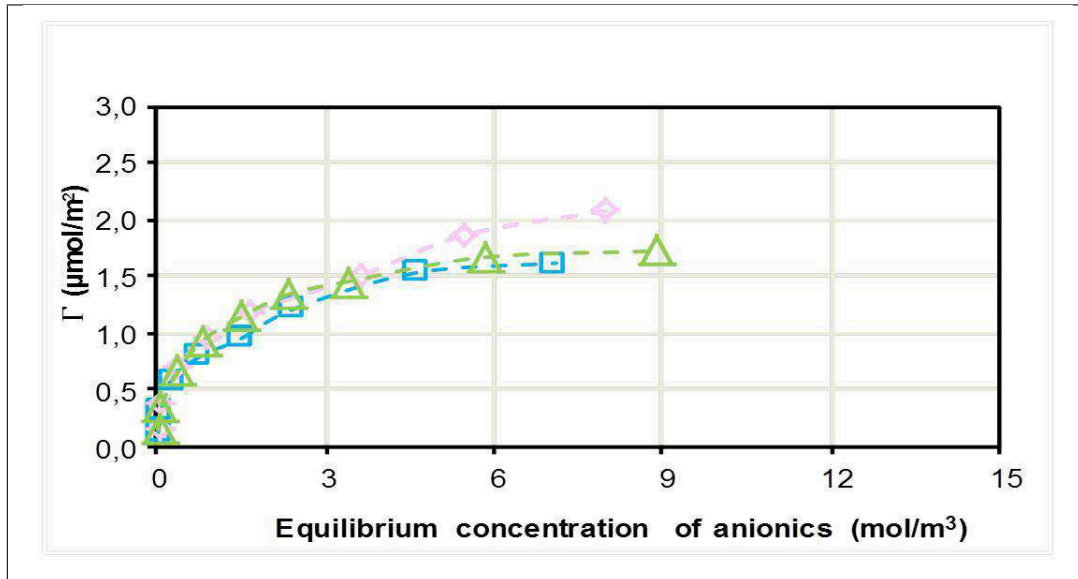


Figure 3.6: Adsorption isotherms for the single anionic surfactants

◇ SDS □ SDBS △ SAS

The results of the adsorption measurements for each mixture of anionic and nonionic surfactant are presented below in form of two graphs:

- Adsorbed amount of anionic surfactants in the mixture compared to the adsorbed amounts of the single anionic surfactants as a function of the

anionic surfactant concentration (figure 3.7)

- Adsorbed amount of the nonionic surfactant in the mixture compared to the adsorbed amount of the single nonionic surfactant as a function of the nonionic surfactant concentration

The adsorbed amounts were calculated from concentration measurements of both surfactants in the mixture.

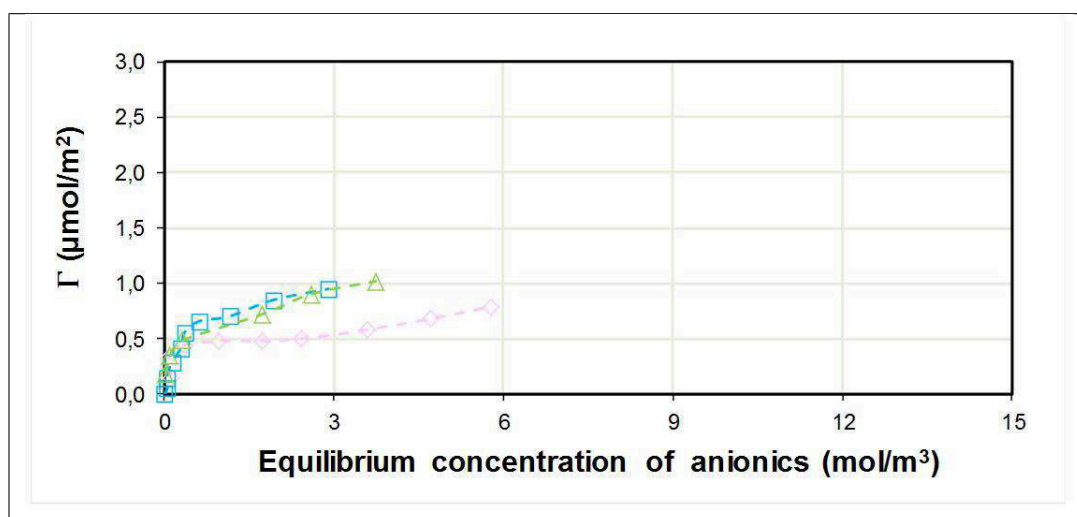


Figure 3.7: Adsorption isotherms for the anionic surfactants in the 1:1 mixture with the nonionic surfactant

◇ SDS □ SDBS △ SAS

The CMC of the studied mixtures (see figure 3.8) have been determined in the same way as already done for the single surfactants (refer to table 3.3) in order to correlate the CMC values for the mixtures with the adsorption isotherms as indicated in figure 3.8. All mixtures with the three different anionic surfactants have nearly the same critical micelle concentration.

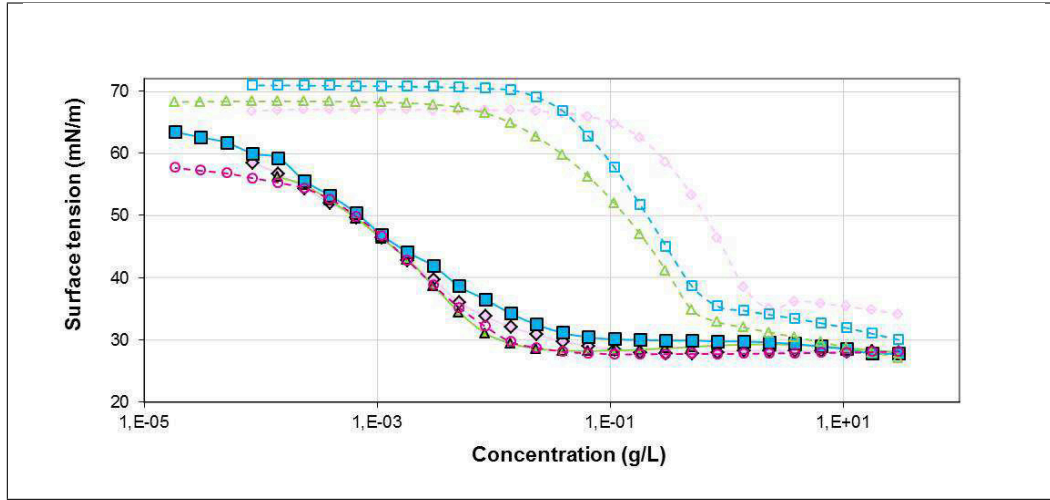


Figure 3.8: Surface tension concentration curves and CMC values for the single anionic surfactants and their mixtures with the nonionic surfactant as function of the total surfactant concentration



Figure 3.8 shows the shifts of the surface tension curves for the mixtures towards lower values compared to the same curves for the single anionic surfactants due to the effect of the nonionic surfactant on the surface tension of the mixtures. The results for the mixtures from the adsorption isotherms show an interesting behavior with mainly two different effects taking place in two different concentration ranges. In fact, at very low surfactant concentrations, the adsorption of the anionic surfactants in the mixtures is slightly increased compared to the single anionic surfactant adsorption. In the second region of higher surfactant concentrations, lower plateau values for the anionic surfactants in mixture with the nonionic surfactant especially for the mixture with SDS are observed. The further determination of the limiting areas per molecule for the mixtures was done using equation 3.1.1. The results for the three mixed systems are presented in table 3.3.

Table 3.3: Limiting area per molecule for the mixture

Surfactant mixture (anio/nio)	Surface excess Γ_{\max} (mol/m ²)	a_S (nm ²)	a_S (v.o) (nm ²)	a_S (h.o) (nm ²)	CMC (mol/m ³)
SDS/C ₁₂₋₁₄ E ₇	2.5	0.66	0.20	1.05	0.03
SDBS/C ₁₂₋₁₄ E ₇	2.2	0.75	0.20	1.05	0.03
SAS/C ₁₂₋₁₄ E ₇	1.8	0.92	0.20	1.05	0.03

The space requirements of the alkyl chain for both surfactants should be comparable in the case of a horizontal orientation of the alkyl chain on the carbon black surface. The adsorption isotherms for the nonionic surfactant in mixture with the anionic surfactants are presented in figure 3.9. In principle, similar effects are observed for the nonionic surfactant in mixture with the anionic surfactants. In fact, a decrease of the plateau values for C₁₂₋₁₄E₇ in the mixture is observed compared to the adsorption isotherm for the single nonionic surfactant. This decrease is strongly dependent from the structure of the anionic surfactant in the mixture as presented in figure 3.9.

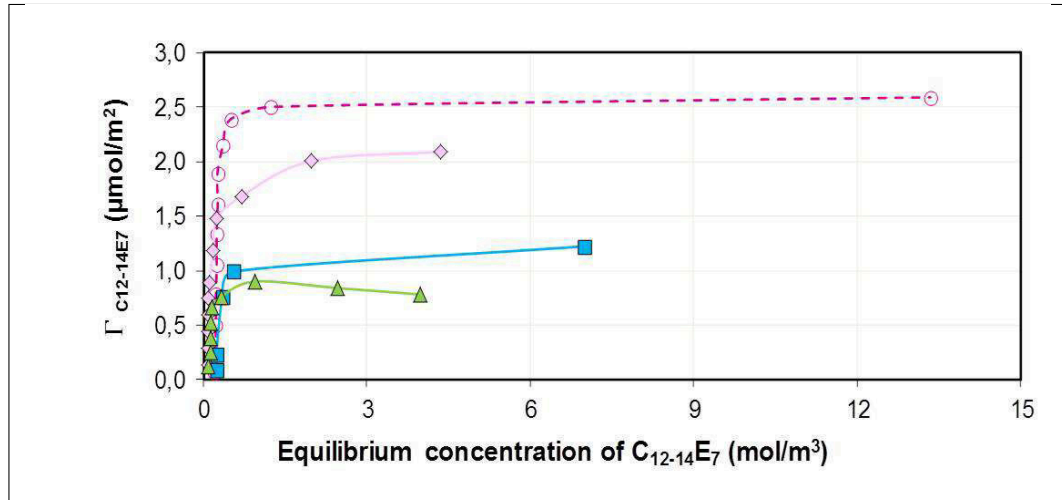


Figure 3.9: Adsorption isotherms of the nonionic surfactant in mixture with the anionic surfactants

○ C₁₂₋₁₄E₇ ◇ SDS/C₁₂₋₁₄E₇ ■ SDBS/C₁₂₋₁₄E₇ ▲ SAS/C₁₂₋₁₄E₇

The adsorption of the nonionic surfactant seems to be only slightly altered by the linear sodium dodecyl sulfate. This is seen in the small decrease of the

3 Results

adsorbed amount of the mixture of this surfactant with the nonionic C₁₂₋₁₄E₇ compared to the adsorbed amount of the single nonionic surfactant. This would suggest a higher displacement of SDS by the nonionic surfactant in the mixture. Schwuger et al [45] suggested that the displacement of the anionic surfactant by the nonionic surfactant is greater the larger the ratio of the nonionic surfactant to that of the ionic surfactant in the mixture is. In this study, a dependence of the ratio of the anionic surfactant and the nonionic surfactant in the adsorbed layer on the total concentration of the surfactants was observed as presented in tables 3.4 to 3.6.

NB:

- The ratios indicated for each mixture are the molar ratios of the nonionic surfactant to the anionic surfactant (for example 0.72/1 for C₁₂₋₁₄E₇/SDS mixture).
- c_i : initial concentration of the surfactant (mol/m³)
- c_{eq} : equilibrium concentration of the surfactant (mol/m³)

Table 3.4: Ratios of the adsorbed amounts for the C₁₂₋₁₄E₇/SDS mixture (0.72/1)

C_{iSDS}	$C_{iC_{12-14}E_7}$	C_{eqSDS}	$C_{eqC_{12-14}E_7}$	$C_{eqC_{12-14}E_7}$	Γ_{SDS}	$\Gamma_{C_{12-14}E_7}$	$\Gamma_{C_{12-14}E_7}$
(mol/m ³)	(mol/m ³)	(mol/m ³)	(mol/m ³)	/ C_{eqSDS}	(μmol/m ²)	(μmol/m ²)	/ Γ_{SDS}
0.86	0.61	0.122	0.090	0.73	0.146	0.133	0.911
1.73	1.2	0.081	0.089	1.09	0.328	0.288	0.878
5.19	3.61	2.427	0.111	0.046	0.499	0.892	1.787
6.92	4.81	3.607	0.173	0.049	0.583	1.184	2.031
8.65	6.01	4.724	0.241	0.051	0.680	1.474	2.168

3.2 Adsorption isotherms for surfactant mixtures

Table 3.5: Ratios of the adsorbed amounts for the $C_{12-14}E_7$ /SDBS mixture (0.87/1)

C_{iSDBS}	$C_{iC_{12-14}E_7}$	C_{eqSDBS}	$C_{eqC_{12-14}E_7}$	$C_{eqC_{12-14}E_7}$	Γ_{SDBS}	$\Gamma_{C_{12-14}E_7}$	$\Gamma_{C_{12-14}E_7}$
(mol/m ³)	(mol/m ³)	(mol/m ³)	(mol/m ³)	/ C_{eqSDBS}	(μ mol/m ²)	(μ mol/m ²)	/ Γ_{SDBS}
0.72	0.63	0.246	0.055	0.223	0.084	0.052	0.619
1.43	1.25	0.235	0.042	0.179	0.226	0.150	0.664
4.31	3.75	0.346	0.293	0.847	0.757	0.414	0.547
5.75	5.00	0.538	0.361	0.671	0.991	0.558	0.563
14.37	12.5	6.995	2.905	0.415	1.223	0.951	0.777

Table 3.6: Ratios of the adsorbed amounts for the $C_{12-14}E_7$ /SAS mixture (0.75/1)

C_{iSAS}	$C_{iC_{12-14}E_7}$	C_{eqSAS}	$C_{eqC_{12-14}E_7}$	$C_{eqC_{12-14}E_7}$	Γ_{SAS}	$\Gamma_{C_{12-14}E_7}$	$\Gamma_{C_{12-14}E_7}$
(mol/m ³)	(mol/m ³)	(mol/m ³)	(mol/m ³)	/ C_{eqSAS}	(μ mol/m ²)	(μ mol/m ²)	/ Γ_{SAS}
0.83	0.63	0.027	0.098	3.629	0.179	0.117	0.654
1.67	1.25	0.080	0.123	1.537	0.353	0.251	0.711
2.50	1.88	0.308	0.126	0.409	0.487	0.389	0.798
3.33	2.50	0.673	0.160	0.237	0.591	0.520	0.879
4.17	3.12	1.182	0.175	0.148	0.663	0.656	0.989
5.00	3.75	1.749	0.275	0.157	0.722	0.772	1.069
6.67	5.00	2.801	0.992	0.354	0.859	0.891	1.037
8.33	6.25	4.409	2.494	0.566	0.872	0.891	1.022

In fact, the ratios calculated for the $C_{12-14}E_7$ /SDS mixture in the adsorption layer at high equilibrium concentrations are comparatively higher than those in the bulk solution. For SAS in the mixture with the nonionic surfactant, the

adsorbed layer at high surfactant concentrations presents similar amounts of both surfactants as the ratio in this concentration region is equal to 1. SDBS is adsorbed in higher quantities than the nonionic surfactant in the mixture in the entire concentration range studied which indicates a different behavior of this surfactant. This means that for the SDBS/C₁₂₋₁₄E₇ mixture, SDBS is preferably adsorbed at high solution concentrations. For the SAS system, the composition in the adsorbed layer is the same as in solution whereas in the mixture with SDS the adsorption of the nonionic surfactant is preferred.

3.3 Enthalpy effects during adsorption

Having determined the adsorption isotherms for the studied systems, it is possible to correlate the adsorbed amounts of surface-active agents at the carbon black-water interface with the overall enthalpy of adsorption in order to get more information about the thermodynamics of the adsorption process, especially in the case of surfactant mixtures and the mechanism of the adsorption process in these mixtures.

3.3.1 Enthalpy effects during the adsorption of single surfactants at the carbon black-water interface

Figure 3.10 represents the cumulative enthalpy of displacement of water by the anionic surfactant sodium dodecyl sulfate at the carbon black surface as a function of surface excess (Γ).

Figure 3.10 is similar in shape to the corresponding adsorption isotherm (figure 3.1). At low Γ values, the signals are less exothermic than at higher values. The differential molar enthalpies of adsorption presented in figure 3.11 are plotted as a function of the surface excess values for SDS at the carbon black/water interface.

The enthalpy of displacement of water by SDS at the carbon black surface decreases regularly with increasing surface excess and the difference becomes less pronounced at higher surface coverage. This difference in the enthalpy values studied in two surface coverage regions (low surface coverage values and higher surface coverage values) could be related to different displacement processes where the one at low surface coverage is more exothermic than the other ones. The values of the enthalpy of adsorption range from -84 to -44 kJ/mol when Γ increases from 0.37 to 1.34 $\mu\text{mol}/\text{m}^2$. For the other anionic surfactants (SDBS and SAS) as well as for the nonionic surfactant, the enthalpies of displacement are presented in figure 3.12 in comparison to the data of SDS.

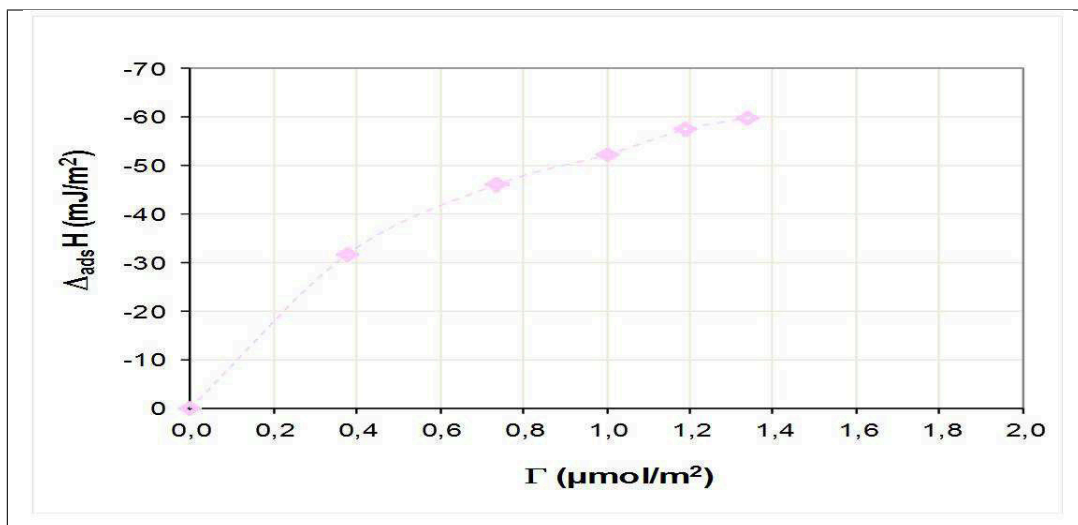


Figure 3.10: Cumulative enthalpy of adsorption on carbon black for SDS

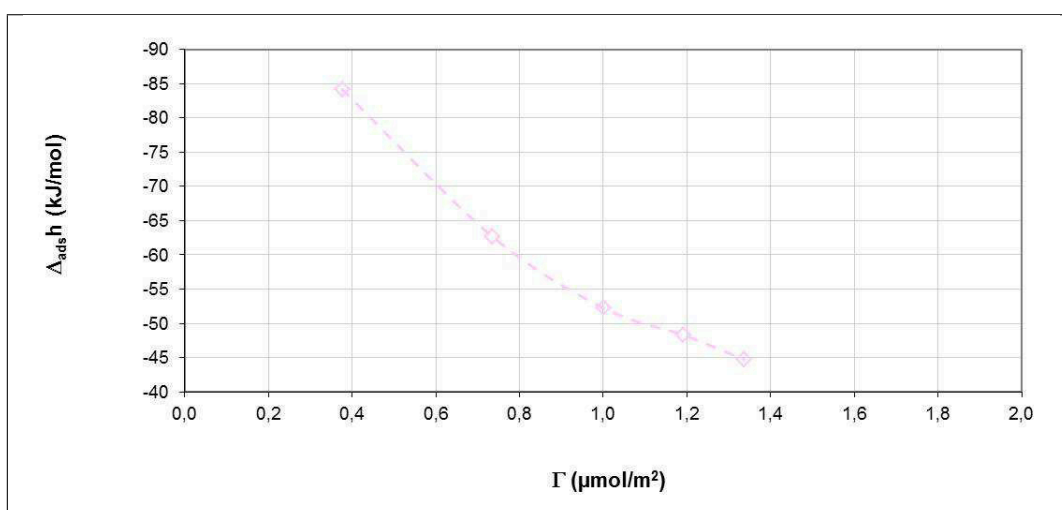


Figure 3.11: Differential molar enthalpy of adsorption on carbon black for SDS

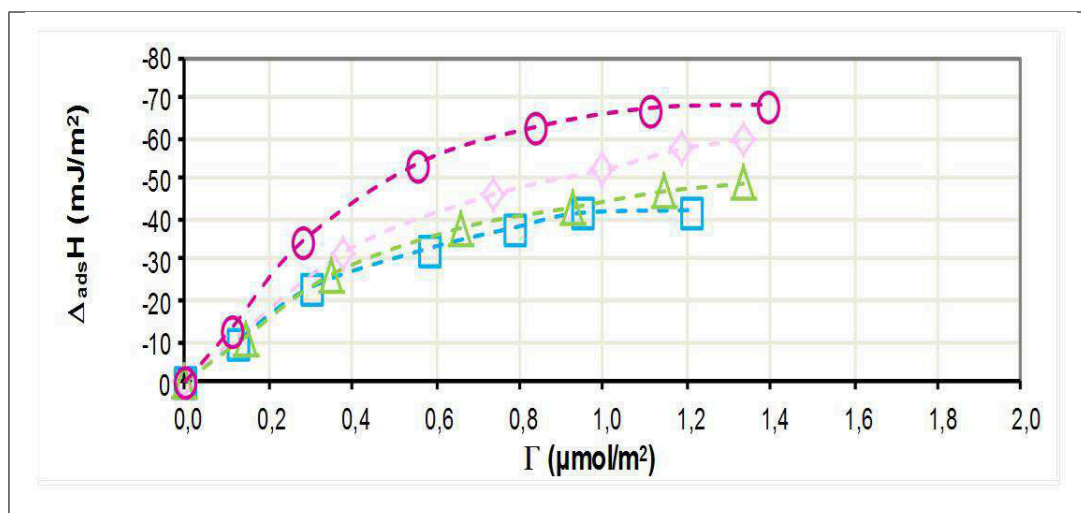


Figure 3.12: Cumulative enthalpies of adsorption on carbon black for SDS, SDBS, SAS and C₁₂₋₁₄E₇

○ C₁₂₋₁₄E₇ ◇ SDS □ SDBS △ SAS

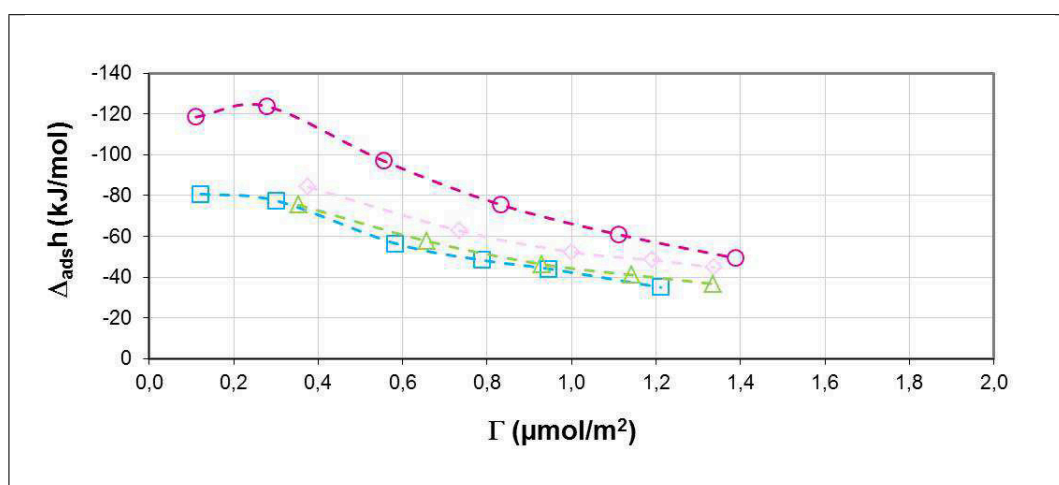


Figure 3.13: Differential molar enthalpies of adsorption on carbon black for SDS, SDBS, SAS and C₁₂₋₁₄E₇

○ C₁₂₋₁₄E₇ ◇ SDS □ SDBS △ SAS

For all anionic surfactants, the curves for the cumulative enthalpy of displacement are similar in shape to the corresponding adsorption isotherms. This is not the case for the nonionic surfactant as both set of curves (figure 3.4

3 Results

and figure 3.12) show differences especially at low surface excess values. The enthalpy of displacement on carbon black for the nonionic surfactant is more exothermic than for the anionic surfactants. SDBS and SAS show comparable enthalpy values on carbon black which are less exothermic than for SDS. The differential enthalpies of displacement for the single surfactants are presented in figure 3.13.

The range of differential molar enthalpies is given as a function of the minimum and the maximum surface excess values for each surfactant in table 3.7.

Table 3.7: Comparison of the differential molar enthalpies of adsorption on carbon black for the single surfactants

Surfactant	$\Gamma_{\min} (\mu\text{mol}/\text{m}^2)$	$\Delta_{\text{ads}}h_{\min} (\text{kJ}/\text{mol})$	$\Gamma_{\max} (\mu\text{mol}/\text{mol})$	$\Delta_{\text{ads}}h_{\max} (\text{kJ}/\text{mol})$
C ₁₂₋₁₄ E ₇	0.11	-118	1.39	-49
SDS	0.37	-84	1.34	-44
SDBS	0.12	-80	1.21	-35
SAS	0.35	-75	1.33	-36

where:

- $\Delta_{\text{ads}}h_{\min}$: molar enthalpy of adsorption at minimum surface coverage
- $\Delta_{\text{ads}}h_{\max}$: molar enthalpy of adsorption at maximum surface coverage
- Γ_{\min} : minimum surface coverage
- Γ_{\max} : maximum surface coverage

Significant differences are observed between the enthalpy values for the single surfactants at low surface excess values. In fact, the nonionic surfactant shows higher values than the anionic surfactants. At higher surface excess values, smaller differences are noted between the nonionic surfactant and the anionic surfactants. SDBS and SAS show very similar enthalpy graphs in the entire surface excess region studied.

3.3.2 Enthalpy effects of adsorption for surfactant mixtures at the carbon black-water interface

For each studied mixture, the enthalpy of adsorption for the mixture will be compared to those for the single compounds.

3.3.2.1 Enthalpy effects of adsorption for SDS/C₁₂₋₁₄E₇ The adsorption enthalpies for SDS, C₁₂₋₁₄E₇ and their 1:1 molar mixture are presented in figure 3.14.

The adsorption enthalpy for the 1:1 mixture is presenting the same progression as the single nonionic surfactant, in fact, both curves are nearly superposed in the entire surface excess region. The same behavior for the mixture is of course observed for the molar enthalpies of adsorption presented in figure 3.15

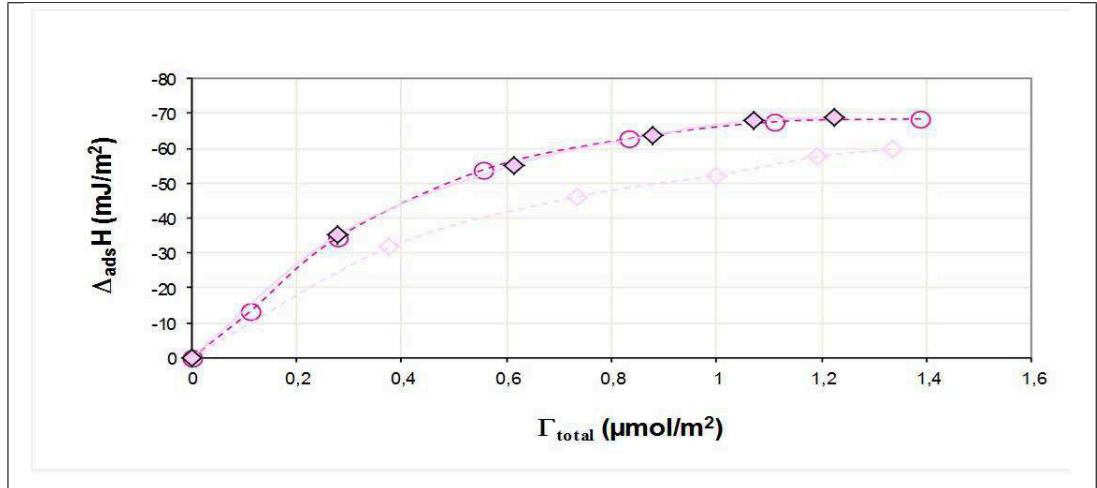


Figure 3.14: Cumulative enthalpies of adsorption of SDS, C₁₂₋₁₄E₇ and their 1:1 mixture as function of the total adsorbed amounts (Γ_{total})

○ C₁₂₋₁₄E₇ ◇ SDS ◇ SDS/C₁₂₋₁₄E₇

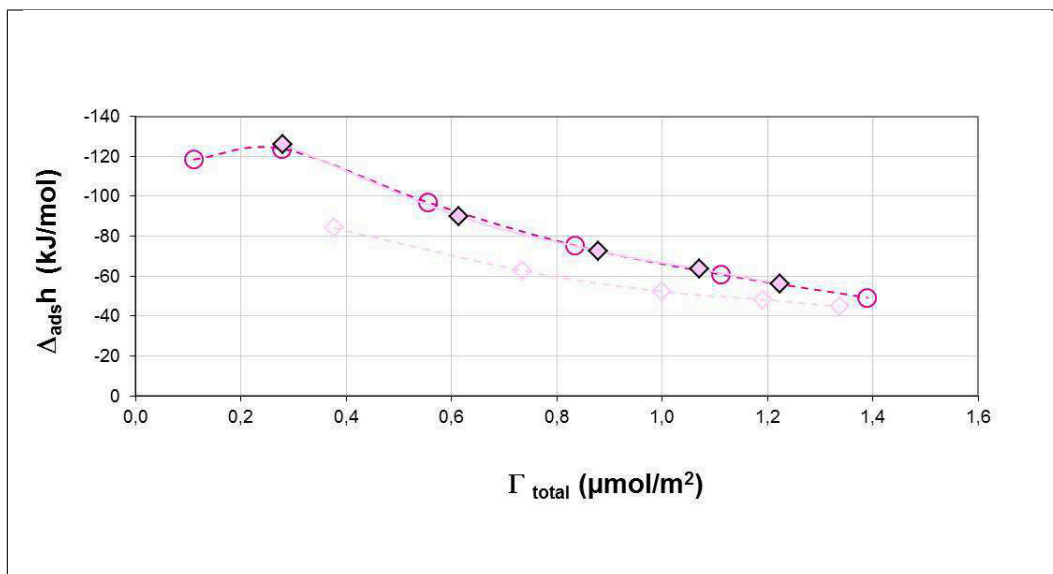


Figure 3.15: Molar enthalpies of adsorption of SDS, C₁₂₋₁₄E₇ and their 1:1 mixture as function of the total adsorbed amounts (Γ_{total})

○ C₁₂₋₁₄E₇
 ◇ SDS
 ◇ SDS/C₁₂₋₁₄E₇

3.3.2.1 Enthalpy effects of adsorption for SDS/C₁₂₋₁₄E₇

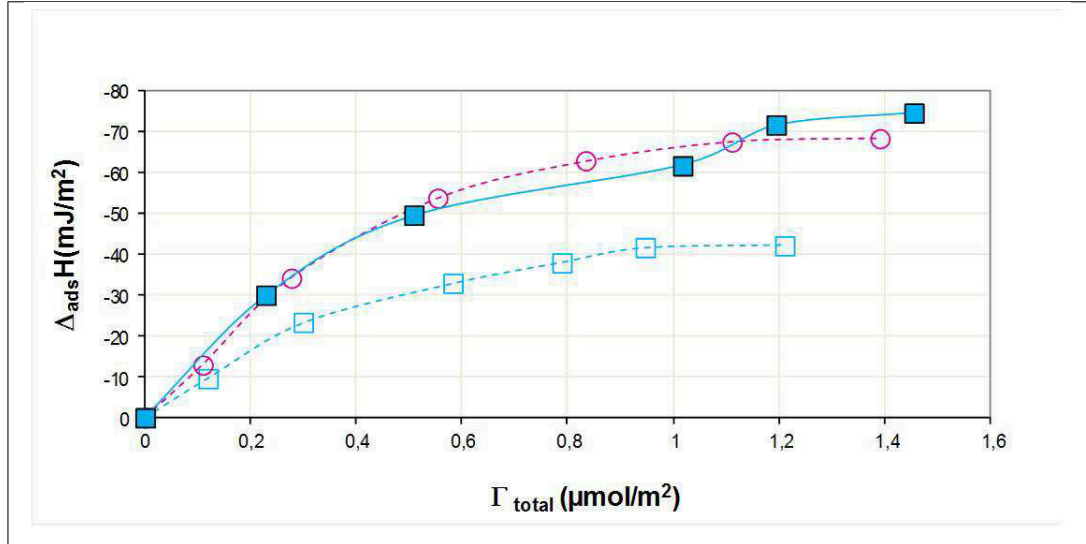


Figure 3.16: Cumulative enthalpies of displacement of SDBS, C₁₂₋₁₄E₇ and their 1:1 mixture as function of the total adsorbed amounts (Γ_{total})

○ C₁₂₋₁₄E₇ □ SDBS ■ SDBS/C₁₂₋₁₄E₇

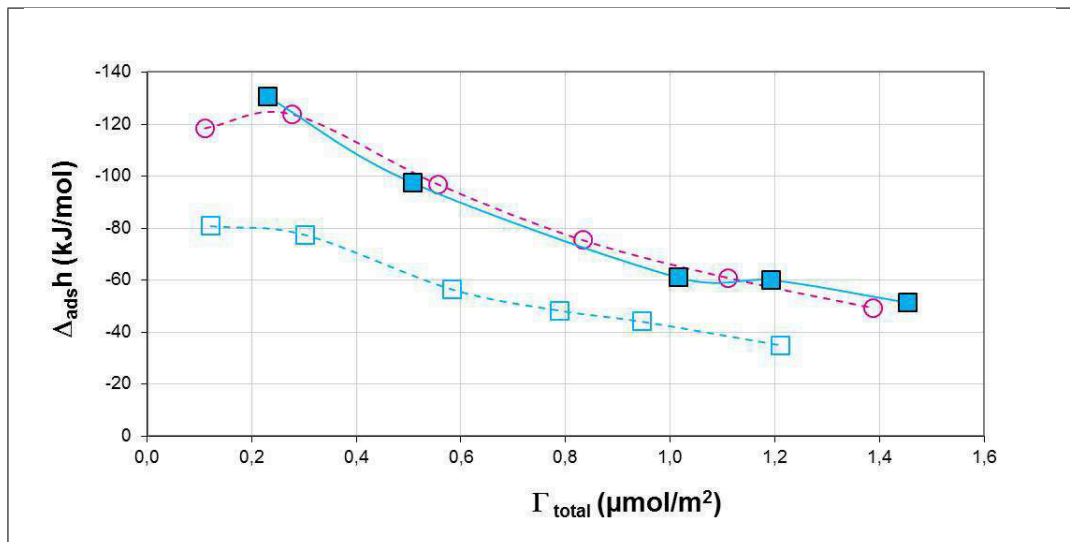


Figure 3.17: Molar enthalpies of adsorption of SDBS, C₁₂₋₁₄E₇ and their 1:1 mixture as function of the total adsorbed amounts (Γ_{total})

○ C₁₂₋₁₄E₇ □ SDBS ■ SDBS/C₁₂₋₁₄E₇

The cumulative enthalpies of adsorption for the anionic surfactant SDBS, the nonionic surfactant $C_{12-14}E_7$ and their 1:1 mixture at the carbon black-water interface are presented in figure 3.16.

The enthalpy of adsorption for the mixture is similar to that for the single nonionic surfactant for low surface excess values. For $\Gamma > 0.50 \mu\text{mol}/\text{m}^2$, $\Delta_{\text{dis}}H$ (displacement enthalpy) for the mixture is lower than that for the single nonionic surfactant and higher than that for SDBS. For $\Gamma > 1.11 \mu\text{mol}/\text{m}^2$, the enthalpy values for the mixture are slightly higher than for the single nonionic surfactant but the differences are not big for both cases. This behavior is better perceived in figure 3.17 which gives the molar enthalpies of adsorption.

3.3.2.3 Enthalpy effects of adsorption for SAS/ $C_{12-14}E_7$ The cumulative as well as the molar enthalpies of adsorption of SAS, $C_{12-14}E_7$ and their mixture are presented respectively in figure 3.18 and 3.19

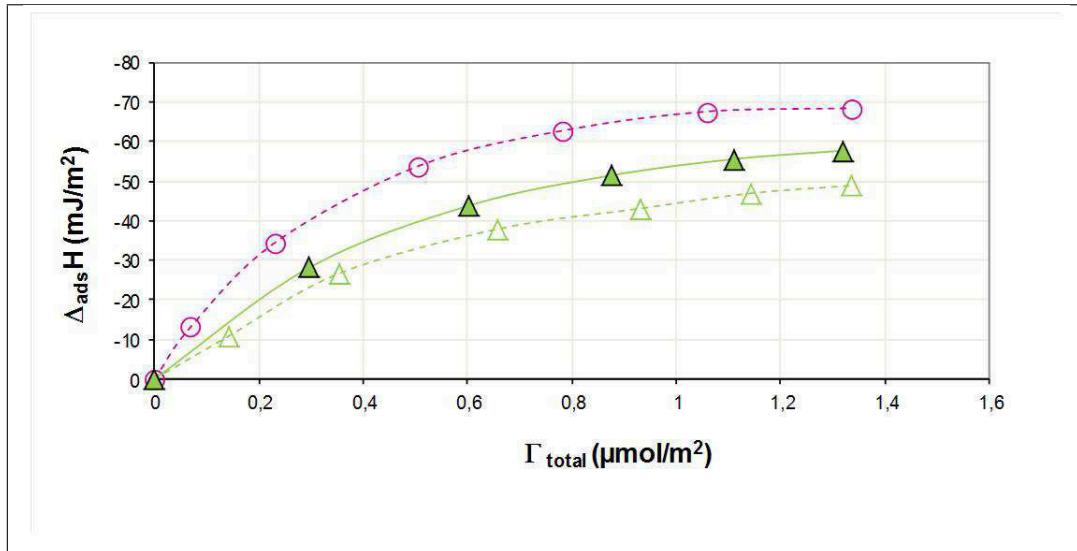


Figure 3.18: Cumulative enthalpies of adsorption of SAS, $C_{12-14}E_7$ and their 1:1 mixture as function of the total adsorbed amounts (Γ_{total})

○ $C_{12-14}E_7$ △ SAS ▲ SAS/ $C_{12-14}E_7$

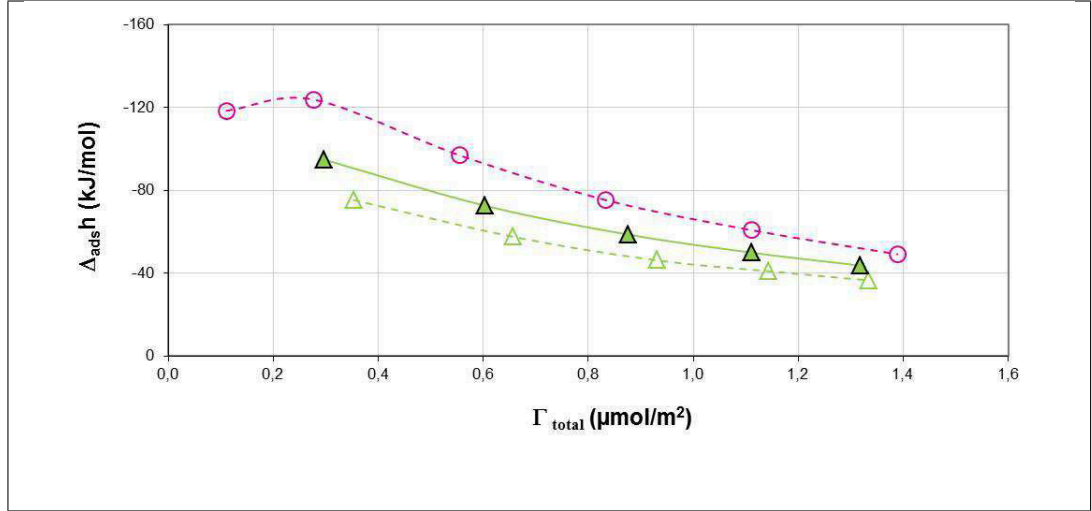


Figure 3.19: Molar enthalpies of adsorption of SAS, C₁₂₋₁₄E₇ and their 1:1 mixture as function of the total adsorbed amounts (Γ_{total})

○ C₁₂₋₁₄E₇ △ SAS ▲ SAS/C₁₂₋₁₄E₇

Table 3.8 gives the range of differential molar enthalpies as a function of the minimum and the maximum surface excess values for each studied surfactant mixture.

Table 3.8: Comparison of the differential molar enthalpies of displacement at the carbon black/water interface for surfactant mixtures

Surfactant mixture	$\Gamma_{\text{min}}^{\text{total}}$ ($\mu\text{mol}/\text{m}^2$)	$\Delta_{\text{dis}} h_{\text{min}}$ (kJ/mol)	$\Gamma_{\text{max}}^{\text{total}}$ ($\mu\text{mol}/\text{m}^2$)	$\Delta_{\text{dis}} h_{\text{max}}$ (kJ/mol)
SDS/C ₁₂₋₁₄ E ₇	0.28	-126	1.22	-56
SDBS/C ₁₂₋₁₄ E ₇	0.23	-130	1.45	-51
SAS/C ₁₂₋₁₄ E ₇	0.29	-95	1.39	-43

3.3.3 Comparison with the results obtained on graphitized carbon black

Király and Findenegg [54] studied the adsorption of SDeS (sodium decyl sulfate) at the graphitized carbon black-water interface. The adsorbed amounts obtained in their study as well as the enthalpies of adsorption at low concentrations are comparable to the results of this study for the adsorption of SDS at the carbon black-water interface as given in table 3.9.

Table 3.9: Comparison between the results of this study and the results of Király et al [54]

Enthalpy values	$\Delta_{\text{ads}}H$ (mJ/m ²)	$\Delta_{\text{ads}}h$ (kJ/mol)	Γ (μmol/m ²)
This study	-59	-44	2.00
Király et al	-62	-35	1.75

This shows that the chemical structures of graphite and the studied carbon black are quite comparable for the adsorption of the studied surfactants.

For a further insight into the structure of the adsorbed layer it seems therefore possible to use flat graphite surfaces. This makes it possible to perform studies with atomic force microscopy which is a method that can not be used for small particles.

3.4 Structure of the adsorbed layer using AFM

AFM was used to further investigate the morphology of the adsorbed layer for the studied systems at the graphite-water interface. In this section, the micrographs for the single anionic surfactants SDS, SDBS and SAS as well as the micrographs for the nonionic surfactant $C_{12-14}E_7$ at the graphite/water interface are presented. All measurements were performed directly in the surfactant solutions at the graphite surface. These micrographs obtained for the single surfactants will be compared in a second section to the following micrographs obtained for the mixtures of the anionic surfactants and the nonionic surfactant:

- SDS/ $C_{12-14}E_7$ adsorption at the graphite-water interface
- SDBS/ $C_{12-14}E_7$ adsorption at the graphite-water interface
- SAS/ $C_{12-14}E_7$ adsorption at the graphite-water interface

All the micrographs presented are height micrographs which means that the contrast observed is given by different positions of the piezo-element. For each studied system, only 1-2 micrographs are presented in this section as an illustration of the structure observed on the graphite surface due to the large data quantity. All micrographs will be presented together with the height profile corresponding to a selected area on the rastered surface in order to calculate the corresponding period of the structures.

3.4.1 Structure of the adsorbed layer for the single surfactants at the graphite-water interface

3.4.1.1 AFM study of SDS adsorption at the graphite-water interface

The atomic force micrograph for a 50 mol/m³ SDS solution at the graphite-water interface is presented in figure 3.20:

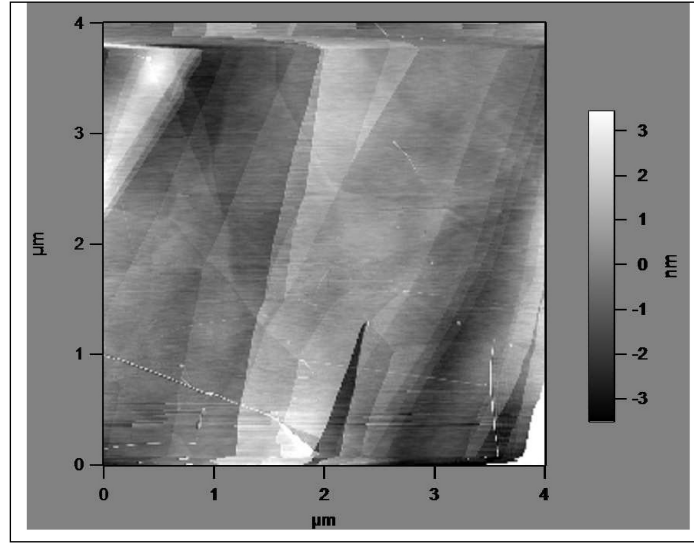


Figure 3.20: 4 μm x 4 μm atomic force micrograph of a 50 mol/m³ SDS solution at the graphite-water interface

This micrograph shows the different layers of the graphite lattice which have been imaged using the so-called soft contact mode [28]. This scan size (4 μm x 4 μm) does not allow the observation of regular structures of surfactants at the surface as these were only observed at smaller scan sizes as described by Manne et al [23]. However, the experiments done in this study show that it is important to start the imaging at higher scan sizes in order to localize bright spots. The bright spots on the graphite surface are usually characteristics of the presence of adsorbed surfactants layers. These were generally observed at the edge of a graphite layer. By zooming in the area where these bright spots appear, the following micrographs have been performed. Force and distance were carefully adjusted during the entire experiment in order to avoid “destroying” the structures observed while the cantilever is rastering the graphite surface.

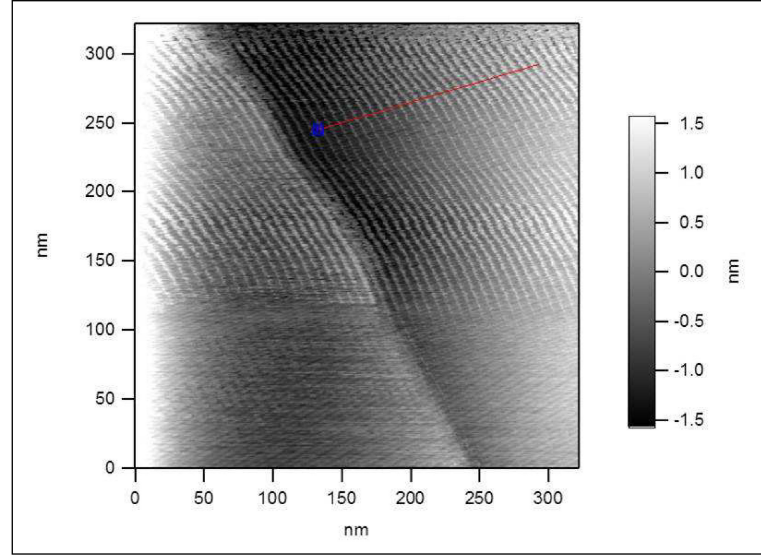


Figure 3.21: 300 x 300 nm atomic force micrograph of a 50 mol/m³ SDS solution at the graphite-water interface

Figure 3.21 shows a higher resolution of the surface with regular parallel structures extending from the top left to the middle of the micrograph.

In the bottom of the micrographs the structures are not observed anymore due to a high force applied on the cantilever. The height profile of the area selected in figure 3.21 (red line) is given in figure 3.22 and enables the estimation of the period between two parallel structures.

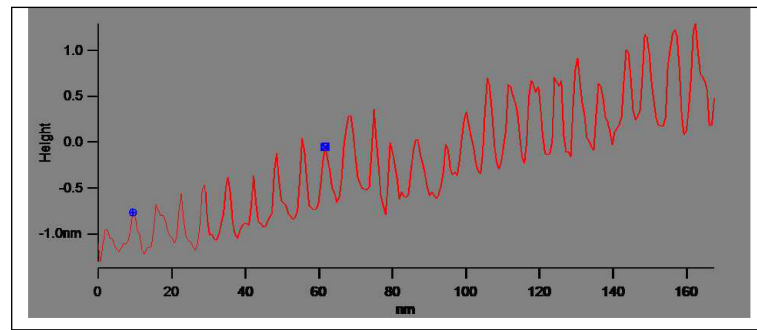


Figure 3.22: Height profile of the selected area in figure 3.21

If the distance between the tip and the surface is not well adjusted, higher forces could result in the destruction of the structures observed. This effect can be seen in figure 3.23 in the regions marked with red arrows. The regular

structures are observed starting from the top left of the micrograph. But with higher forces applied on the cantilever tip, the structures are destroyed. This shows the importance of a constant adjustment of the tip-sample distance during imaging in order to assure a good quality of the micrographs. Moreover, this permanent adjustment of the cantilever position represents the main challenge while imaging soft matter in general and surfactants in particular using AFM.

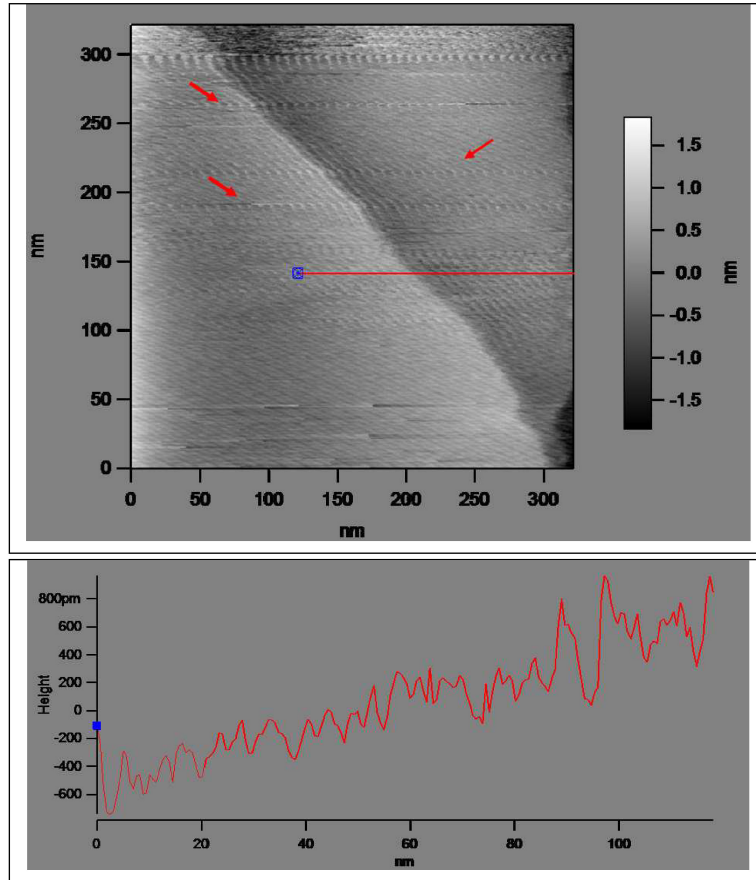


Figure 3.23: Destruction of the structure of the adsorbed SDS layer when using higher imaging forces

As already described above, the morphologies observed in figure 3.21 represent parallel structures with regular periods. The calculation of the period is done using different micrographs for the same sample at the same scan size (mainly at 300 nm) to make sure that the calculated period value is representative for the studied system. The software used enables the measurement of the

height profile in the area of choice. Consequently, the height profile enables the measurement of the period of the observed structures. This is done by calculating the number of the maxima in the height profile. Each maximum represents one stripe. In the height profile presented in figure 3.22, at a distance of 50 nm on the x-axis, 9 maxima can be found. The corresponding period is calculated by dividing this distance (50 nm) through the number of stripes : $50 \text{ nm} / 9 = 5.6 \text{ nm}$. This calculation was done for 3 different 300 nm x 300 nm atomic force micrographs of a 50 mM SDS solution at 1-2 positions in the micrograph. Each experiment was repeated twice which gave an average period of 5.6 nm with a standard deviation of about $\pm 10\%$ as presented in table 3.10:

Table 3.10: Calculation of the period for 50 mol/m³ SDS at the graphite-water interface

Distance (nm)	Number of stripes	Period (nm)
50	9	5.6
50	8	6.3
50	10	5
50	9	5.6
50	9	5.6

The average period calculated for the 50 mol/m³ SDS solution at the graphite surface (5.6 nm) is comparable to the period reported in the literature for SDS at the graphite/water interface by Wanless et al [30] which is 5.3 nm.

3.4.1.2 AFM study of SDBS adsorption at the graphite-water interface

For the anionic surfactant sodium dodecyl benzene sulfonate (SDBS) which presents a phenyl ring in its structure, different experiments were conducted at different SDBS concentrations starting from 50 mol/m³ with higher (100 mol/m³) and lower (0.1 and 10 mol/m³) concentrations. In all experiments conducted, no regular structures were observed which makes it difficult to conclude on the morphology of the adsorbed structure of this surfactant at the graphite/water interface. Some micrographs show the presence of adsorbed surfactant molecules that are displaced by the cantilever tip during imaging

as it is shown in figure 3.24. In the marked region, it is possible to distinguish bright lines between the two graphite layers which could be adsorbed surfactant molecules. This confirms assumptions made by Patrick et al [55] according to which regular structures at the graphite surface should not be possible for surfactants presenting aromatic groups in their structure.

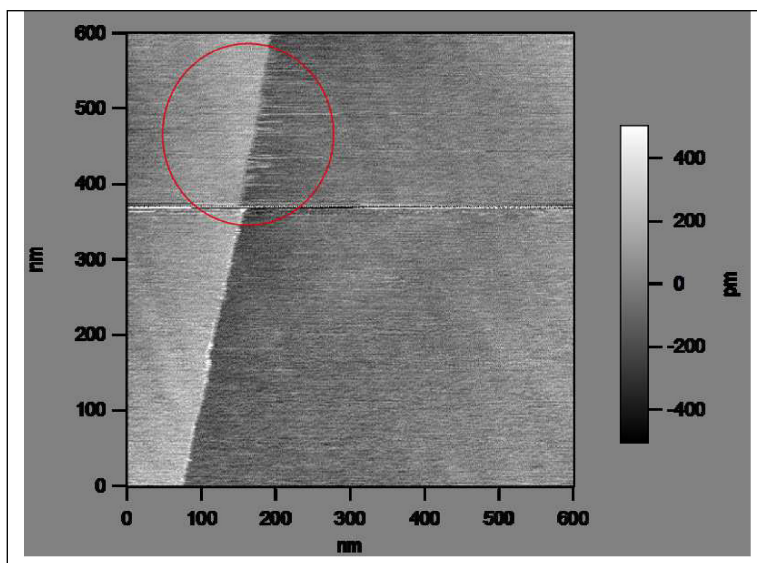


Figure 3.24: 600 x 600 nm atomic force micrograph of a 50 mol/m³ SDBS solution at the graphite-water interface

In the case of SDBS, the structure at the graphite surface can not be predicted from the micrographs as it is the case for SDS for which the hemicylindrical structure at the graphite surface was suggested. The hemicylinders at the graphite surface were correlated to the three-dimensional structure of the surfactant molecules in the aqueous phase [24]. The half of a cylindrical micelle is quite similar in shape to the hemicylindrical structure of the aggregate at the graphite surface. In order to find out if SDBS presents cylindrical micelles in solution, the phase diagram of this surfactant in water gives the necessary information. The phase diagram for SDBS in water has been reported by Sein et al [56] and is given in figure 3.25.

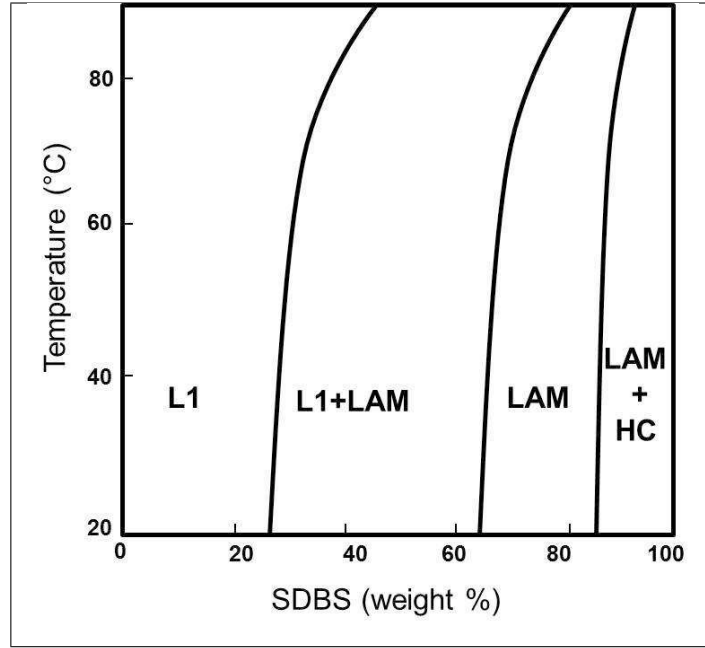


Figure 3.25: SDBS/water phase diagramm [56]

With:

- L_1 = micellar phase
- LAM = lamellar phase
- HC = (hydrated) crystals
- L1+LAM = two-phases domain (L1+ LAM)
- LAM+HC = two-phases domain (LAM+HC)

The phase diagram for SDBS in water presents no hexagonal phase, which means that no cylindrical micelles are formed in solution for this surfactant. This can be an explanation for the absence of a regular structure at the graphite surface and gives indication for the analogy between the surfactant's structure in the aqueous phase and at the graphite surface. This aspect will be further described in the section "discussion".

3.4.1.3 AFM study of SAS adsorption at the graphite-water interface

Figure 3.26 illustrates the atomic force micrographs of a 50 mol/m^3 SAS solution at the graphite-water interface.

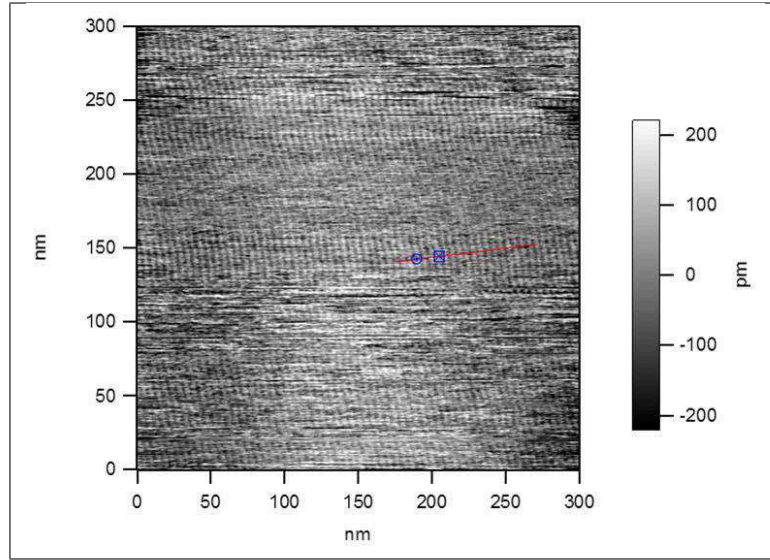


Figure 3.26: 300 x 300 nm atomic force micrograph of a 50 mol/m³ SAS solution at the graphite-water interface

Regular stripes are visible in the entire micrographs with the exemption of small domains located in the center of the micrograph due to higher forces applied on the cantilever tip which do generally result in the structures disappearing. These structures are seen again immediately after adjusting the force applied on the z-piezo. The corresponding structures are similar to the one observed for the 50 mM SDS solution at the graphite surface. In order to determine the period of these structures for SAS, the height profile has been performed and is given in figure 3.27:

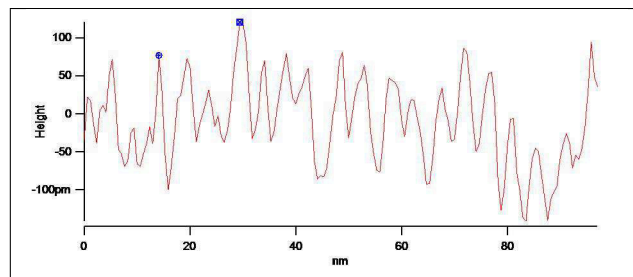


Figure 3.27: Height profile for the 50 mol/m³ SAS solution given in figure 3.26

The estimation of the period of the structures observed at the graphite surface for the 50 mol/m³ SAS solution was done using the same procedure applied

for the determination of the periods observed for the 50 mol/m³ SDS solution. Table 3.11 summarizes the different values obtained:

Table 3.11: Calculation of the period for 50 mol/m³ SAS at the graphite-water interface

Distance (nm)	Number of stripes	Period (nm)
50	11	4.5
50	11	4.5
50	11	4.5
50	11	4.5
50	11	4.5
50	10	5
50	10	5

This gives an average period value of 4.7 nm with a standard deviation of about +/- 6%. The period measured for SAS is smaller than for SDS. This difference could be related to the structural differences between the two alkyl chains of these surfactants. In fact, SDS presents a linear alkyl chain whereas SAS presents a branched alkyl chain. This branching could result in lower periods for the structures observed at the graphite surface. These differences between the measured periods for SDS and SAS will be discussed further in the chapter “discussion”.

3.4.1.4 AFM study of C₁₂₋₁₄E₇ adsorption at the graphite-water interface An example of the micrographs obtained for the nonionic surfactant C₁₂₋₁₄E₇ adsorption at the graphite surface is given in figure 3.28:

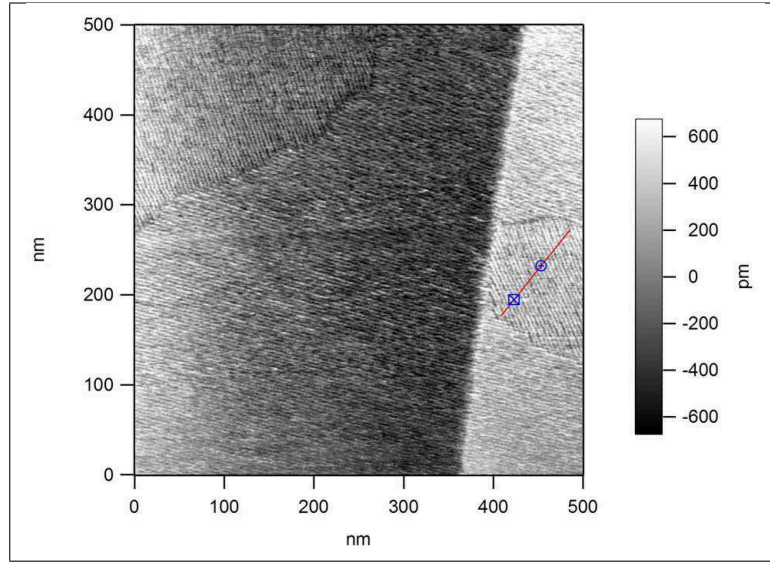


Figure 3.28: 500 x 500 nm atomic force micrographs of a 50 mol/m³ C₁₂₋₁₄E₇ at the graphite-water interface

Different domains are observed in figure 3.28 due to the presence of 3 graphite layers with different orientations. In the top left of the micrograph, a frontier is observed between two domains after which the periodic structures present another orientation angle towards the graphite surface. In the third domain in the bottom right of the micrograph, yet another orientation is observed. This shows the dependence of the periodic structures orientation on the graphite layer from the orientation angle of the graphite surface. The height profile measured for this domain is given in figure 3.29.

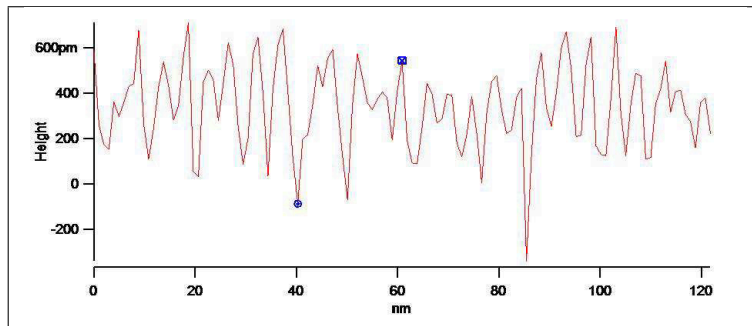


Figure 3.29: Height profile for the third domain in figure 3.28

The same experiment was repeated different times for a better estimation of

the period. A second example of the obtained micrograph with a smaller scan size is given in figure 3.30:

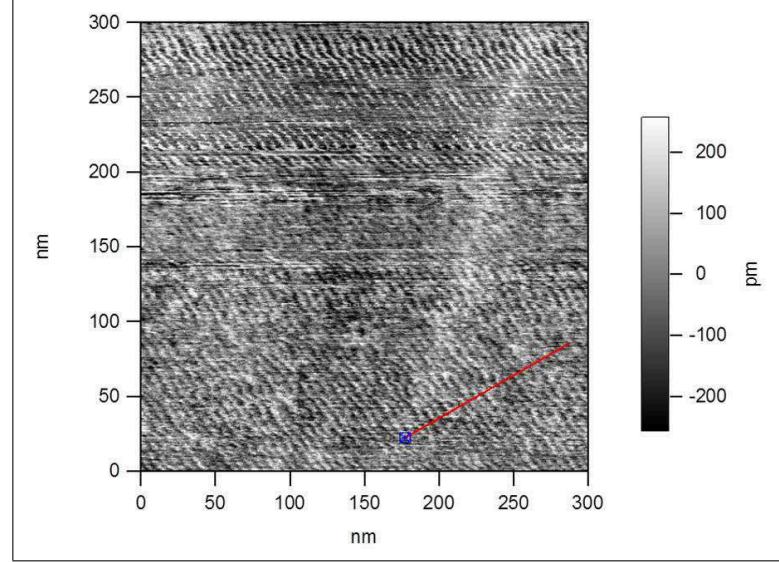


Figure 3.30: 300 x 300 nm atomic force micrographs of a 50 mol/m³ C₁₂₋₁₄E₇ at the graphite-water interface

The height profile in the indicated area was determined and is given in figure 3.31.

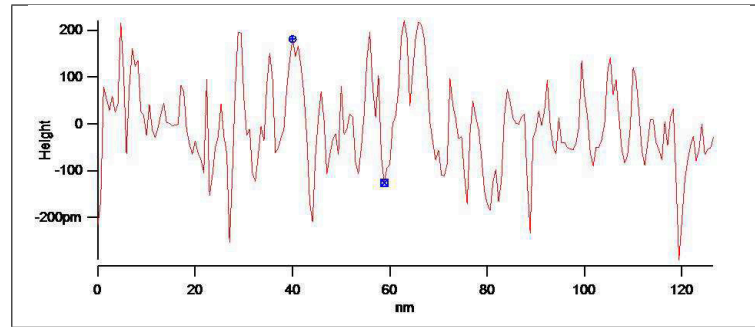


Figure 3.31: Height profile for the indicated area in figure 3.30

From the different micrographs obtained for the 50 mol/m³ C₁₂₋₁₄E₇ solution at the graphite/water interface, an estimation of the period of the observed structures was done following the same procedure used to determine the period of the structures observed for the anionic surfactants SDS and SAS at the graphite-water interface. The results are given in table 3.12.

3 Results

Table 3.12: Calculation of the period for 50 mol/m³ C₁₂₋₁₄E₇ at the graphite-water interface

Distance (nm)	Number of stripes	Period (nm)
50	9	5.6
50	9	5.6
100	20	5
100	20	5
40	8	5

The average period is equal to 5.2 nm with a standard deviation of about +/- 7%. This period is similar to that registered for SDS in the calculated standard deviation range. Other studies [31] reported higher spacing between the periodic parallel stripes for C₁₂E₃ and C₁₂E₅ on graphite but similar periods were registered for C₁₂E₈ as indicated in table 3.13:

Table 3.13: Comparison between the values of the periods measured using AFM for different C₁₂E_n at the graphite surface

Author	Surfactant used	Period measured (nm)
Patrick et al [31]	C ₁₂ E ₃	5.7
Patrick et al [31]	C ₁₂ E ₅	5.6
Jabnoun	C ₁₂ E ₇	5.2
Patrick et al [31]	C ₁₆ E ₈	5.3

3.4.2 Structure of the adsorbed layer for surfactant mixtures at the graphite-water interface

3.4.2.1 SDS/C₁₂₋₁₄E₇ mixture Figure 3.32 illustrates the structure observed for the SDS/C₁₂₋₁₄E₇ mixture at the graphite surface.

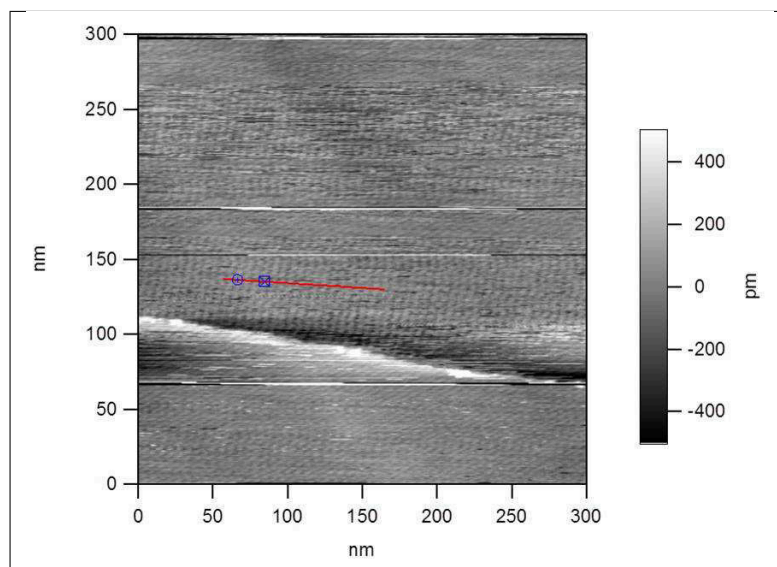


Figure 3.32: 300 x 300 nm micrograph of a 50 mol/m³ SDS/C₁₂₋₁₄E₇ 1:1 mixture at the graphite-water interface

The height profile of the area indicated in figure 3.32 is given below:

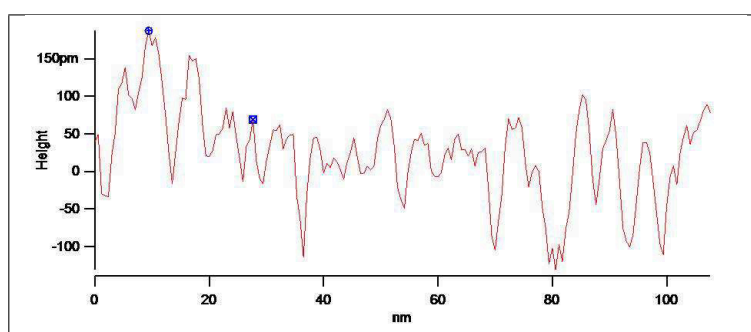


Figure 3.33: Height profile for the indicated area in figure 3.32

The period for the mixture is measured at different positions of the performed micrographs following the same procedure as for the single compounds. The results are given in table 3.14.

Table 3.14: Calculation of the period for 50 mol/m³ SDS/C₁₂₋₁₄E₇ mixture at the graphite-water interface

Distance (nm)	Number of stripes	Period (nm)
50	9	5.6
50	9	5.6
50	9	5.6
50	9	5.6
50	9	5.6

The period was the same in all parts of the micrographs where the structures were observed and the periods measured. The period for the mixture is equal to the period registered for the single compounds when considering the standard deviations registered for both SDS and C₁₂₋₁₄E₇.

3.4.2.2 SDBS/C₁₂₋₁₄E₇ mixture The morphology of the single anionic surfactant SDBS presented no regular parallel structures, but a featureless adsorbed layer. In contrast, the nonionic surfactant C₁₂₋₁₄E₇ did present regular periodic structures. Different mixing ratios have been studied for the SDBS/C₁₂₋₁₄E₇ mixture where the concentration of the anionic surfactant SDBS was progressively increased as follows.

- SDBS/C₁₂₋₁₄E₇ 1/9 mixture
- SDBS/C₁₂₋₁₄E₇ 2:8 mixture
- SDBS/C₁₂₋₁₄E₇ 1:1 mixture

The results of this mixing are presented in figures 3.34, 3.35 and 3.36:

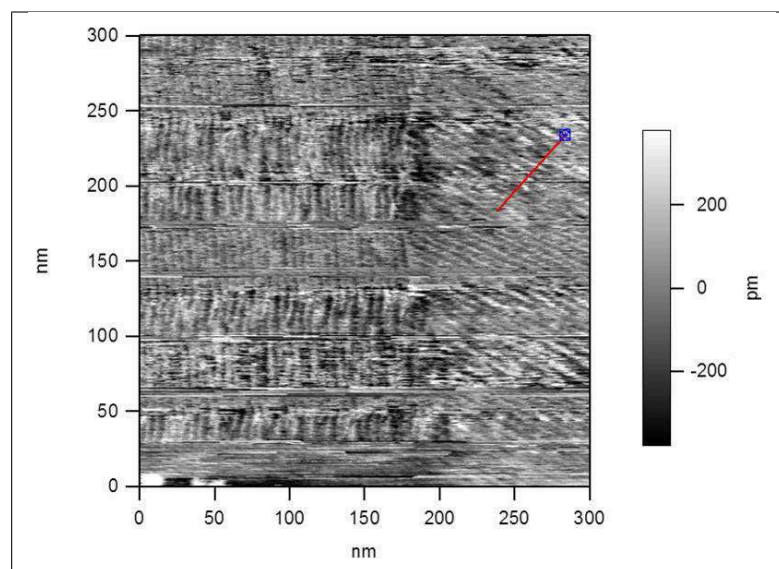


Figure 3.34: 300 x 300 nm micrograph of a 50 mol/m³ SDBS/C₁₂₋₁₄E₇ 1: 9 mixture at the graphite-water interface

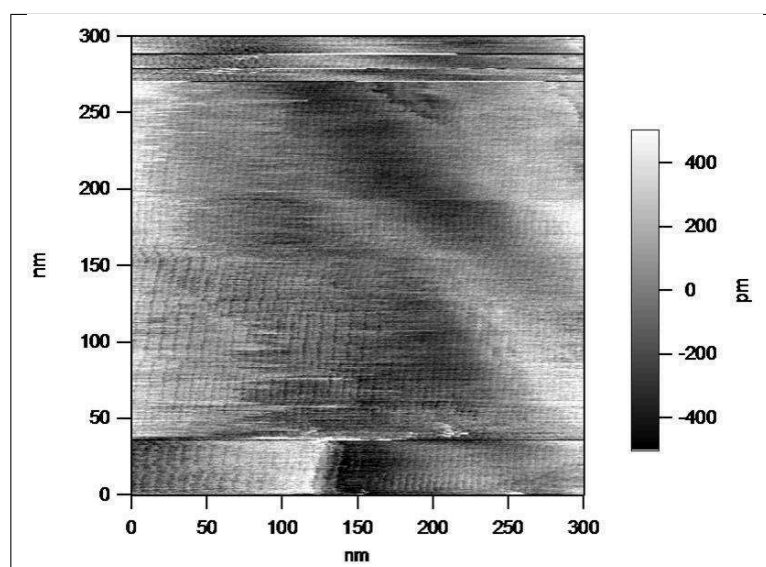


Figure 3.35: 300 x 300 nm micrograph of a 50 mol/m³ SDBS/C₁₂₋₁₄E₇ 2:8 mixture at the graphite-water interface

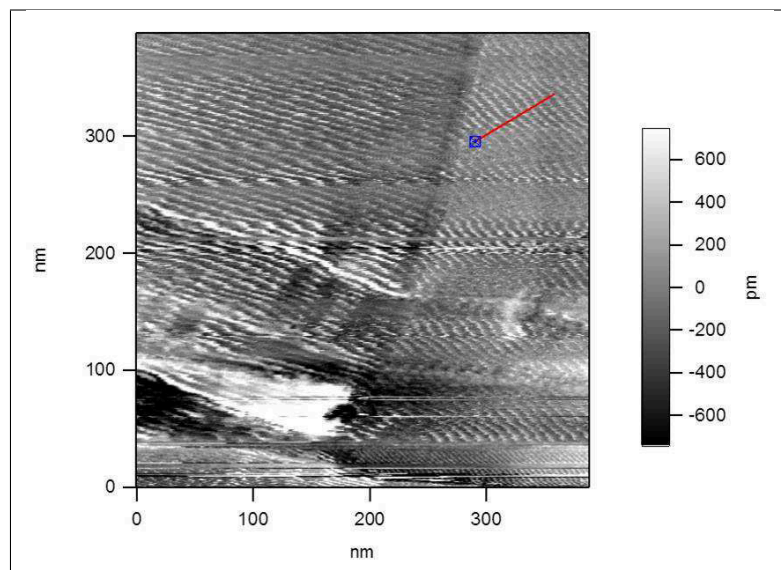


Figure 3.36: 400 x 400 nm micrograph of a 50 mol/m³ SDBS/C₁₂₋₁₄E₇ 1:1 mixture at the graphite-water interface

The different micrographs obtained for the SDBS/C₁₂₋₁₄E₇ mixtures presented differences related to the mixing ratios of both compounds. In figure 3.34, the anionic surfactant SDBS is represented in the mixture with only 10%. At this mixing ratio, the structures observed for the single nonionic surfactant were still observed for its mixture with SDBS. By increasing the concentration of SDBS in the mixture, the regular structures were still observed but imaging was made more difficult. In fact, the structure observed in figure 3.36 for the highest SDBS concentration in the mixture is different from the periodic and parallel stripes observed so far for the single nonionic surfactant in that way that these structures seem to be flattened by the cantilever tip. This effect can be observed in the top left of figure 3.36 and is due to the fact that the force applied on the cantilever tip was constantly adjusted due to the higher repulsion observed for this mixture between the cantilever tip and the structures formed at the graphite surface.

This can be further observed in the values of the periods determined for the different mixtures in table 3.15.

Table 3.15: Calculation of the periods for 50 mol/m³ SDBS/C₁₂₋₁₄E₇ mixtures at the graphite-water interface

SDBS/C ₁₂₋₁₄ E ₇ mixing ratio	Distance (nm)	Number of stripes	Period (nm)	Standard deviation (%)
1:9	50	9	5.6	0
2:8	50	10	4.8	3
1:1	100	16	5.3	17

The value of the period obtained for the lower concentration of SDBS in the mixture is similar to the one registered for the single nonionic surfactant. But with higher SDBS concentration in the mixture, the periods present a broader range. The standard deviation increases with increasing SDBS concentration in the mixture. The results obtained for the mixture support the assumptions made for the single anionic surfactant SDBS. The structure of this surfactant and especially the presence of an aromatic group does not enable imaging using AFM for the single anionic surfactant. The presence of the nonionic surfactant in the mixture allows images up to an SDBS/C₁₂₋₁₄E₇ ratio of 1:1. This means that when SDBS is present in the mixture until a 1:1 ratio, cylindrical structures are still observed at the graphite-water interface.

3.4.2.3 SAS/C₁₂₋₁₄E₇ 1:1 mixture The results of the AFM study for the 1:1 mixture of SAS and the nonionic surfactant are presented in figure 3.37:

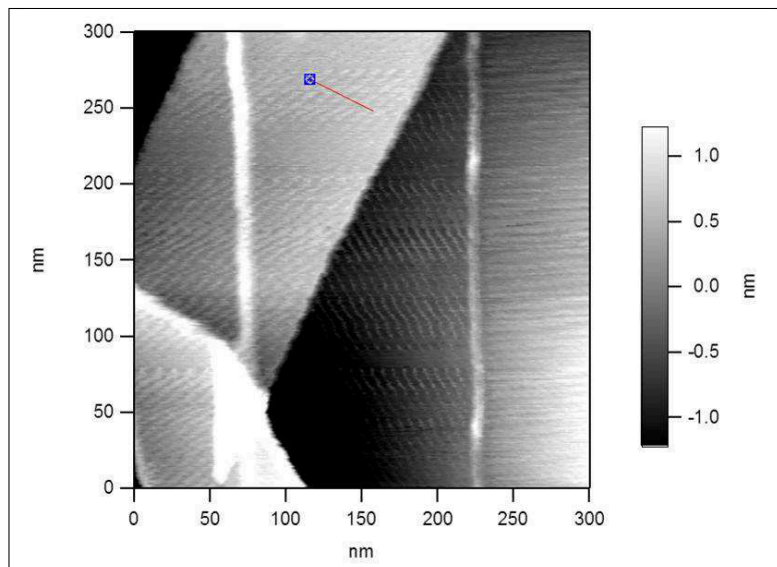


Figure 3.37: 300 x 300 nm micrograph of a 50 mol/m³ SAS/C₁₂₋₁₄E₇ 1:1 mixture at the graphite-water interface

This micrograph shows regular structures with different orientations towards the graphite surface. In the center of the micrograph, the observed structures presented different orientation angles; similar structures were observed for both single compounds SAS and C₁₂₋₁₄E₇. The height profile of the area mentioned in figure 3.37 is given below:

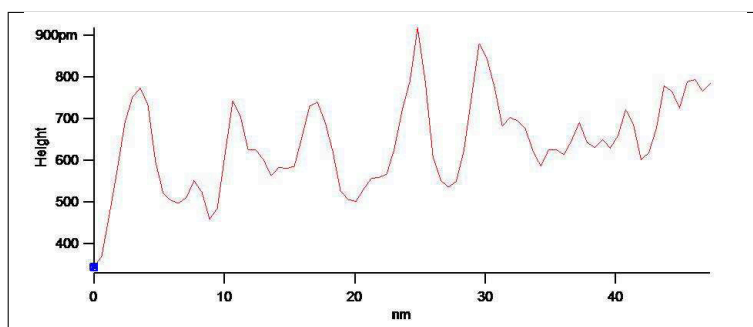


Figure 3.38: Height profile for the indicated area in figure 3.37

This height profile as well as the measurement done using different micrographs of the same SAS/C₁₂₋₁₄E₇ mixture gave a period value of 5.4 nm (+/-5). The

structure observed for the mixture contradicts assumptions made by Patrick et al [31] according to which these periodic structures can not be observed for surfactants presenting branching in the alkyl chain.

3.4.2.4 Summary of the results of the adsorbed layer Table 3.16 presents the period values registered for all the studied systems.

Table 3.16: Periods of the structures observed for the studied systems

Surfactant	Period (nm)	Deviation (%)
SDS	5.6	10
SAS	4.7	6
SDBS	no periodic structure	-
C ₁₂₋₁₄ E ₇	5.2	7
SDS/C ₁₂₋₁₄ E ₇ 1:1	5.6	0
SAS/C ₁₂₋₁₄ E ₇ 1:1	5.3	5
SDBS/C ₁₂₋₁₄ E ₇ 1:1	5.3	17
SDBS/C ₁₂₋₁₄ E ₇ 2:8	4.8	3
SDBS/C ₁₂₋₁₄ E ₇ 1:9	5.6	0

For the SDS/C₁₂₋₁₄E₇ mixture, the period measured is comparable to both single compounds. For the SAS/C₁₂₋₁₄E₇ mixture, the value is similar to that of the nonionic surfactant. Obviously, the longer period of the nonionic surfactant dominates in the mixture due to a high concentration of the nonionic surfactant in the mixture.

For SDBS and a high nonionic surfactant content in the 1:1 mixture, the period is also determining the dimension of the structure. At a higher content of SDBS, the period decreases and the structure becomes not that homogeneous. This may be caused by the increasing influence of the adsorbed SDBS molecules at the graphite surface which interfere with the regular built-up of cylindrical structures.

4 Discussion

4.1 Adsorption behavior of single surfactants and mixtures

The adsorbed amounts of the surfactant mixtures at the carbon black/water interface show differences compared to the adsorbed amounts of the single surface-active agents. This indicates a complex adsorption behavior in the mixture compared to the single compounds as mentioned in the beginning of this work.

Zettlemoyer et al [46] interpreted the shape of the adsorption isotherm of SDS on graphon, which did present an inflection point, as having two regions where in the first region (at low surfactant concentration) the alkyl chains of SDS adsorb parallel to the surface to maximize favorable hydrophobic interactions between the alkyl chains and the hydrophobic surface. In the second region characterized by higher surfactant concentrations, the alkyl chains are then oriented vertically towards the surface and at saturation, a vertically oriented monolayer is then formed.

The driving free energy of adsorption above the point of inflection is attributed to associative chain-chain as well as chain-solid hydrophobic interactions.

The absence of the inflection point in the adsorption isotherm (in the case of SDS adsorption on Spheron 6) studied by Day et al [47] has been related to the heterogeneous surface of the used carbon black Spheron 6 which would hinder the formation of a uniform layer oriented horizontally towards the surface.

In a review of 1983, Hough and Rendall [57] discussed the thorough analysis of adsorption isotherms of surfactants based on reviews and original publications in the matter, among them the already mentioned studies of Zettlemoyer et al [46] as well as Day et al [47]. One striking aspect treated was the thorough interpretation of the shape of the adsorption isotherms.

In fact, the presence of an inflection point in the CMC region supposes two domains above and below the inflection point with a different geometry or orientation of the adsorbed species of mainly anionic surfactants on the surface of the adsorbent (carbon black).

Somasundaran et al [58, 59, 60, 61, 62, 63, 64] by studying the adsorption

of alkyl and alkylbenzene sulfonates at the mineral oxide/water interface further confirmed the model first introduced by Gaudin and Fuerstenau in 1955 [65] and further developed by Fuerstenau and Somasundaran. This model presented the concept of hemi-micelle concentration which is defined as the concentration at which two-dimensional self-assembly aggregates form at interfaces. Basically 50 years later, this model is still commonly used and will be also discussed in the current study. The above-mentioned studies brought important insights into the interpretation of adsorption isotherms in order to predict the adsorption behavior of surface-active agents at interfaces but few have been dedicated to the study of the behavior of surface-active agents with different chemical structures in mixtures especially at hydrophobic surfaces which is the main goal of this work.

4.1.1 Adsorbed amounts of single surface-active agents

4.1.1.1 Adsorption isotherms for the anionic surfactants The adsorption isotherms for the anionic surfactants sodium dodecyl sulfate (SDS), sodium dodecyl benzene sulfonate (SDBS) and the secondary alkane sulfonate (SAS) presented a strong increase at low concentrations and plateau values at concentrations above the CMC of the corresponding surfactants in solution (refer to figure 3.4). The strong increase towards plateau values in the first part of the adsorption isotherms can be explained by the strong adsorption of the surfactant monomers in solution at the carbon black-water interface. With higher surfactant concentration in solution, micelles begin to form. Saturation in solution is reached and a monolayer or multilayer is formed at the solid-liquid interface. SDBS and SAS present adsorption isotherms with a similar shape, the increase towards plateau values takes place at comparable equilibrium concentration values with slightly higher (Γ) values for SAS. The increase towards the plateau region takes place at comparable equilibrium concentrations for both surfactants ($c_{eq} = 5.8 \text{ mol/m}^3$). This behavior can be related in a first approximation to the similar CMC values of both surfactants. SDS presents due to the higher CMC a higher monomer concentration than SDBS and SAS which explains the higher adsorption (Γ values) registered for this surfactant at concentrations underneath the CMC (especially for $c_{eq} > 4 \text{ mol/m}^3$). SDS presents as well higher plateau values than the one starting to form for SDBS

and SAS. Aggregates tend to form at the carbon black-water interface at higher concentration following the same dependence of plateau values on the CMC value of the corresponding surfactant. The structural differences between the linear SDS and the branched SDBS and SAS can also explain the differences observed between the adsorption isotherms of these surfactants. In fact, the values calculated for the limiting area per molecule for SDBS (0.93 nm^2) and SAS (1.03 nm^2) are comparatively higher than the value reported for SDS (0.83 nm^2), this means that the molecules adsorbed at saturation for SDBS and SAS at the carbon black/water interface occupy a larger area than the one formed for the linear SDS. Another structural difference between the studied anionic surfactants is the structure of the head group. In fact, both SAS and SDBS have a sulfonate group, SDS on the other hand has a sulfate group in its structure. This could result in a different electrostatic repulsion between the head groups of SDS compared to SDBS and SAS.

4.1.1.2 Adsorption isotherm for the nonionic surfactant Contrarily to anionic and cationic surfactants, nonionic surfactants have no or little effect on surface charge [45]. Therefore, their mode of adsorption cannot be related to changes in the surface charge. Instead, the effect is strongly influenced by the hydrophobic interactions between the nonionic surfactant and the surface as well as between the adsorbed surfactant molecules. Compared to anionic surfactants, the adsorption of nonionic surfactants is quite steep at hydrophobic, weakly polar interfaces. This is illustrated in Figure 4.1 which is derived from figure 3.2 for the adsorption of $\text{C}_{12-14}\text{E}_7$ and SDS at the carbon black surface.

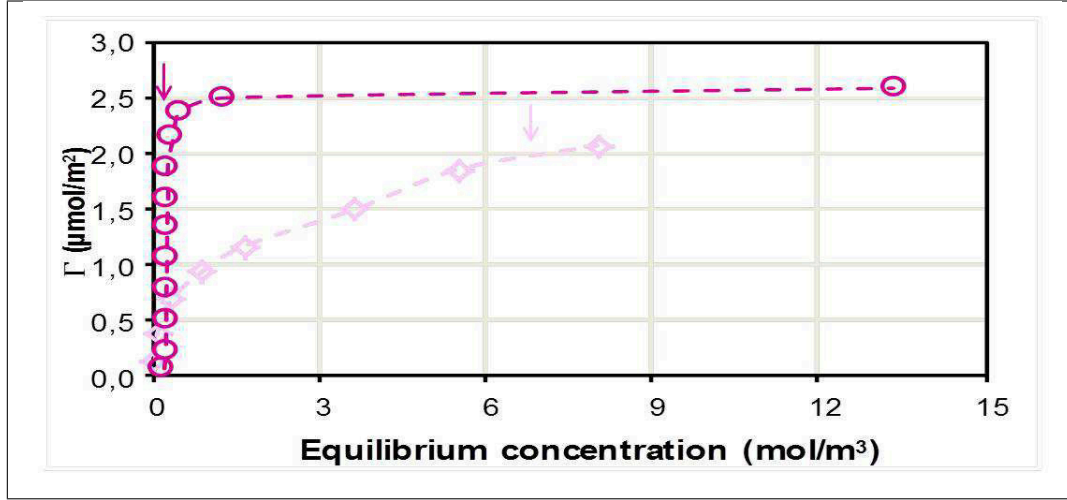


Figure 4.1: Adsorption isotherm at $T = 25^\circ\text{C}$ and $\text{pH} = 10$ for $\text{C}_{12-14}\text{E}_7$

○ $\text{C}_{12-14}\text{E}_7$ ◇ SDS

The adsorption isotherm for the nonionic surfactant at the carbon black/water interface presents a different shape than the one observed for the anionic surfactant SDS which was related to the lower CMC value for this surfactant compared to SDS. A comparison between the adsorption behavior of the nonionic surfactant $\text{C}_{12-14}\text{E}_7$ and the anionic surfactant SDS is important for an estimation of the effect of the head group of the surfactant on the adsorption isotherm. In fact, both surfactants show similar structures for the non polar part of the molecule (a linear alkyl chain of mainly twelve carbon atoms) with a single difference which is the structure of the head group. Investigations done by Ma and Xia [66] as well as Bossetti [67] suggest that at low concentrations, the nonionic surfactant presents a molecular structure on the carbon black surface with the alkyl chain lying parallel to the surface and the ethylene oxide groups coiling at the solid/liquid interface. The results already reported at saturation for the value of the area per molecule (see table 3.2) of the nonionic surfactant (0.66 nm^2) are comparatively smaller than that for the anionic surfactant SDS (0.83 nm^2). Both results (at low and high concentrations) show the effect of the chemical structure and the charge of the head group on the adsorption behavior of the surfactant. The higher surface activity of the nonionic surfactant due to its lower CMC value and the absence of electrostatic repulsion due to the uncharged head group for this surfactant explain the lower

values of the area occupied by each molecule of this surfactant at the carbon black/water interface.

4.1.1.3 Correlation between the adsorption isotherms obtained experimentally and theoretical models The adsorption isotherms obtained experimentally for the studied systems are compared with models presented in the literature to further investigate the possible adsorption mechanism at the carbon black-water interface. The well-known Langmuir isotherm [68, 69] is a commonly used model also for the adsorption at the solid-liquid interface and was already introduced in the first chapter of this thesis. In the following chapter, we present the comparison between the adsorption isotherms obtained experimentally and the adsorption isotherms calculated using the Langmuir model. In this chapter, C_{ads} rather than Γ is used ($C_{ads} = \Gamma$).

$$c_{ads} = \frac{\Gamma_{max} K c_{sol}}{(1 + K c_{sol})} \quad (4.1)$$

With:

- c_{ads} : concentration of the adsorbed surfactant at the surface (mol/m²)
- c_{sol} : concentration of the adsorbed surfactant in the bulk solution (mol/m³)
- Γ_{max} : maximum adsorbed amount per unit area (mol/m²)
- K : Langmuir constant (m³/mol)

4.1.1.4 Langmuir model for anionic surfactant adsorption at the carbon black-water interface In figure 4.2, 4.3 and 4.4, the experimental results obtained for each anionic surfactant are presented in each graph together with the fit using the Langmuir model.

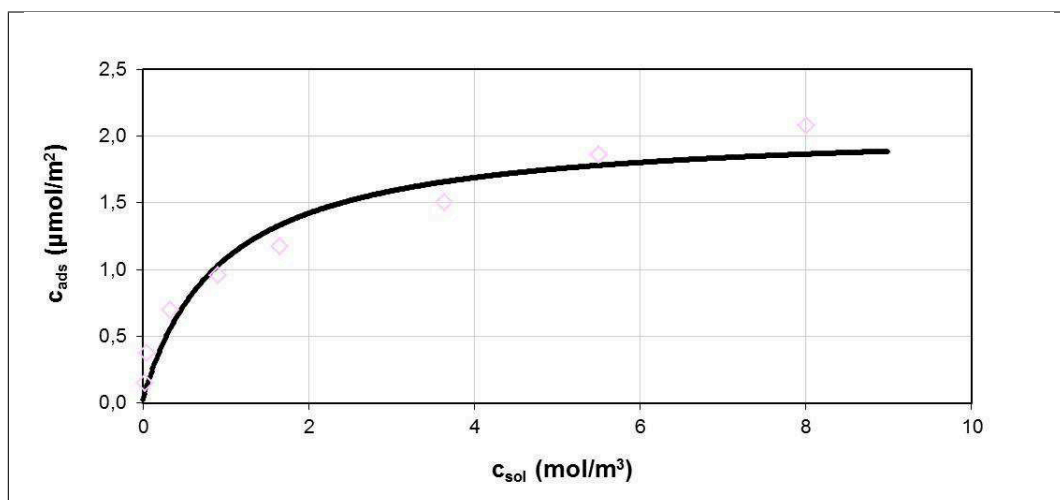


Figure 4.2: Experimental results and adsorption isotherms obtained using the Langmuir model for SDS (experimental data from figure 3.2)

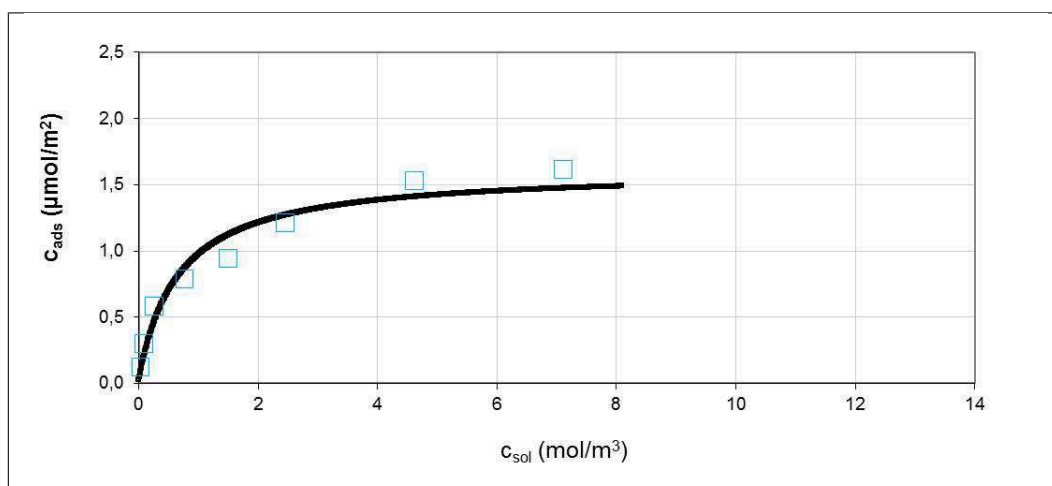


Figure 4.3: Experimental results and adsorption isotherms obtained using the Langmuir model for SDBS (experimental data from figure 3.2)

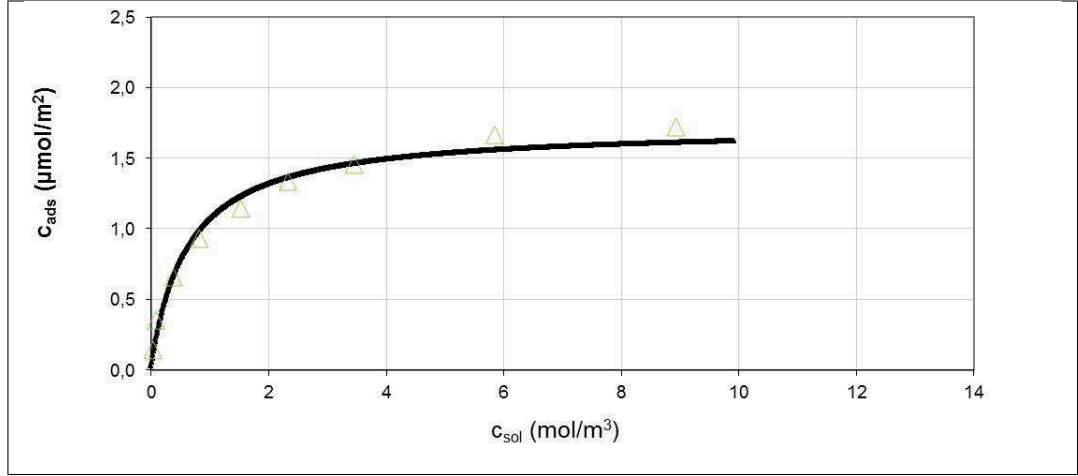


Figure 4.4: Experimental results and adsorption isotherms obtained using the Langmuir model for SAS (experimental data from figure 3.2)

All isotherms for the anionic surfactants present a quite good agreement between the experimental results and the Langmuir model. The values of K for each surfactant extrapolated from the Langmuir fits are given in table 4.1.

Table 4.1: Values of K using the Langmuir model

Surfactant	K (m^3/mol)
SDS	1.07
SDBS	1.52
SAS	1.84

SDS presents a quasi-Langmuir adsorption behavior ($K \approx 1$). This would mean that the adsorption of SDS at the carbon black-water interface seems to be Langmuir-like. However, when having a closer look to the adsorption isotherm of SDS at the carbon black/water interface, it is possible to distinguish deviations between the experimental results and the graph given by the Langmuir model. The values obtained for the Langmuir model are lower than the experimental values at low concentration ($< 0.5 \text{ mol/m}^3$). In the concentration range from 1 to 5 mol/m^3 , the values obtained for the Langmuir model are higher than the experimental values and at concentrations higher than 5 mol/m^3 , this trend is again inverted. These differences observed between the Langmuir values and the experimental values might be an explanation for the average value

obtained for K which does apparently describe a Langmuir-like behavior for SDS but does not directly correlate with the differences observed between the experimental results and the Langmuir model. The same case was observed for SAS and SDBS where both K values were higher than 1. The adsorption process for both surfactants is not fully described by the Langmuir equation. The higher K values for SAS and SDBS compared to SDS show that the interactions of these molecules with the carbon black surface are stronger than SDS, which is supported by the results for the surfactant mixtures (see below).

4.1.1.5 Langmuir model for the nonionic surfactant adsorption at the carbon black-water interface A similar calculation has been done for the nonionic surfactant as presented in figure 4.5.

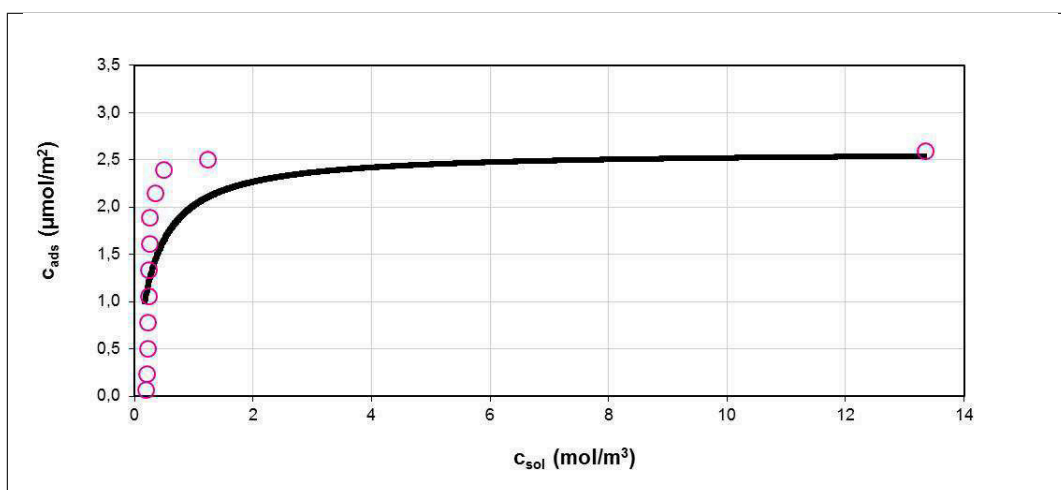


Figure 4.5: Experimental results and adsorption isotherms obtained using the Langmuir model for $C_{12-14}E_7$ (experimental data from figure 3.2)

The nonionic surfactant presents an adsorption behavior which is different from the Langmuir model. In fact, the increase towards plateau values in the adsorption isotherm of this surfactant takes place at much lower values than the values given by the Langmuir model. This supposes a stronger interaction between the nonionic surfactant and the carbon black surface than predicted by the Langmuir model or an interaction between the nonionic surfactant molecules. For the nonionic surfactant, $K=3.46 \text{ m}^3/\text{mol}$. This is much

higher than the values obtained for the anionic surfactants. This result further confirms the stronger interaction of the nonionic surfactant with the carbon black surface compared to the anionic surfactants and is also supported by the results obtained for the surfactant mixtures.

4.1.1.6 Zhu model for anionic surfactant adsorption at the carbon black-water interface This model has been originally developed to describe the adsorption of surfactants which are supposed to form so-called hemi-micelles. The Zhu equation [70, 71, 72] is expressed as follows:

$$c_{\text{ads}} = \Gamma = \frac{\Gamma_{\text{max}} K_1 c_{\text{sol}} \left(\frac{1}{n} + K_2 c_{\text{sol}}^{n-1} \right)}{1 + K_1 c_{\text{sol}} (1 + K_2 c_{\text{sol}}^{n-1})} \quad (4.2)$$

Where:

- $c_{\text{ads}} = \Gamma$: concentration of adsorbed surfactant at the surface (mol/m²)
- c_{sol} : concentration of adsorbed surfactant in the bulk solution (mol/m³)
- Γ_{max} : maximum adsorbed amount per unit area (mol/m²)
- K_1 : equilibrium constant for the adsorption of single molecules (m³/mol)
- K_2 : equilibrium constant describing the adsorption of clusters of n molecules (m³/mol)
- n: number of molecules per cluster formed

In order to use the Zhu equation for fitting the experimental results of this study, a first calculation has been done in order to determine the value of the parameter n corresponding to an $R^2 = 1$ fit (which represents a good agreement between the experimental results and the fitted values). R^2 was calculated using the following equation:

$$R^2 = 1 - \frac{\sum w_i (y_i - \hat{y}_i)^2}{\sum w_i (y_i - \bar{y})^2} \quad (4.3)$$

Where:

- R^2 : coefficient of determination
- w_i : mean value
- y_i : observed value
- \hat{y}_i : predicted value
- \bar{y} : mean of the observed value

The graphs presenting the variation of n as a function of R^2 show good results (R^2 nearly equal to 1) values for $n=3$ (refer to Appendix). It is possible to deduce that each aggregate formed at the surface of the adsorbent presents 3 surfactant molecules according to the fit. In fact, the best fits were obtained for $n=3$. In a second step, K_1 and K_2 as given by the Zhu equation need to be determined. This is done by fitting the experimental results to the graphs given by the Zhu equation for $n=3$. Both graphs (experimental results (single values) and Zhu fit for $n=3$) for each surfactant are given below:

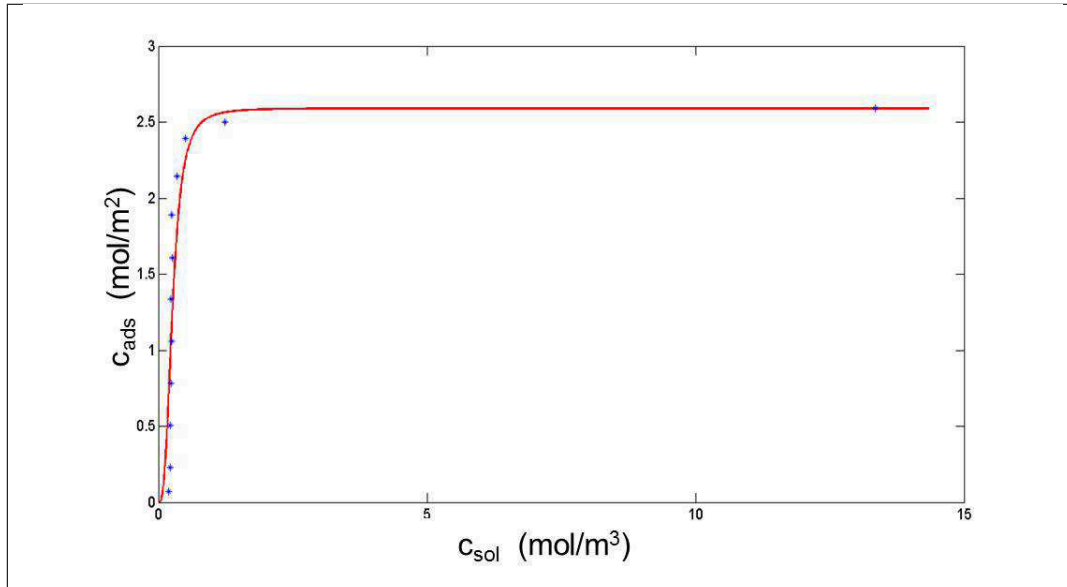


Figure 4.6: Concentration of the adsorbed $C_{12-14}E_7$ at the surface (c_{ads}) as a function of the bulk solution concentration (c_{sol}) for $n=3$

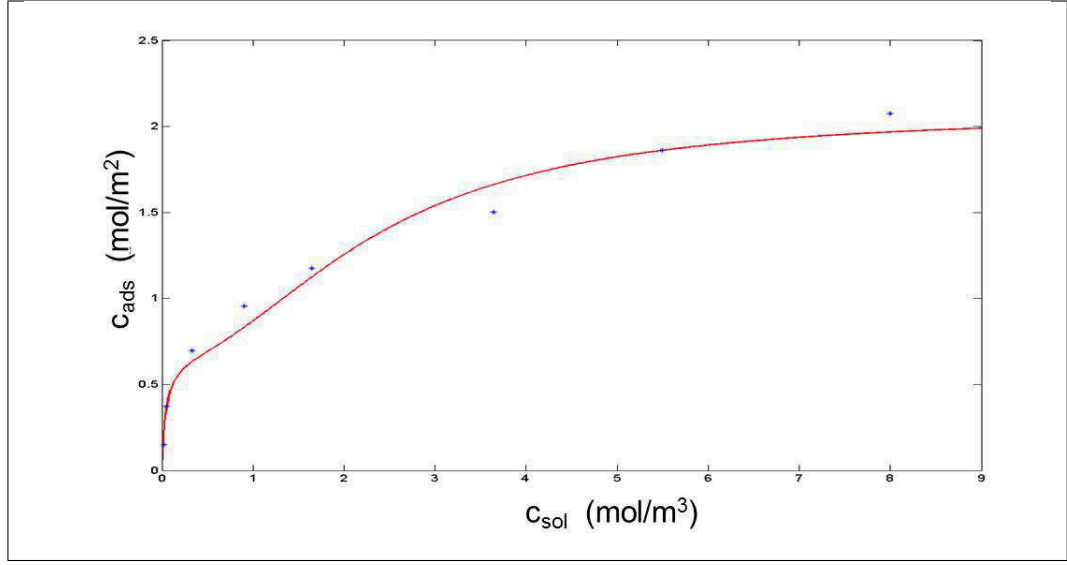


Figure 4.7: Concentration of the adsorbed SDS at the surface (c_{ads}) as a function of the bulk solution concentration (c_{sol}) for $n=3$

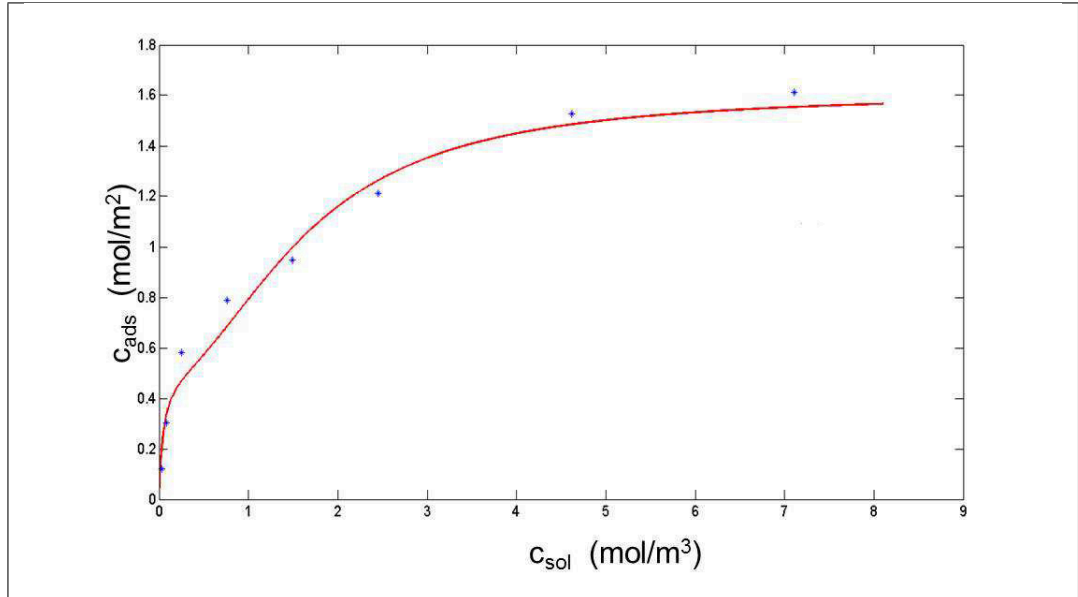


Figure 4.8: Concentration of the adsorbed SDBS at the surface (c_{ads}) as a function of the bulk solution concentration (c_{sol}) for $n=3$

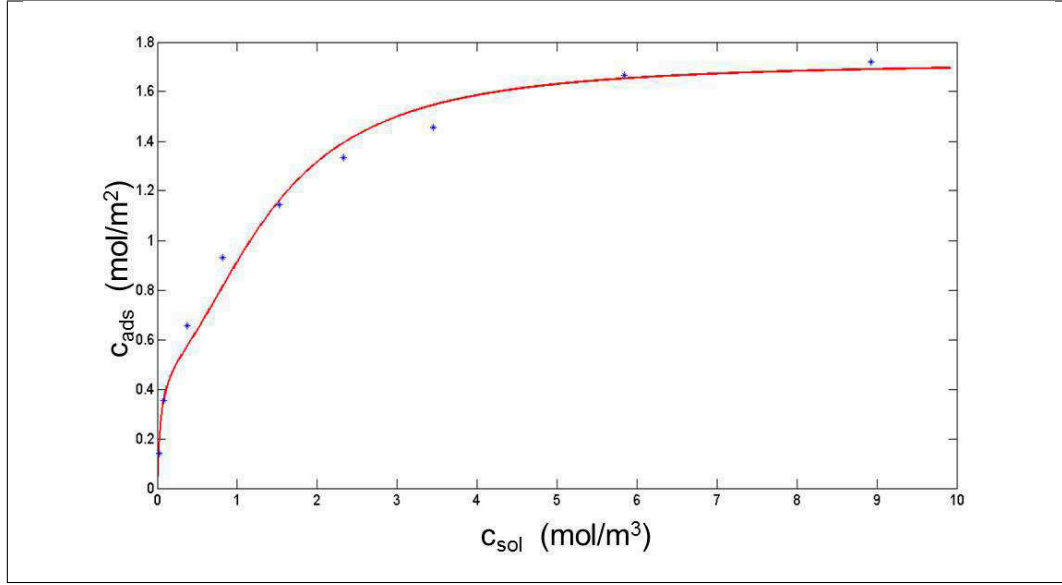


Figure 4.9: Concentration of the adsorbed SAS at the surface (c_{ads}) as a function of the bulk solution concentration (c_{sol}) for $n=3$

- For the nonionic surfactant $C_{12-14}E_7$, the fit in figure 4.6 for c_{ads} according to the Zhu model is given by the following equation:

$$c_{ads} = \frac{2.59 \times 3.610^{-3} c_{sol} \left(\frac{1}{3} + 14013.75 c_{sol}^{3-1} \right)}{1 + 3.610^{-3} c_{sol} (1 + 14013.75 c_{sol}^{3-1})} \quad (4.4)$$

- For SDS, the fit in figure 4.7 for c_{ads} according to the Zhu model is given by the following equation:

$$c_{ads} = \frac{2.08 \times 21.21 c_{sol} \left(\frac{1}{3} + 0.18 c_{sol}^{3-1} \right)}{1 + 21.21 c_{sol} (1 + 0.18 c_{sol}^{3-1})} \quad (4.5)$$

- For SDBS, the fit in figure 4.8 for c_{ads} according to the Zhu model is given by the following equation:

$$c_{ads} = \frac{1.72x20c_{sol}(\frac{1}{3} + 0.48c_{sol}^{3-1})}{1 + 20c_{sol}(1 + 0.48c_{sol}^{3-1})} \quad (4.6)$$

- For SAS, the fit in figure 4.9 for c_{ads} according to the Zhu model is given by the following equation:

$$c_{ads} = \frac{1.72x20c_{sol}(\frac{1}{3} + 0.48c_{sol}^{3-1})}{1 + 20c_{sol}(1 + 0.48c_{sol}^{3-1})} \quad (4.7)$$

Table 4.2 summarizes the values of K_1 and K_2 given by equations 4.4 to 4.7 for $n = 3$.

Table 4.2: Values of K_1 and K_2 for $n=3$ for the single surfactants using the Zhu equation

Single surfactant	$K_1(\text{m}^3/\text{mol})$	$K_2(\text{m}^3/\text{mol})$
$\text{C}_{12-14}\text{E}_7$	$3.6 \cdot 10^{-3}$	$14.01 \cdot 10^3$
SDS	21.21	0.18
SDBS	19.52	0.36
SAS	20.00	0.48

Differences are observed between the values of K_1 and K_2 obtained for the nonionic surfactant compared to the one obtained for the anionic surfactants. These differences can be summarized as follows:

- The K_1 values are much higher for the anionic surfactants
- The K_2 values are much higher for the nonionic surfactant

Knowing that K_1 represents the equilibrium constant for the adsorption of single molecules at the solid-liquid interface, it is possible to conclude that for the anionic surfactants, the adsorption of the single surfactant molecules at the carbon black-water interface predominates. For the nonionic surfactant, the interaction between the adsorbed surfactant molecules is predominant. This gives indication for different adsorption behaviors for the surfactants

used which could be further investigated by changing the values of n , K_1 and K_2 in the Zhu equation for each surfactant and comparing the given graphs to the experimental results (single values in figures 4.10 to 4.13) which enables the investigation of the effect of the variation of each parameter on the fits.

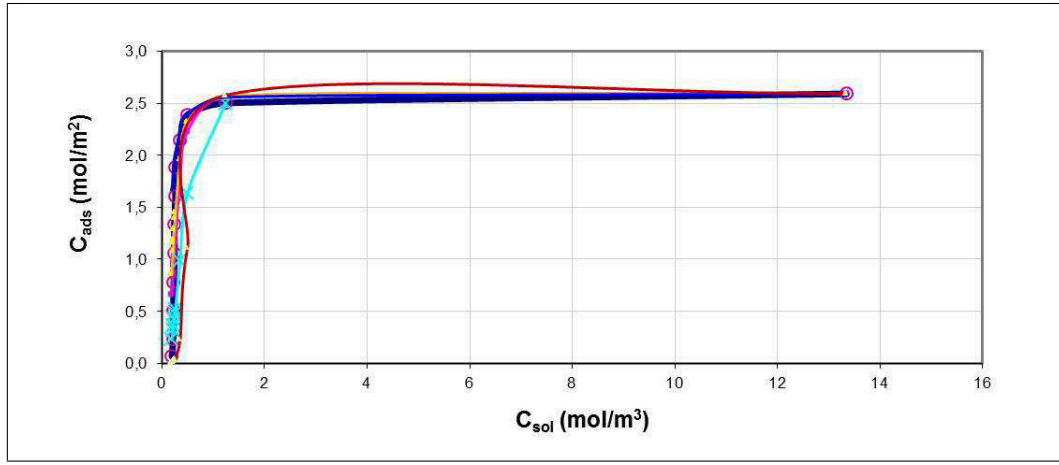
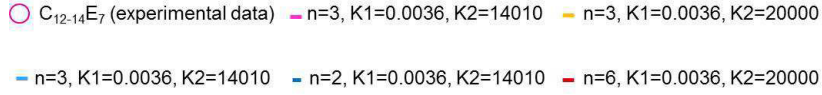


Figure 4.10: Variation of the constants n , K_1 and K_2 in the Zhu equation for $C_{12-14}E_7$



For $C_{12-14}E_7$, the best fit is obtained for $n=3$; $K_1=0.0036 \text{ m}^3/\text{mol}$ and $K_2=14010 \text{ m}^3/\text{mol}$. The adsorption isotherm of the nonionic $C_{12-14}E_7$ presents no significant dependance on the values of n , K_1 or K_2 as all graphs determined using the Zhu model present a similar progression as a function of c_{sol} and are in good agreement with the experimental results except for $n=3$ and a lower value of K_1 ($K_1=0.001$). This indicates that aggregation seems to be the dominant process (n values between 3 and 6) for this surfactant. Only for lower K_1 values, a shift between the experimental results and the fit is observed.

4.1 Adsorption behavior of single surfactants and mixtures

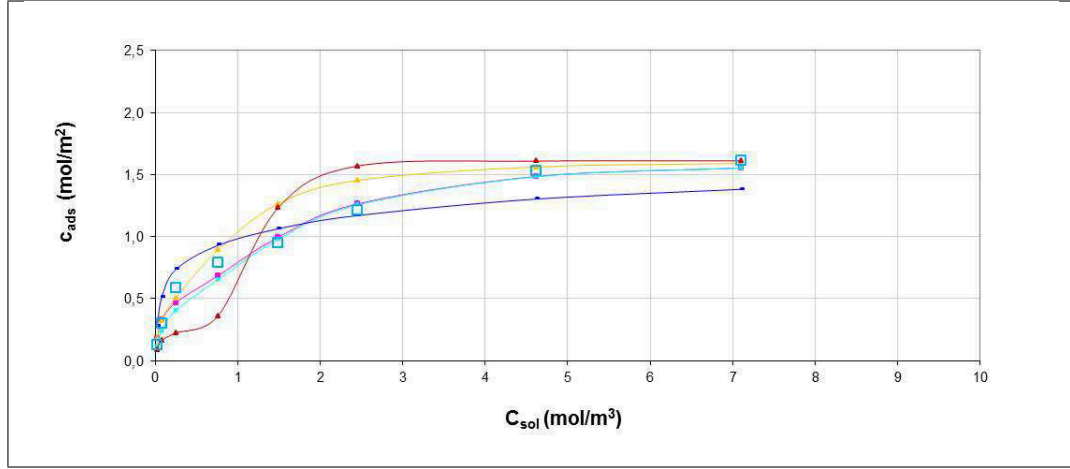


Figure 4.11: Variation of the constants n , K_1 and K_2 in the Zhu equation for SDS

SDS (experimental data) $n=3, K_1=21.2, K_2=0.18$ $n=3, K_1=21.2, K_2=0.5$
 $n=3, K_1=10, K_2=0.18$ $n=2, K_1=21.2, K_2=0.18$ $n=6, K_1=21.2, K_2=0.18$

For SDS, the best fit is obtained for $n=3$; $K_1=10 \text{ m}^3/\text{mol}$ and $K_2=0.18 \text{ m}^3/\text{mol}$.

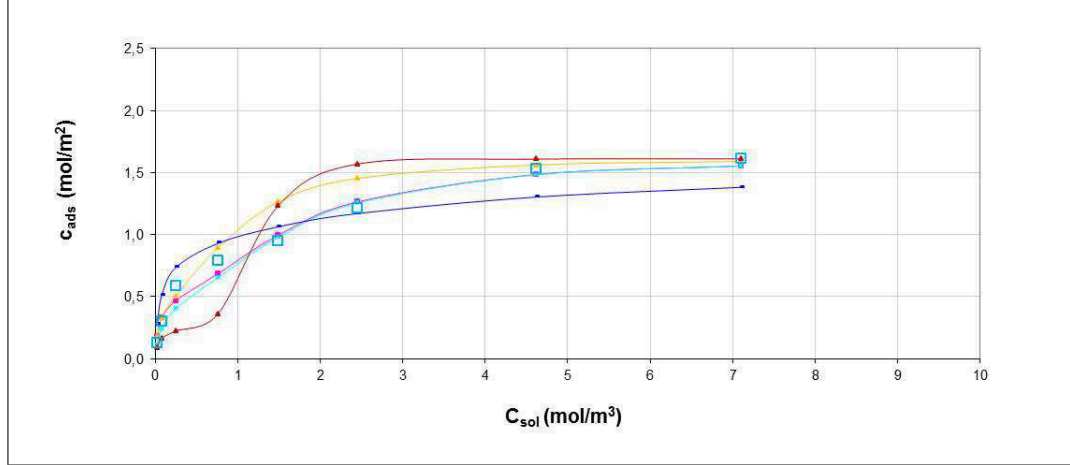


Figure 4.12: Variation of the constants n , K_1 and K_2 in the Zhu equation for SDBS

SDBS (experimental data) $n=3, K_1=19.5, K_2=0.36$ $n=3, K_1=19.5, K_2=1$
 $n=3, K_1=10, K_2=0.36$ $n=2, K_1=0.19.5, K_2=0.36$ $n=6, K_1=0.0036, K_2=0.36$

For SDBS, the best fit is obtained for $n=3$; $K_1=10 \text{ m}^3/\text{mol}$ and $K_2=0.36 \text{ m}^3/\text{mol}$.

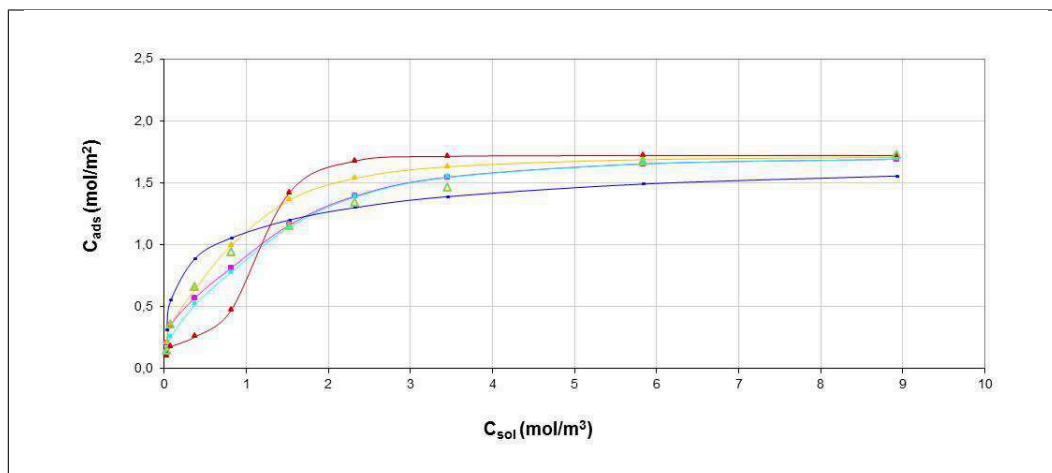
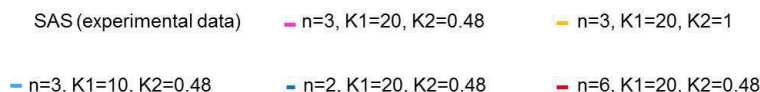


Figure 4.13: Variation of the constants n , K_1 and K_2 in the Zhu equation for SAS



For SAS, the best fit is obtained for $n=3$; $K_1=10 \text{ m}^3/\text{mol}$ and $K_2=0.48 \text{ m}^3/\text{mol}$. For the anionic surfactants SDS, SDBS and SAS the best fits were obtained for $n=3$. The variation of the value n towards higher and lower values presented a shift of the corresponding graphs from the best fit. The variation of the values of K_1 and K_2 presented similar results, but the shift observed when varying n was higher which shows a dependence of the adsorption behavior of the anionic surfactants on the number of molecules per aggregate formed at saturation on the surface of carbon black. The anionic surfactant adsorption at the carbon black/water interface seems to be better described by the Langmuir isotherm than by the Zhu isotherm. The aggregation process for the anionic surfactants seems to be less strong than for the nonionic surfactant. This study of the significance of the parameters of the Zhu equation supports the drawn conclusion of a significantly different adsorption mechanism for the nonionic surfactant compared to the anionic surfactants. The best fit for $n=3$ could mean that either small aggregates with 3 molecules per aggregate or aggregates of different single molecules are adsorbed in a mixed layer at the carbon black/water interface. For the anionic surfactant, even at high surfactant concentrations, the interaction between the surfactant and the hydrophobic carbon black surface predominates whereas for the nonionic surfactant, the interaction between

the adsorbed surfactant molecules predominates. The results mentioned above show that the mechanism of adsorption of the single surfactants at the carbon black-water interface is strongly dependent on the nature of the surfactant and its structure. Moreover, differences have been noticed between the models used to describe the adsorption behavior of the single surfactants. In fact, the Langmuir model could be applied for the interpretation of the adsorption isotherms of the anionic surfactants at the carbon black-water interface whereas for the nonionic surfactant, the Zhu model seems to describe at best the adsorption behavior. In fact, the Zhu model gives indication for the formation of surfactant aggregates at the hydrophobic surface which will be further investigated using atomic force microscopy.

4.1.2 Adsorbed amounts of surfactant mixtures at the carbon black-water interface

The adsorption isotherms for the studied mixtures are given in figure 4.14:

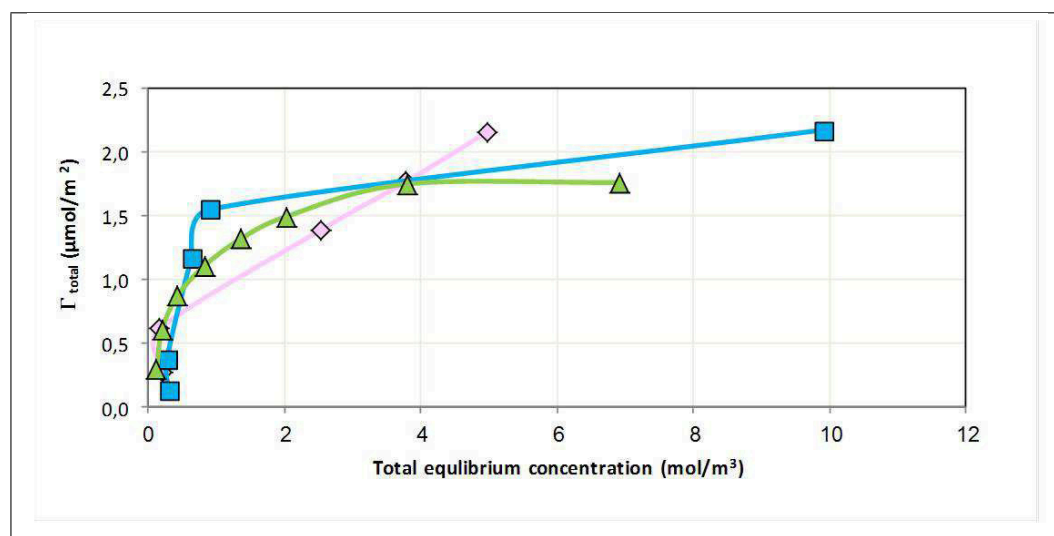


Figure 4.14: Adsorption isotherms for surfactant mixtures at the carbon black-water interface

◇ SDS/C₁₂₋₁₄E₇ ■ SDBS/C₁₂₋₁₄E₇ ▲ SAS/C₁₂₋₁₄E₇

Here the adsorbed amount (Γ_{total}) as well as the equilibrium concentration

represent the sum of the quantities obtained for the anionic surfactants and the nonionic surfactant in the mixture which have been measured separately. At low total equilibrium concentrations (up to 0.5 mol/m^3), the total adsorbed amounts for the studied systems were quite the same. At higher concentrations and up to 4 mol/m^3 , differences were observed between the 3 mixtures. SDBS/ $\text{C}_{12-14}\text{E}_7$ and SAS/ $\text{C}_{12-14}\text{E}_7$ present higher adsorbed amounts than the mixture $\text{SDS}/\text{C}_{12-14}\text{E}_7$, which shows a linear increase of the adsorbed amounts as a function of the equilibrium concentration. In this concentration range, $\text{SDS}/\text{C}_{12-14}\text{E}_7$ presented lower adsorbed amounts than $\text{SDBS}/\text{C}_{12-14}\text{E}_7$ and $\text{SAS}/\text{C}_{12-14}\text{E}_7$. But at higher concentrations, $\text{SDS}/\text{C}_{12-14}\text{E}_7$ presented higher adsorbed amounts. The adsorption isotherms for all the studied mixtures presented a similar feature which is the decrease of the adsorbed amount at saturation of either the anionic surfactant or the nonionic surfactant with increasing initial concentration of the other component with differences observed depending on the structure of the anionic surfactant used as presented in figures 4.15 and 4.16.

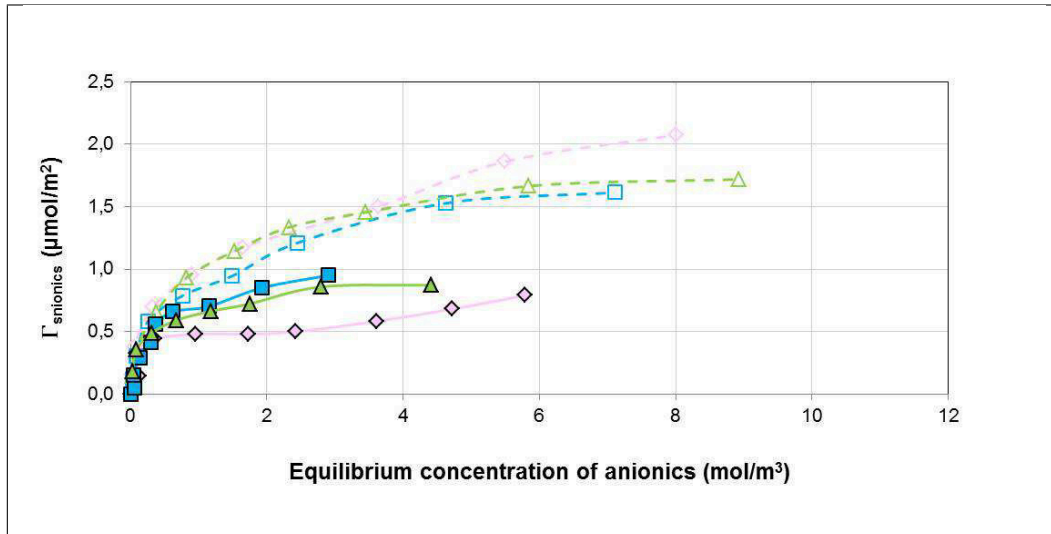
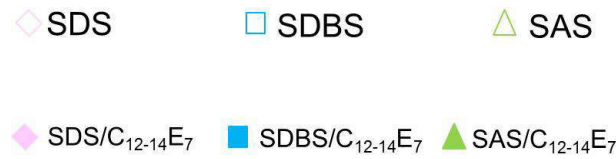


Figure 4.15: Adsorption isotherms for the anionic surfactants in the mixture at the carbon black-water interface



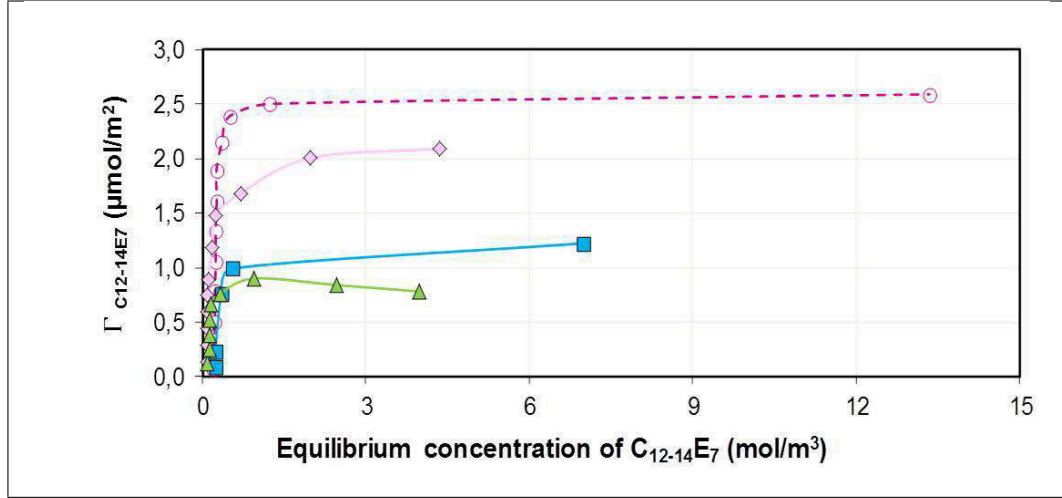


Figure 4.16: Adsorption isotherms for the nonionic surfactant in the mixture at the carbon black-water interface

○ $C_{12-14}E_7$ ◇ $SDS/C_{12-14}E_7$ ■ $SDBS/C_{12-14}E_7$ ▲ $SAS/C_{12-14}E_7$

In fact, the decrease of the adsorbed amount of SDS in the mixture with the nonionic surfactant is comparatively higher than that for SDBS and SAS. These results, especially for SDS, confirm the conclusions reported by Chobanu and Ropot [73] who investigated the adsorption of cationic and nonionic surfactants from their mixed solutions on carbon black as well as Gao et al [74] who studied the adsorption of Triton X-100 (nonionic surfactant) and sodium dodecyl sulfate as well as cetyltrimethylammonium bromide (cationic surfactant) from their mixed solutions on active carbon. In fact, the results of these studies show that the adsorption of ionic surfactants at saturation decrease markedly in the presence of a nonionic surfactant. Depending on the anionic surfactant in the mixture, the following interpretation can be done based on figure 4.14 and in relation to the values obtained in tables 3.4 to 3.6:

- For the $SDS/C_{12-14}E_7$ mixture: at low equilibrium concentration in the mixture, both anionic surfactant and nonionic surfactant are adsorbed equally at the carbon black surface. In fact, the mixing ratio up to a total equilibrium concentration of 0.17 mol/m^3 is very close to 1.

At higher concentrations, a strong increase is observed which is due to

the mutual adsorption of SDS and $C_{12-14}E_7$. Starting from this concentration range, a higher adsorption of $C_{12-14}E_7$ is observed, SDS is less adsorbed. This is given by the higher equilibrium concentration of this surfactant in solution. This is the linear part of the adsorption isotherm. In this mixture, the adsorption of the nonionic surfactant at the carbon black/water interface predominates. This results in a higher packing of the nonionic surfactant (aggregation) and a higher occupation of the carbon black surface due to the absence of electrostatic repulsion.

- For the SAS/ $C_{12-14}E_7$ mixture: at low concentrations, the anionic surfactant is more adsorbed at the carbon black/water interface and results in a continuous increase of the adsorption isotherm. Starting from a total equilibrium concentration of 1.35 mol/m^3 , the effect of the adsorption of the nonionic surfactant increases but the mixing ratios did not exceed 1 which results in plateau values reached at lower equilibrium concentration for the SDS/ $C_{12-14}E_7$ mixture.
- For the SDBS/ $C_{12-14}E_7$ mixture: the adsorption of the anionic surfactant predominates which results in a continuous increase of the adsorption isotherm in the initial region and plateau values starting already at a total equilibrium concentration of 0.9 mol/m^3 . In the studied concentration range, no dominance of the nonionic surfactant was observed.

Table 4.3 summarizes the mixing ratios at high concentrations for the studied mixtures.

Table 4.3: Ratios of the adsorbed amounts in the mixtures

Mixture:	C^i (mol/m ³)	$C^i_{C_{12-14}E_7}$ (mol/m ³)	C^i_{anionic} (mol/m ³)	$\Gamma_{C_{12-14}E_7}$ ($\mu\text{mol/m}^2$)	Γ_{anionic} ($\mu\text{mol/m}^2$)	$\Gamma_{C_{12-14}E_7}$ / Γ_{anionic}
SDS/ $C_{12-14}E_7$	14.66	6.01	8.65	1.474	0.680	2.16
SDBS/ $C_{12-14}E_7$	10.75	5.00	5.75	0.558	0.991	0.56
SAS/ $C_{12-14}E_7$	14.58	6.25	8.33	0.891	0.872	1.02

In this section, the most important result gained from the study of the adsorption behavior of surfactant mixtures at hydrophobic surfaces is the direct correlation between the structure of the alkyl chain of the anionic surfactant and the amount of nonionic surfactant adsorbed. The correlation between the

structure of the alkyl chain of the ionic surfactant in the mixture with a non-ionic surfactant and the adsorbed amount of the latter has been suggested in the literature, but has not been directly confirmed yet [45]. This aspect will be further discussed in the next section especially under the thermodynamic aspects of the adsorption process for mixtures.

4.2 Enthalpy effects during adsorption for single surfactants and mixtures

The cumulative molar enthalpies of adsorption for the single surfactants presented the same shape as the adsorption isotherms except for the nonionic surfactant. For a further evaluation of the adsorption process, the molar enthalpies of adsorption as a function of (Γ) will be considered in this section in order to study the thermodynamics of the adsorption process. Figure 4.17 shows the enthalpies of adsorption obtained for the single surfactants.

A high exothermic step at low Γ values is followed by a less exothermic adsorption process at higher Γ values for all surfactants. In the first region, the higher enthalpies of adsorption are due to the strong hydrophobic interaction between the hydrocarbon tail of the surfactants and the hydrophobic carbon black surface as suggested by Király et al [54]. As already noted in the section results, higher enthalpy values are registered for the nonionic surfactant compared to the anionic surfactants at the carbon black-water interface for low Γ values. The direct comparison between the adsorption enthalpy of the nonionic surfactant at the carbon black-water interface and the linear anionic surfactant SDS is presented in figure 4.18.

Both surfactants have similar hydrophobic tails (linear with similar hydrocarbon length) but different headgroups. The interactions between the carbon black surface and the head groups are probably small but seem to have an effect on the enthalpies of adsorption. In fact, differences in the values of the adsorption enthalpies ranging from 20 kJ/mol at low Γ values (for example for $\Gamma=0.38 \mu\text{mol}/\text{m}^2$) to about 5 kJ/mol at higher Γ values are registered between both surfactants (with higher values for the nonionic surfactant). This difference observed for the enthalpies of adsorption between the anionic surfactant

and the nonionic surfactant can be related to three effects resulting in the decrease of the overall adsorption enthalpy:

- the interaction between the charged head groups of the anionic surfactant and the carbon black surface presents a partial $\Delta h > 0$ (the total $-\Delta h$ decreases)
- the mutual repulsion between the charged head groups of the anionic surfactant molecules in the adsorbed layer results a partial $\Delta h > 0$ (the total $-\Delta h$ decreases)
- the adsorption at the carbon black surface results in the dehydration of the ionic head group (the total $-\Delta h$ decreases)

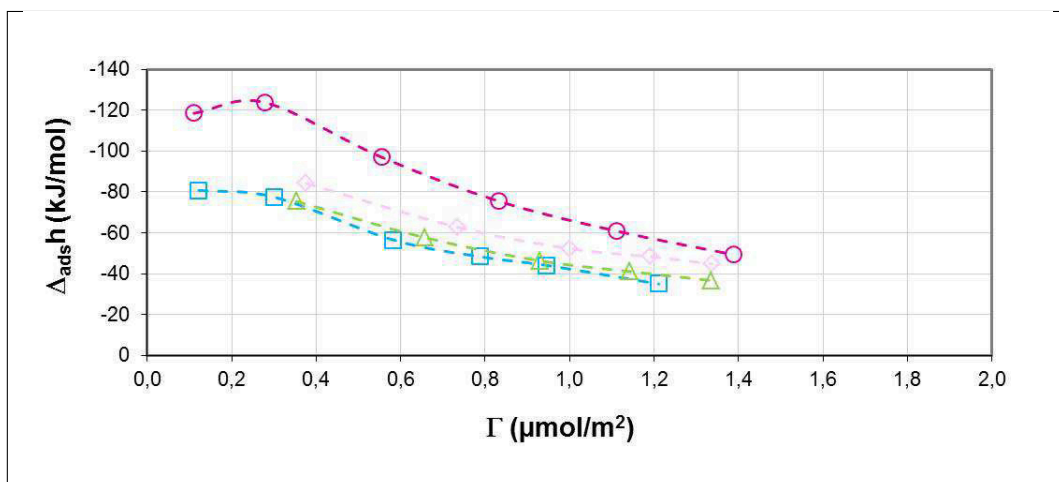


Figure 4.17: Differential molar enthalpies of adsorption of the single surfactants at the carbon black-water interface (corresponds to figure 3.13)

○ $\text{C}_{12-14}\text{E}_7$ ◇ SDS □ SDBS △ SAS

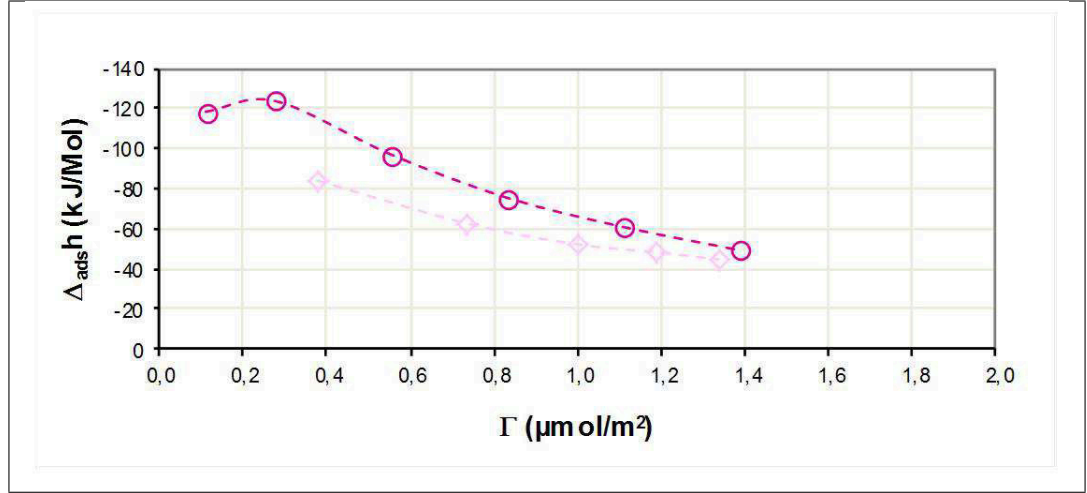


Figure 4.18: Effect of the surfactant head group

○ C₁₂₋₁₄E₇ ◇ SDS

This results in an overall decrease of the enthalpy of adsorption for the anionic surfactant compared to the nonionic surfactant. Lower values were reported by Király et al [18] for the cationic surfactant C₁₂TAB as presented in table 4.4 which further confirms the effect of the charge and probably also the structure of the head group on the thermodynamics of the adsorption process. Another important aspect is related to the chain length of the surfactants. In fact, results obtained by Király et al [54] for the adsorption of sodium dodecylsulfate (SDeS) at the graphitized carbon black-water interface reported lower enthalpy values for this surfactant compared to the values reported in this study for SDS (Table 4.4). This supports the horizontal arrangement of the surfactant at the surface with less carbon atoms at the surface for SDeS compared to SDS.

Table 4.4: Headgroup and chain length effects on the adsorption enthalpies

Surfactants	Δh_{\max} (kJ/Mol)	Δh_{\min} (kJ/Mol)	CMC (Mol/m ³)	$\Delta h_{\text{micellization}}$ (kJ/Mol)
C ₁₂₋₁₄ E ₇	-115	-50	0.03	2.4
SDS	-85	-45	6.8	1.02
C ₁₂ TAB [18]	-61	-61	14.8	-1.20
SDeS [54]	-42	-10	33.2	1.6
C ₁₀ TAB [18]	-43	-43	68	-

In table 4.4, Δh_{\min} and Δh_{\max} represent the lower and the higher enthalpy values obtained. CMC is the critical micelle concentration for the studied surfactants and $\Delta h_{\text{micellization}}$ is the micellization enthalpy. The interaction between the adsorbed surfactant molecules in the adsorbed layer at high concentrations is comparable to the interaction in the micelles in that way that both mechanisms (interaction in the adsorbed layer and in the micelles) show lower enthalpy variations. In fact, the comparison of the enthalpy values for SDS, for example between $\Gamma=1.0 \text{ } \mu\text{mol}/\text{m}^2$ and $\Gamma=1.2 \text{ } \mu\text{mol}/\text{m}^2$ shows a very small difference in the enthalpy of adsorption ($\Delta h = 2 \text{ kJ}/\text{mol}$; where Δh is the difference between the two enthalpy of adsorption measured at the given $\Gamma = 1.0 \text{ } \mu\text{mol}/\text{m}^2$ and $\Gamma = 1.2 \text{ } \mu\text{mol}/\text{m}^2$) which is comparable to the enthalpy of micellization obtained for this surfactant. An additional parameter seems to have an effect on the adsorption enthalpies of the anionic surfactants which is the structure of the hydrophobic tail and especially the presence or absence of an aromatic group or branching (refer to table 4.2). In fact, the comparison between the enthalpies of adsorption measured for SDS and both SDBS and SAS shows the effect of branching. Both SDBS and SAS present branching in the hydrophobic tail and exhibit slightly lower enthalpy values than the linear SDS as presented in table 4.2. These lower enthalpy values can be due to the steric effects generated by the branched alkyl chain compared to a linear alkyl chain.

Table 4.5: Comparison between the differential molar enthalpies of adsorption at the carbon black surface

Surfactant	$\Gamma_{\min} (\mu\text{mol}/\text{m}^2)$	$\Delta_{\text{dis}} h_{\min} (\text{kJ}/\text{mol})$	$\Gamma_{\max} (\mu\text{mol}/\text{mol})$	$\Delta_{\text{dis}} h_{\max} (\text{kJ}/\text{mol})$
C ₁₂₋₁₄ E ₇	0.11	-118	1.39	-49
SDS	0.37	-84	1.34	-44
SDBS	0.12	-80	1.21	-35
SAS	0.35	-75	1.33	-36

The mixtures of the three studied anionic surfactants with the nonionic surfactant exhibited different behaviors depending on the structure of the anionic surfactant used. In fact, the enthalpy of adsorption for the SDS/C₁₂₋₁₄E₇ mixture was similar to that of the single nonionic surfactant in the entire Γ region studied which suggests that the thermodynamic parameter of adsorp-

tion in the mixture is governed by the nonionic surfactant. This supports the assumption that the electrostatic repulsion of the polar group of the anionic surfactant is reduced in the mixture and therefore the adsorption enthalpy in the mixture is equal to that of the nonionic surfactant. By correlating the adsorption enthalpies in the mixture to the ratio of the adsorbed amounts, this aspect is further confirmed. In fact, and as presented in figure 4.19, the ratio ($\Gamma_{C_{12-14}E_7}/\Gamma_{SDS}$) is mostly equal or higher than 1, which means that the nonionic surfactant in the mixture adsorbs preferentially at the carbon black surface and exhibits enthalpy values which are equal to the one registered for the single nonionic surfactant.

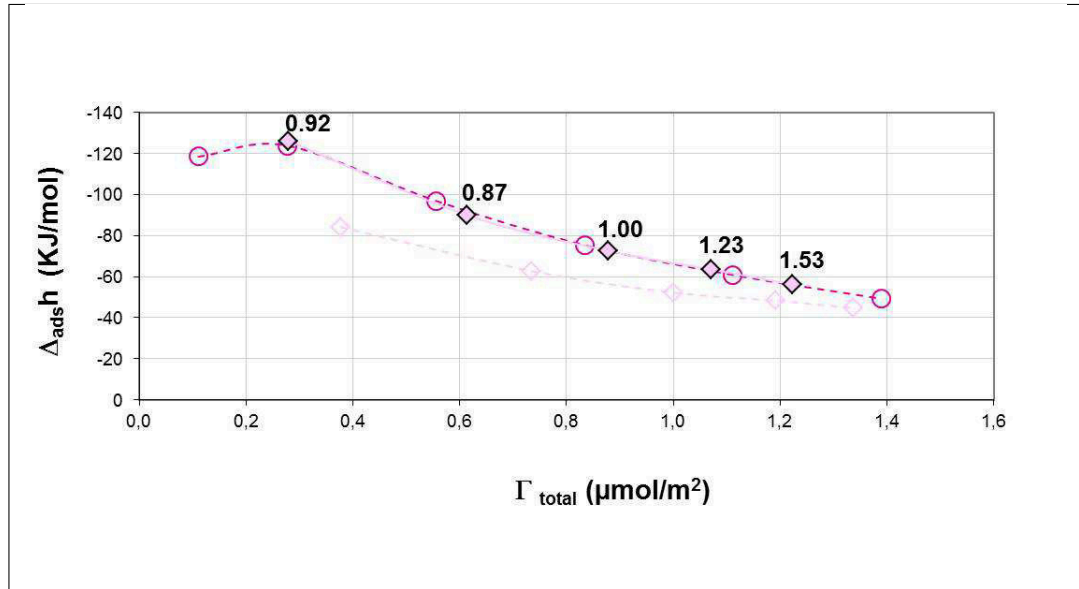


Figure 4.19: Correlation between the enthalpies of adsorption and the ratio of the adsorbed amounts (corresponds to figure 3.15)

○ $C_{12-14}E_7$ ◇ SDS ◇ $SDS/C_{12-14}E_7$

For the other mixtures, the following behavior was observed:

- For the SDBS/ $C_{12-14}E_7$ mixture, the adsorption behavior was quite comparable to the one registered for the $SDS/C_{12-14}E_7$ mixture (refer to figure 3.17). A mixed adsorbed film is also formed for this mixture at the carbon black-water interface, but with a higher concentration of the anionic

surfactant than for the SDS/C₁₂₋₁₄E₇ mixture. This results in a low electrostatic repulsion between the adsorbed anionic surfactant molecules.

- For the SAS/C₁₂₋₁₄E₇ mixture, a different behavior was observed. The graph representing the adsorption enthalpy for the mixture is located under the one for the single nonionic surfactant (refer to figure 3.19). The effect of the nonionic surfactant on the adsorbed amounts of the anionic surfactant for SAS was lower than the one registered for SDS (refer to table 3.4 and 3.6). Moreover, the adsorption enthalpy for SAS in the mixture with the nonionic surfactant as a function of the total adsorbed amount is different from the one registered for SDS. This could be due to the fact that the nonionic surfactant has little effect on the electrostatic repulsion between the head groups of SAS. This might be related to a heterogeneous adsorbed film where domains of single surfactants are adsorbed at the carbon black-water interface rather than an homogeneous distribution of anionic and nonionic surfactant molecules in the adsorbed film.

4.3 Structure of the adsorbed layer using AFM

4.3.1 Structure observed for the single surfactants

The micrographs obtained for the single surfactants with exception of the anionic surfactant SDBS gave indication for an ordered structure with regular periods as indicated in Table 4.6.

Table 4.6: Periods registered for the single surfactants using AFM

Surfactants	Periods (nm)	Standard deviation (%)
C ₁₂₋₁₄ E ₇	5.2	7
SDS	5.6	10
SAS	4.7	6
SDBS	-	-

The value of the period calculated for the nonionic surfactant C₁₂₋₁₄E₇ and the anionic surfactant SDS are quite comparable due to the similar alkyl chains of

both surfactants. The higher value for SDS compared to $C_{12-14}E_7$ may be due to the electrostatic repulsion between the ionic groups of two horizontal molecules at the surface of two neighboring structures. These values, and especially for SDS, were in agreement with the values reported in the literature by Ducker et al [75] who did also study the adsorption of SDS at the graphite surface and reported a period of 5.6 nm.

From the results of the enthalpy study as well as the shape of the measured adsorption isotherms, the following conclusions can be made:

- at low concentrations, the alkyl chains of the surfactants are oriented horizontally towards the carbon black surface
- at higher concentrations, aggregates form in the solution and at the carbon black surface with an interaction between the molecules forming these aggregates

In their study of the adsorption of $C_{16}TAB$ at the graphite-water interface using atomic force microscopy, Manne et al [29] suggested that the structures observed in the AFM micrographs are hemimicelles forming at the graphite surface which can be either spherical or cylindrical. This suggestion is based on the sudden increase of the adsorbed amount of the surfactant at high concentration which is an indication for the formation of hydrophobic aggregates known so far as hemimicelles and first suggested by Gaudin and Fuerstenau [65]. In this study, the proposal for the shape of the aggregates observed at the graphite surface will be made according to the following assumptions:

1. Space occupied by the cross section area of the head group or the alkyl chain at the graphite surface according to the Langmuir film measurements [69]
2. Space occupied by the length of an alkyl chain of 12-14 carbon atoms at the graphite surface
3. Comparison between the number of molecules in a spherical micelle and the number of molecules suggested using geometrical considerations at the surface

The length of each C_{12} chain equals 2.02 nm as suggested by Dörfler et al [53], which means that 2 alkyl chains with 12 carbon atoms would occupy 4.08 nm

at the graphite surface.

$$Length(C_{12}chain) = 2.02nm \quad (4.8)$$

Considering a circular head group for a linear surfactant, the area given by the Langmuir measurement as reported by Ohba et al [76] is 0.52 nm^2 (figure 4.20)

$$A = \pi r^2 \quad (4.9)$$

where:

- A: Area of the head group
- r: radius of the head group

which corresponds to a radius of 0.41 nm and a distance (d) occupied by each head group of 0.82 nm as given by the following equation:

$$d = lenght_{headgroup} = 2r \quad (4.10)$$

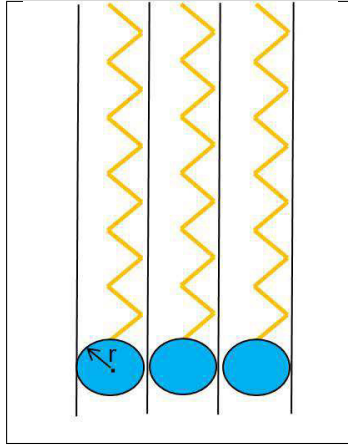


Figure 4.20: Space occupied by the cross sectional area of the head group according to the Langmuir film measurements

By applying the following equation:

$$Period_{AFM} = 2x(lenght_{C_{12}chain}) + 2x(lenght_{headgroup}) \quad (4.11)$$

$$Period_{AFM} = 2 \times 2.02 + 2 \times 0.8 \quad (4.12)$$

The distance obtained corresponds to 5.64 nm, the distance between two neighboring head groups is not included. This distance could correspond to the following structures presented in figure 4.21:

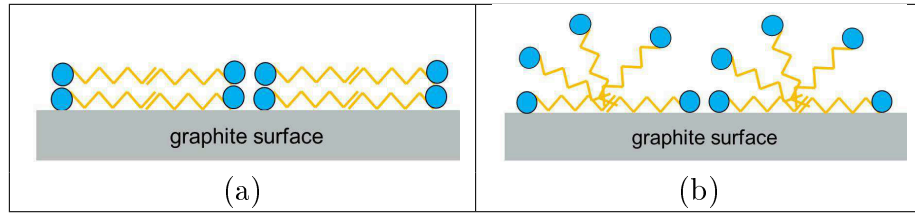


Figure 4.21: Structure of the adsorbed layer: (a) bilayer and (b) hemimicelle

It is now important to estimate the number of molecules per aggregate formed considering the parameters mentioned in figure 4.22:

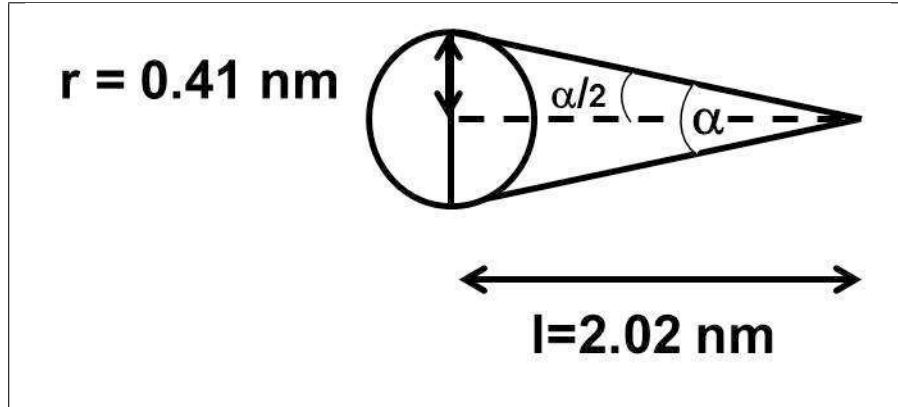


Figure 4.22: Number of molecules per aggregate

where:

- l : length of the alkyl chain
- r : radius of the head group
- α : curvature of the angle formed between the head group and the alkyl chain of the surfactant molecule

The tangent of the angle α ($\tan(\alpha)$) is given by the following equation:

$$\tan(\alpha) = \frac{r}{l} = \frac{0.41}{2.02} = 0.2 \quad (4.13)$$

$$\alpha = \tan^{-1}(0.2) = 11.5^\circ \quad (4.14)$$

where $\tan^{-1}(\alpha)$: inverse tan (α)

Assuming a 180° angle for the entire aggregate in a half-circle at the surface, the number of molecules per aggregate (N) is given by the following equation:

$$N = \frac{180}{2\alpha} = \frac{180}{2 \times 11.5} \approx 8 \quad (4.15)$$

Comparing this surface structures to the dimension of a micelle in bulk solution and supposing a spherical aggregate structure as in figure 4.21 (b), where the sphere radius is given by the length of an alkyl chain ($r = 2.02$ nm), the surface of the sphere at the graphite surface is given by the following equation:

$$A = 4\pi r^2 \quad (4.16)$$

This corresponds to a surface area of 55.4 nm^2 .

Knowing that the surface area occupied by each molecule is 0.52 nm^2 , the number of molecule per spherical micelle (N) is equal to 106. Myers et al [77] reported a number of molecules in spherical micelles for SDS of 30-70 which is for the upper limit (70 molecules per micelle) comparable to the number obtained above. This shows that the structure estimated from the period given by the AFM measurements fits quite well to that of spherical micelles in a bulk solution.

Table 4.7: Comparison between the number of molecules in micelles

Model	N
Number of molecules in micelles obtained in this study	106
Number of molecules in spherical micelles according to Myers et al [77]	30-70

These three aspects treated above which are the estimation of the space occupied by the cross section area of the headgroup or the alkyl chain at the

graphite surface as well as the space occupied by the length of an alkyl chain of 12-14 carbon atoms at the graphite surface together with the comparison between the number of molecules in a spherical micelle and the number of molecules per aggregate at the surface give indication for a hemimicelle structure at the graphite surface rather than bilayers. The height values for all the studied systems could not be used to estimate the height of the structures observed at the graphite surface due to the fact that these values did vary from one scan to the other, in contrast to the values of the periods which remained nearly constant. This variation of the height values can be explained by the slightly changing force applied by the piezo-element on the cantilever tip. An important aspect revealed in this study is the fact that the anionic surfactant SDBS is the only surfactant that does not present these regular structures. When studying the phase diagrams in water for the single surfactants SDS, SAS, SDBS and $C_{12-14}E_7$, one striking difference is observed which is the absence of a hexagonal phase in the phase diagram of SDBS (refer to figure 3.25). The hexagonal phase of a surfactant consists of close packed cylindrical micelles. Obviously there is a similarity between the structure formation in bulk solution and at the surface. Surfactants which are not able to build-up a hexagonal phase in bulk solution can also not form cylindrical aggregates at the graphite surface, although this structure is also favored by the orientation of the graphite surface. In fact, and as already presented in the section “Materials & Methods”, the distance between two neighboring carbon atoms for the used graphite is about 0.142 nm [78]. The distance between two neighboring carbon atoms in the alkyl chain of the surfactants is about 0.152 nm as measured by Groszek et al [79] for the adsorption of n-dotriacontane and n-butanol dissolved in n-heptane onto graphitized carbon black. These similar values could explain the preferential orientation of the alkyl chains of the surfactants at the graphite surface. This means that the formed aggregates are rather cylindrical than spherical hemimicelles. The aggregates can be referred to as hemicylinders. Consequently, an orientation of the alkyl chains lying horizontally head-to-head should be favored building a row of these structures along the three symmetry axis of the hexagonal structure of the graphite surface. These hexagonal structures can be seen in the AFM micrographs for example figures 3.26 and 3.28. A study done by Patrick et al [55] suggests that

the structure of the surfactant is another important aspect which can help, in addition to the phase diagram of the corresponding surfactant, to predict the formation or not of the hemicylindrical structures at the graphite surface. Patrick et al [55] suggest that surfactants presenting branching and/or aromatic groups in their alkyl chains would not present regular structures at the graphite surface when imaged using AFM as they hinder the strong registry with the graphite lattice resulting in a featureless monolayer. For SAS, which is an anionic surfactant presenting branching in its alkyl chain, regular structures at the graphite surface were observed and it was possible to measure the corresponding period which contradicts the assumptions made by Patrick et al [55]. But for the anionic surfactant SDBS which presents an aromatic group (phenyl group), these structures were not observed even at different initial concentrations of the surfactant and also when using electrolytes which agrees with the assumption done by Patrick et al [55]. This means that not simply the structure should be the parameter considered for the interpretation of the AFM micrographs, but it is also very important to consider the aggregation of the surfactants in bulk solution.

4.3.2 Structure observed for the surfactant mixtures

For the mixtures studied, the periods calculated show some interesting characteristics compared to the values obtained for the single surfactants (refer to table 3.16). For both $C_{12-14}E_7$ /SDS and $C_{12-14}E_7$ /SAS, imaging conditions were comparable to the corresponding single systems. In fact, no adhesion of the cantilever tip was observed (the so-called snap-on effect) and reproducible measurements were possible which enables the determination of the periods. The periods measured correspond to the structure considered for the single surfactants at the graphite surface (figure 4.21 (b)). The corresponding aggregates can be mixed aggregates containing anionic surfactant molecules as well as nonionic surfactant molecules and/or aggregates of each surfactant adsorbed in a random manner at the graphite surface. For surfactant mixtures, mixed micelles are formed in solution. For the studied mixtures, these mixed micelles are formed at low concentrations starting at 0.03 mol/m³ driven by the low nonionic surfactant concentration. It is possible to consider mixed

aggregates adsorbed at the graphite surface comparable to the mixed micelles in solution. And due to the higher affinity of $C_{12-14}E_7$ towards the graphite surface due to its linear alkyl chain and the absence of charges on its head group, the following aggregate structures can be considered at the graphite surface:

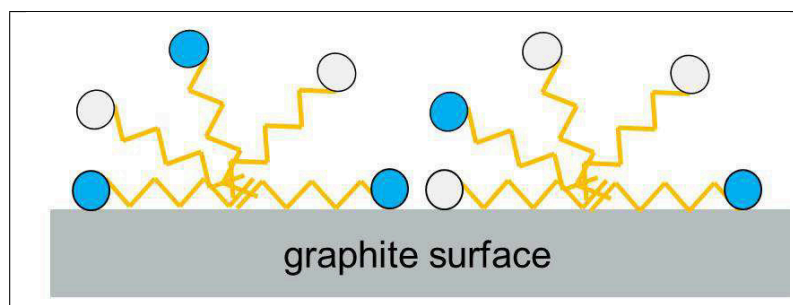


Figure 4.23: Aggregate structure at the graphite surface for surfactant mixtures

In figure 4.23, the nonionic surfactant molecules are lying parallel to the graphite surface and further anionic surfactant molecules are adsorbed from the solution. An important aspect was observed for the mixture $C_{12-14}E_7$ /SDBS. In fact, the presence of regular structures at the graphite surface is dependent on the $C_{12-14}E_7$ concentration in the mixture. At low $C_{12-14}E_7$ concentrations, the snap-on effect of the cantilever made imaging difficult. With higher non-ionic surfactant concentrations, imaging was possible and regular structures were observed up to 50% SDBS concentration in the mixture. This could be due to the fact that the hemicylindrical structure of the nonionic surfactant is stabilizing the adsorbed SDBS at the graphite surface.

4.3.3 Conclusion

The AFM study enables the further investigation of the special adsorption behavior of SDBS in the mixture which was not revealed while studying the adsorption isotherms and the enthalpies of the mixtures. This shows the importance of this technique for studying surfactant adsorption at the solid/liquid interface as the obtained micrographs in combination with the results of the

adsorption isotherms and the enthalpy values enable the proposal of the structure of the adsorbed layer.

5 Importance for the application

The adsorption of single surfactants and surfactant mixtures at the solid-liquid interface was studied under different aspects. In fact, the adsorbed quantities, the enthalpies of adsorption and the structure of the adsorbed layer were investigated. The adsorption of single surfactants as well as surfactant mixtures resulted in a change of the surface properties of the studied solid substrates (carbon black as well as graphite). This gives an important prerequisite for the stabilization of particles in liquids. To prevent an aggregation and therefore an increase of the particle size of the solids in the liquids, repulsive forces have to be present in order to keep the particles at a certain distance. An increase in particle size results in an increased sedimentation or creaming velocity which can be described by the Stokes equation [80]:

$$F_d = 6\pi\mu r V_S \quad (5.1)$$

where:

F_d : frictional force acting on the interface between the fluid and the particle (N),

μ : dynamic viscosity (Ns/m²),

r : radius of the spherical particle (m),

V_s : particle's settling velocity (m/s).

The stability of the resulting dispersions is dependent on the properties of the adsorbed surfactant layer. Generally speaking, the stability of solid particles in a liquid medium is governed by two fundamental mechanisms [1]:

- Steric stabilization: It is mainly achieved by adding polymers or nonionic surface active agents which adsorb onto the particle surface preventing the agglomeration of the particles. This is governed by the thickness of the adsorbed layer. At a certain concentration of the additive, the thickness of the adsorbed layer keeps the particles separated at a certain distance where the attractive van der Waals forces are not any more sufficient to cause the particles to agglomerate.
- Electrostatic stabilization: This is the effect generated by charge distri-

bution at the particle surface which generates repulsion between particles having a same surface charge inhibiting agglomeration.

Both effects are presented in figure 5.1:

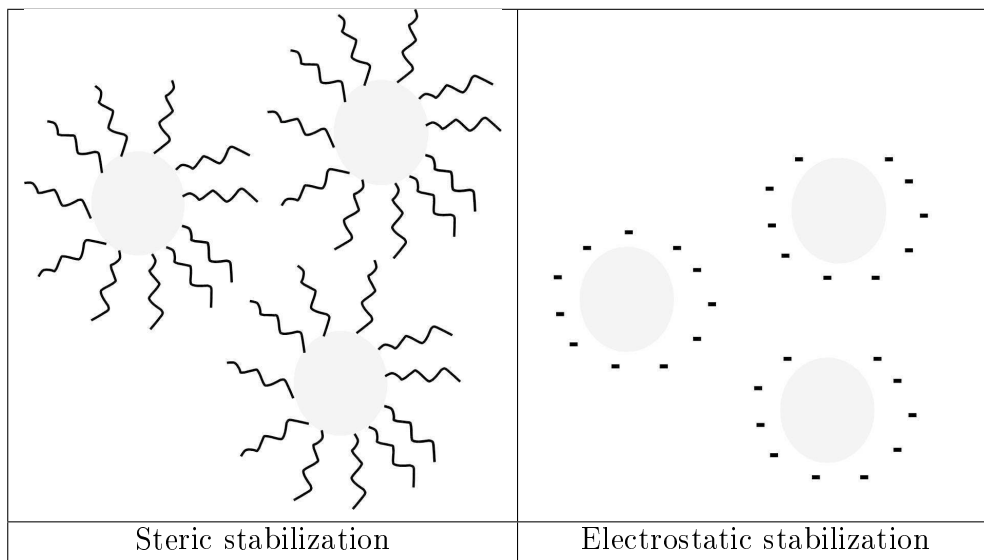


Figure 5.1: Dispersion stabilization

These two mechanisms play an important role in many industrial applications where dispersions need to be stabilized. One other example of application of the stabilization effect is the removal of soil particles during the washing process. In this case, it is the interaction of a small particle with a flat surface on a macroscopic scale. During the washing process, the adsorbed soil particles (P) on the flat textile surfaces (solid substrate) are removed according to one of the following mechanisms suggested by M.J. Schwuger [81]:

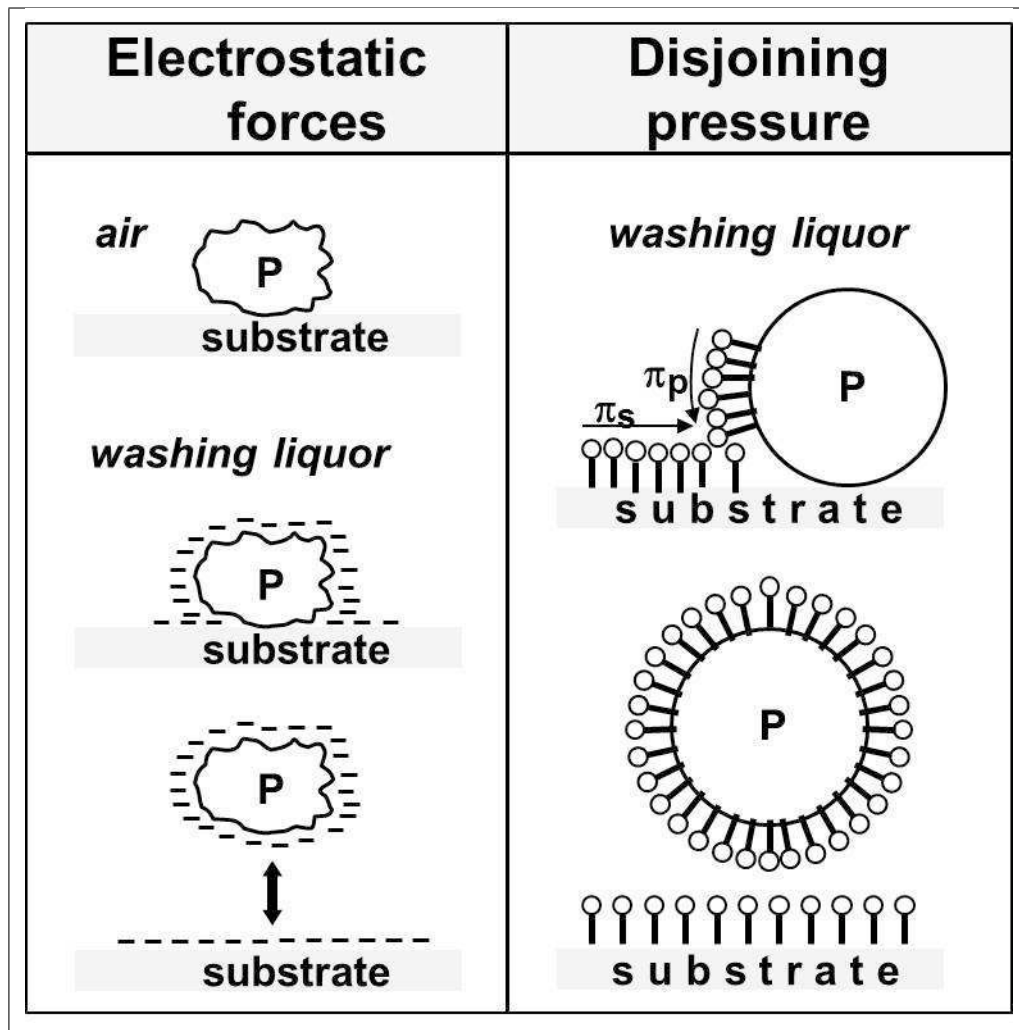


Figure 5.2: Mechanisms involved during the washing process [81]

The aspect presented on the left part of figure 5.2 is a typical case of electrostatic stabilization. The adsorption of anionic surfactants at the surface of the soil particle as well as the formation of an adsorbed layer of the same anionic surfactant at the textile surface result in a mutual repulsion between the textile surface and the soil particle which enables its removal and hinders its redeposition. The second part in figure 5.2 describes a further aspect related to the presence of an adsorbed layer at the substrate surface (textile). The surfactant molecules (mainly nonionic surfactant molecules) adsorb at the soil particle (P) and at the substrate surface which creates the so-called disjoining pressure which is the pressure difference between the adsorbed layer at the soil

particle and at the textile surface resulting in the release of the soil particle from the substrate. The mechanism of stabilization involved here is a steric stabilization.

5.1 Study of dispersion stability

The continuous measurement of light transmission as a function of time during centrifugation of solid-liquid dispersions can be applied to determine the concentration at which a dispersion is not stable any more. The advantages of this method are the decrease of time to study dispersion stability and to show the effect of different gravitational forces on the stability of dispersions. This is done by measuring the transmission factor (T) as a function of time during centrifugation (see chapter methods). A high transmission factor per unit time (dT/t) indicates that sedimentation takes place which means that the solid particles are not any more stable in the aqueous medium resulting in an unstable dispersion. This technique has been applied in this study in order to correlate the results of the fundamental study of surfactant adsorption at the solid-liquid interface with the light transmission curves for the same systems during centrifugation. This was done for the single surfactants and the surfactant mixtures.

5.2 Dispersion stability using single surfactants

Different concentrations of the studied single surfactants (the anionic surfactants SDS, SAS and SDBS as well as the nonionic surfactant $C_{12-14}E_7$) have been added to the same carbon black concentration in solution (30 g/l). The light transmission curves obtained for each surfactant are given in figure 5.3.

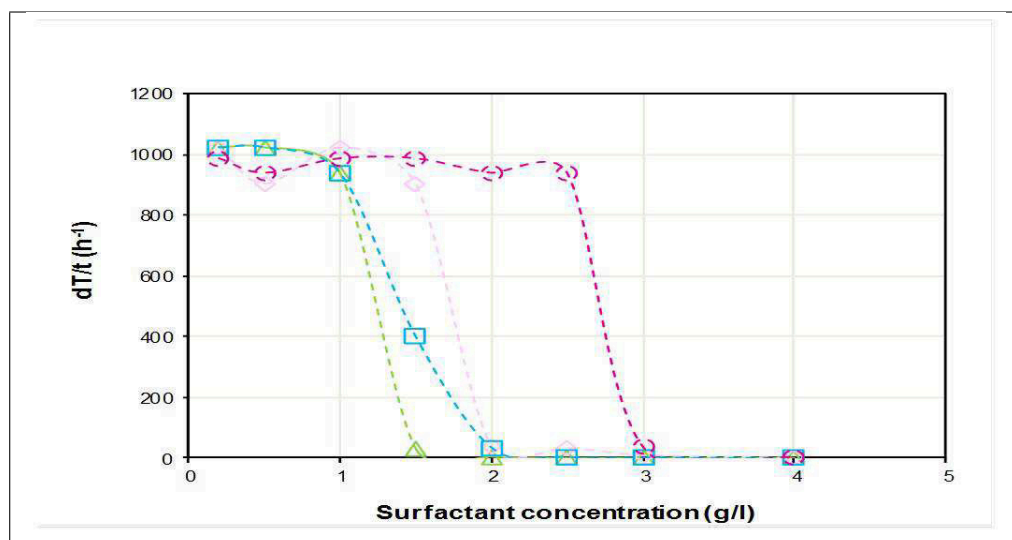


Figure 5.3: Light transmission measurements of carbon black dispersions for the single surfactants

○ C₁₂₋₁₄E₇ ◇ SDS □ SDBS △ SAS

The dispersions with the anionic surfactants are stable at lower concentrations than with the nonionic surfactant. The single nonionic surfactant stabilizes the dispersions at a concentration almost two times higher than the concentration of the anionic surfactants. This indicates a better stabilization of the carbon black dispersions using anionic surfactants. The stabilization of the dispersions using anionic surfactants is due to the electrostatic stabilization whereas for the nonionic surfactant the stabilization of the carbon black dispersions is due to steric stabilization. Obviously, the steric stabilization needs more surfactant molecules being present in the solution to build up a layer which is thick enough to counterbalance the attractive van der Waals forces between the particles. Differences are to be noted between the anionic surfactants: SDBS and SAS seem to stabilize dispersions at lower concentrations than SDS. This behavior can be correlated to the head groups of these surfactants. The head group for both SDBS and SAS is a sulfonate group and for SDS, the head group is a sulfate group. The sulfonate group seems to result in a higher repulsion between the carbon black particles than the sulfate group.

5.3 Dispersion stability using surfactant mixtures

The stabilizing effect of the mixed surfactant systems was studied for the 1:1 molar mixtures (figure 5.4). The dispersions using surfactant mixtures were stable at higher concentrations than the sum of the concentrations for the single compounds.

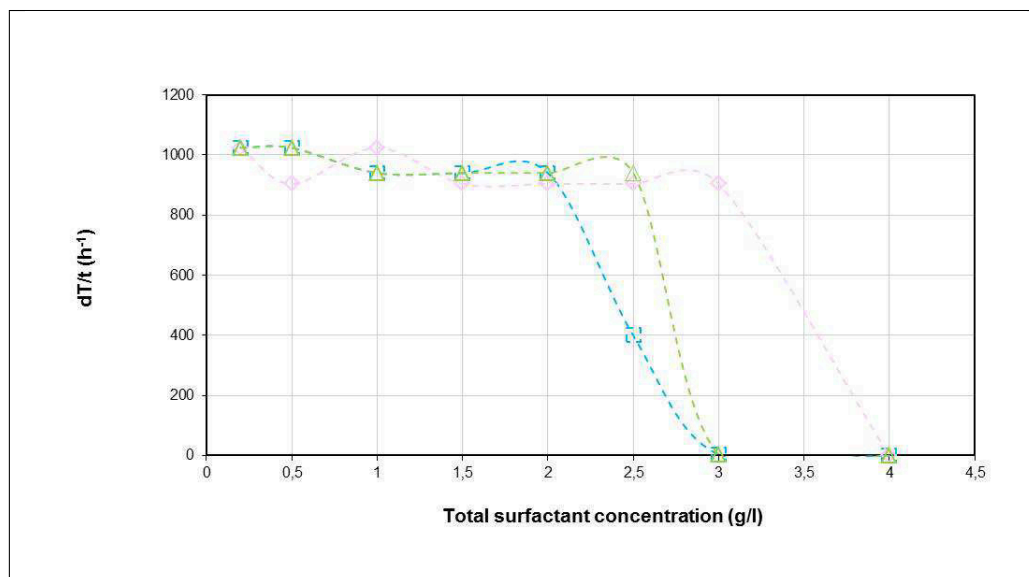


Figure 5.4: Light transmission measurements for the surfactant mixtures

◆ SDS/C₁₂₋₁₄E₇ ■ SDBS/C₁₂₋₁₄E₇ ▲ SAS/C₁₂₋₁₄E₇

As already presented above, all used single surfactants stabilize the carbon black particles, but in different manner. The stabilization resulting from the adsorption of SDS, SDBS and SAS at the carbon black/water interface is an electrostatic stabilization whereas the stabilization resulting from the adsorption of C₁₂₋₁₄E₇ at the same interface is a steric stabilization. In the mixed systems, differences were observed between SDS and the other anionic surfactants SDBS and SAS. SDS was more easily substituted by the nonionic surfactant in the mixture as given by the results of the adsorption isotherms for the mixture as well as the results of the calorimetric study and AFM. The results of the dispersion stability can be explained as follows: The addition of SDS results in the decrease of the steric stabilization of the nonionic surfactant due to the lower adsorbed amount of the nonionic surfactant in the adsorbed

layer. However, the adsorbed SDS amount does not seem to generate an electrostatic repulsion sufficient for stabilizing the carbon black dispersions. At higher concentrations, the mixing ratios in the adsorbed layer are characterized by the increase of the adsorbed amount of the nonionic surfactant (refer to table 5.1) which results in a higher steric stabilization and an overall increase in the stabilization of the carbon black dispersion.

Table 5.1: Ratios of the adsorbed amounts for the $C_{12-14}E_7$ /SDS mixture

$c^i_{\text{mixture}}(\text{mol/m}^3)$	$\Gamma_{C_{12-14}E_7} (\mu\text{mol/m}^2)$	$\Gamma_{\text{SDS}} (\mu\text{mol/m}^2)$	$\Gamma_{C_{12-14}E_7}/\Gamma_{\text{SDS}}$
1.47	0.133	0.146	0.911
2.93	0.288	0.328	0.878
8.80	0.892	0.499	1.787
11.73	1.184	0.583	2.031
14.66	1.474	0.680	2.168

The mixtures for SDBS and SAS presented stabilization of the carbon black dispersions at lower concentrations. This can be related to the fact that both surfactants do not substitute $C_{12-14}E_7$ as it is the case for SDS. This results in a higher steric stabilization in these two mixtures compared to the mixture with SDS. Another effect is the higher part of the electrostatic stabilization of SDBS and SAS in the mixtures as both surfactants are adsorbed in higher amounts at the carbon black/water interface compared to SDS (refer to table 5.2 and 5.3), especially for SDBS.

Table 5.2: Ratios of the adsorbed amounts for the $C_{12-14}E_7$ /SDBS mixture

$c^i_{\text{mixture}}(\text{mol/m}^3)$	$\Gamma_{C_{12-14}E_7} (\mu\text{mol/m}^2)$	$\Gamma_{\text{SDBS}} (\mu\text{mol/m}^2)$	$\Gamma_{C_{12-14}E_7}/\Gamma_{\text{SDBS}}$
1.35	0.052	0.084	0.612
2.69	0.150	0.226	0.664
8.06	0.414	0.757	0.547
10.75	0.558	0.991	0.563
26.87	0.951	1.223	0.777

Table 5.3: Ratios of the adsorbed amounts for the C₁₂₋₁₄E₇/SAS mixture

$c_{\text{mixture}}^i (\text{mol/m}^3)$	$\Gamma_{\text{C}_{12-14}\text{E}_7} (\mu\text{mol/m}^2)$	$\Gamma_{\text{SAS}} (\mu\text{mol/m}^2)$	$\Gamma_{\text{C}_{12-14}\text{E}_7}/\Gamma_{\text{SAS}}$
1.46	0.117	0.179	0.654
2.92	0.251	0.353	0.711
4.38	0.389	0.487	0.798
5.83	0.520	0.591	0.879
7.29	0.656	0.663	0.989
8.75	0.772	0.722	1.069
11.67	0.891	0.859	1.037
14.58	0.891	0.872	1.022

This results for the mixture with SDBS in a stabilization of the carbon black dispersion at lower concentrations compared to the single compounds. These results of the dispersion stability further confirm the results from the adsorption isotherms, the calorimetry study as well as the AFM micrographs: They allow to optimize mixed systems for the stabilization of solid particles in liquids.

6 Conclusion

The results of this study revealed an important aspect which is the difference observed between the effect of single surfactants and surfactant mixtures on the stability of dispersions of fine carbon black particles in the aqueous medium.

The anionic surfactants resulted in a better stabilization of the fine solid particles than the mixed systems.

Moreover, the properties of the adsorbed layer in the case of single surfactants seem to be more favorable for the stabilization of solid-liquid dispersions.

The AFM study done for the same systems revealed differences between the properties of the adsorbed layer on the graphite surface using single surfactants and surfactant mixtures as also seen for the stability of dispersions.

This correlation between the results of the AFM study and the results of the dispersion stability study was possible despite the different structures of graphite and carbon black.

However, and for a better understanding of the mechanisms involved during the stabilization of the carbon black dispersions, a study of the structure of the adsorbed layer on carbon black is needed.

AFM gave important insights about the possible structure of the adsorbed surfactants on the graphite surface but imaging using this technique is only possible on flat surfaces.

The porosity and the irregular structure of carbon black makes it difficult to perform such kind of micrographs and reinforces the need for imaging techniques which can be used to study the structure of the adsorbed surfactants on porous particles.

7 Presentations in scientific conferences

1. Poster presentation at ECIS 2010 “Calorimetric study of surfactants and their mixture at the solid/liquid interface”; M. Jabnoun, W. von Rybinski; Prague/Czech Republic; September 2010
2. Lecture at Zsigmondy-Kolloquium 2011 “Calorimetric study of surfactants and their mixture at the solid/liquid interface”; M. Jabnoun, W. von Rybinski; University of Münster/Germany; February 2011
3. Lecture at ProcessNet meeting 2011 “Calorimetric study of surfactants and their mixture at the solid/liquid interface”; M. Jabnoun, W. von Rybinski, M. Dreja; Clausthal-Zellerfeld/Germany; March 2011
4. Lecture at Bunsentagung 2011 “Calorimetric study of surfactants and their mixture at the solid/liquid interface”; M. Jabnoun, W. von Rybinski, F. Österheld, M. Dreja; Freie Universität Berlin/Germany; June 2011
5. Lecture at ECIS 2011 “Adsorption layers of surfactant mixtures on non-polar solid-particles and stability of dispersions”; M. Jabnoun, W. von Rybinski, F. Österheld, M. Dreja; MPI Berlin/Germany; September 2011

References

- [1] B. Dobiás, X. Qiu, and W. von Rybinski. *Solid-liquid dispersions*. Marcel Dekker, 1999.
- [2] Ethymology Dictionary. 2010.
- [3] W. Ostwald. *Z. Phys. Chem. (Leipzig)*, 34:295, 1907.
- [4] Th.F. Tadros. *Solid liquid dispersions*. Academic Press Inc (London) Ltd, 1987.
- [5] S. Voyutsky. *Colloid Chemistry*. MIR Publishers, 1978.
- [6] H.G. Hauthal. *SÖFW-Journal*, 130:3, 2004.
- [7] S. Brunauer, P.H. Emmett, and E. Teller. *J. Am. chem. Soc.*, 60:309, 1938.
- [8] W.C. Griffin. Classification of surface-active agents by hlb. *J. Soc. Cosmetic Chemists*, 1:311, 1949.
- [9] M.J. Rosen. *Surfactant and Interfacial Phenomena*. Wiley, New York, 1978.
- [10] W. Röhl. *Adsorption von Tensiden an niedrig geladenen Schichtsilikaten*. PhD thesis, Mathematisch-Naturwissenschaftliche Fakultät der Heinrich-Heine-Universität Düsseldorf, 1992.
- [11] W. von Rybinski and M.J. Schwuger. Surfactant mixtures as collectors in flotation. *Colloids and surfaces*, 26:291, 1987.
- [12] B. Andersson and G. Olofsson. *J. Chem. Soc., Faraday Trans. 1*, 84:4087, 1988.
- [13] S. Paula, W. Süss, J. Tuchtenhagen, and A. Blume. *J. Phys. Chem.*, 99:11742, 1995.
- [14] M. Lindheimer, E. Keh, S. Zaini, and S. Partyka. *Colloid Interfaces Science*, 138:83, 1990.
- [15] S. Partyka, M. Lindheimer, and B. Faucompre. *Colloids Surfaces*, 76:267, A 1993.
- [16] Z. Király, R.H.K. Börner, and G.H. Findenegg. *Langmuir*, 13:3308, 1997.

- [17] G.H. Findenegg, B. Pasucha, and H. Strunk. *Colloids and surfaces*, 37:223, 1989.
- [18] Z. Király and G.H. Findenegg. *J. Phys. Chem.*, 102:1203, 1998.
- [19] P.J. Scales. *Modern characterization methods of surfactant systems*. Marcel Dekker, INC, 1999.
- [20] D. Fennell Evans and Hakan Wennerström. *The colloidal domain*. WILEY-VCH, 1999.
- [21] G. Binnig, C.F. Quate, and Ch. Gerber. *Phys. Rev. Lett.* 56, page 930, 1986.
- [22] W.Richard Bowen. *Surface Chemistry and Electrochemistry of Membranes*, chapter Atomic Force Microscope Studies of Membrane Surfaces, pages 1–28. Marcel Dekker, INC.
- [23] S. Manne, J.P. Cleveland, H.E. Gaub, G.D. Stucky, and P.K. Hansma. *Langmuir*, 10:4409, 1994.
- [24] W. Ducker and E.J. Wanless. *J. Phys. Chem.*, 100:3207, 1996.
- [25] F.G. Greenwood, G.D. Parfitt, N.H. Picton, and D.G. Wharton. *Eds. American chemical society*, 28:343, 1968.
- [26] A.J. Groszek. *Proc. Royal Soc. London*, 314:473, A 1970.
- [27] J.P. Rabe and S. Buchholz. *Science*, 253:424, 1995.
- [28] S. Manne and H.E. Gaub. *Science*, 270:1480, 1995.
- [29] S. Manne, T.E. Schäffer, Q. Huo, P.K. Hansma, D.E. Morse, G.D. Stucky, and I.A. Aksay. *Langmuir*, 13:6382, 1997.
- [30] E.J. Wanless and W.A. Ducker. *Langmuir*, 13:1463, 1997.
- [31] H.N. Patrick, G.C. Warr, S. Manne, and I.A. Aksay. *Langmuir*, 13:4349, 1997.
- [32] L.M. Grant, F. Tiberg, and W.A. Ducker. *J.Phys. Chem.*, 102:4288, 1998.
- [33] N.B. Holland, M. Ruegsegger, and R.E. Marchant. *Langmuir*, 14:2790, 1998.
- [34] W. Ducker and L.M. Grant. *J.Phys. Chem.*, 100:11507, 1996.
- [35] E. Smulders and P. Krings. *China surfactant Detergents & Cosmetics 1*, page 18, 1993.

-
- [36] H.G. Hauthal. Anionic surfactants: Organic chemistry. *Surfactant Sci. Ser.*, 56:143, 1996.
- [37] H.G. Hauthal, B. Makowka, and M. Pieroth. *Proceedings of the 5. World Surfactants Congress (CESIO)*, page 873, 2000.
- [38] F. Asinger. *Chemie und Technologie der Paraffinkohlenwasserstoffe*. Akademie Verlag, Berlin, 1959.
- [39] J.M. Quack and M. Trautman. *Tenside Deterg.*, 22:281, 1985.
- [40] K. Holmberg, editor. *Handbook of applied surface and colloid chemistry Volume 2*. John Wiley and Sons, 2002.
- [41] S. I. Park and C. f. Quate. *Appl. Phys. Lett.*, 48:112, 1986.
- [42] M. Tsubouchi, N. Yamasaki, and K. Yanagisawa. *Anal. Chem.*, 57:783, 1985.
- [43] R. Atkins, V.S.J. Craig, E.J. Wanless, and S. Biggs. *Advances in colloids and interfaces Science*, 103:219, 2003.
- [44] A. Blom. *structure and physical properties of surfactant films at the solid-liquid interface*. PhD thesis, University of Sydney, 2005.
- [45] M.J. Schwuger and H.G. Smolka. *Coll. Polym. Sci.*, 255:589, 1977.
- [46] A.C. Zettlemoyer. *J. Colloid Interface Sci.*, 28:343, 1968.
- [47] R. E. Day, F.G. Greenwood, and G.D. Parfitt. *4th International Congress of Surface Active Substances*, 2B:1005, 1967.
- [48] A. C. Zettlemoyer. *J. Coll. Int. Sci.*, 28:343, 1962.
- [49] H. Rupprecht. *J. Pharm. Sci.*, 61:700, 1972.
- [50] H. Rupprecht and T. Gu. *Coll. Polym. Sci.*, 269:506, 1991.
- [51] H. Rupprecht, E. Ullmann, and K. Thoma. *Fortsch. Kolloid Polym.*, 55:45, 1971.
- [52] A. Thibault, A.M. Misselyn-Baudin, J. Grandjean, G. Broze, and R. Jerome. *Langmuir*, 16:203, 2002.
- [53] H.D. Dörfler. *Grenzflächen und kolloid-disperser Systeme*. Springer-Verlag, Heidelberg 2002.
- [54] Z. Király. *Langmuir*, 17:2423, 2001.
- [55] N. Patrick and G.G. Warr. *Coll. Surf. A.*, 162:149, 2000.

- [56] A. Sein and J.B.N. Engberts. *Langmuir*, 12:2913, 1996.
- [57] D.B. Hough and H.M. Rendall. *Adsorption from solutions at the Solid/Liquid Interface*. Academic Press, London, 1983.
- [58] T.W. Healy, P. Somasundaran, and D.W. Fuerstenau. *Int. J. Miner. Process.*, 72:3, 2003.
- [59] P. Somasundaran, T.W. Healy, and D. Fuerstenau. *J. Phys. Chem.*, 68:3562, 1964.
- [60] P. Somasundaran and D.W.Fuerstenau. *J.Phys. Chem.*, 70:90, 1966.
- [61] P. Somasundaran, T.W. Healy, and D. Fuerstenau. *J. Colloid Interface Sci*, 22:599, 1966.
- [62] P. Somasundaran and D. Fuerstenau. *Trans. AIME*, 252:275, 1972.
- [63] P. Somasundaran and H.S. Hanna. *In Improved Oil Recovery by Surfactant and Polymer Flooding (D.O. Shah and R.S. Schechter, eds)*. Academic Press, London, 1977.
- [64] P. Somasundaran and E.D. Goddard. *Mod. Aspects Electrochem.*, 13:207, 1979.
- [65] A.M. Gaudin and D.W. Fuerstenau. *Trans. AIME*, 202:958, 1955.
- [66] C. Ma and Y. Xia. *Coll. Surf.*, 66:215, 1992.
- [67] L.Bossoleti, R. Ricceri, and G. Gabrielli. *J. Disp. Sci. Technol.*, 16:205, 1995.
- [68] I. Langmuir. *J. Am. Chem. Soc*, 38:2221, 1916.
- [69] I. Langmuir. *J. Am. Chem. Soc*, 39:1848, 1917.
- [70] B.Y. Zhu and T. Gu. *J. Chem. Soc. Farad. T.*, 87:2745, 1991.
- [71] B.Y. Zhu and T. R. Gu. *J. Chem. Soc. Farad. T. 1*, 85:3813, 1989.
- [72] B. Y. Zhu, T. Gu, and L. Zhao. *J. Chem. Soc. Farad. T. 1*, 85:3819, 1989.
- [73] M.M. Cobanu and V.M. Ropot. *Zh. Prikl. Khim.*, 54:2221, 1981.
- [74] Y. Gao, Y. Zhang, Z. Huang, and T. Gu. *Acta Sci. Nat. Univ. Pckincnsis*, 25:726, 1989.
- [75] E.J. Wanless and W.A. Ducker. *Langmuir*, 13:1463, 1997.
- [76] N. Ohba and A. Takahashi. *Chimie, physique et applications pratiques*

- des agents de surface: compte-rendus du 5ème Congrès International de la Détergence, Band 2.* 1969.
- [77] D. Myers. *Surfaces, interfaces, and Colloids - Principles and Applications.* VCH Publishers Inc, 1990.
- [78] S. I. Park and C.F. Quate. *Appl. Phys. Lett.*, 48:112, 1986.
- [79] A.J. Groszek. *Proc. R. Soc. London*, 314:473–498, 1970.
- [80] J. McNown and J. Malaika. *Americal Geophysical Union*, 31:74, 1950.
- [81] M.J. Schwuger. *Ber. Bunsenges. Phys. Chem.*, 83:1193, 1979.
- [82] W. Ostwald. *Z. Phys. Chem.*, 34:294, 1907.
- [83] F. Schambil and J. Schwuger. *Proceedings of the 2.World Surfactants Congress (CESIO)*, page 505, 1988.
- [84] T. Wakamatsu and D.W. Fuerstenau. *Advances in chemistry.* 79:161, 1968.
- [85] S. G. Dick, D.W. Fuerstenau, and T.W. Healy. *J.Coll. Int. Sci.*, 37:595, 1971.
- [86] D. Fan, P. Somasundaran, and N.J.Turro. *Langmuir*, 13:506, 1997.
- [87] C.A. Hunter, K.R. Lawson, J. Perkins, and C.J. Urch. *J. Chem. Soc. Perkin Trans.*, 2:651, 2001.
- [88] W.N. Rowlands and R.J. Hunter. *Clays and clay minerals.* 40:287, 1992.
- [89] F. Z. Saleeb and J.A. Kitchener. *J.Chem.Soc.*, page 911, 1965.
- [90] M.A. Yeskie and J.H. Harwell. *J. Phys. Chem.*, 92:2346, 1988.
- [91] Z. király, R.H.K. Börner, and G.H. Findenegg. *Langmuir*, 13:3308, 1997.
- [92] H.P. Boehm. *Angew. Chem.*, 78:617, 1966.
- [93] J.M. Corkill, J.F. Goodman, and J.R. Tate. *Trans. Faraday Soc.*, 63:2264, 1967.
- [94] R. Denoyel, F. Rouquerol, and J. Rouquerol. In proceedings of the 2nd engineering foundation conference on fundamentals of adsorption. *American Institute of Chemical Engineers, New York*, page 199, 1987.
- [95] A. Gellan and C.H. Rochester. *J. Chem. Soc., Faraday Trans. 1*, 82:953, 1986.
- [96] A. Gellan and C. Rochester. *J. Chem. Soc., Faraday Trans. 1*, 81:3109, 1985.

- [97] M.J. Hey, J.W. Mac Taggart, and C.H. Rochester. *J. Chem. Soc., Faraday Trans. 1*, 80:699, 1984.
- [98] Z. Király and I. Dékány. *Coll. Surf.*, 49:95, 1990.
- [99] Z. Király, I. Dékány, E. Klumpp, H. Lewandowski, H. Narres, and M.J. Schwuger. *Langmuir*, 12:423, 1996.
- [100] N.A. Klimenko. *Colloid J. USSR*, 42:466, 1980.
- [101] M. Lindheimer, S. Zaini, E. Keh, and S. Partyka. *J. Colloid Interface Sci.*, 138:83, 1990.
- [102] L.A. Noll. *Calorim. Anal. Therm.*, 16:12, 1985.
- [103] S. Partyka, M. Lindheimer, S. Zaini, E. Keh, and B. Brun. *Langmuir*, 2:101, 1986.
- [104] J. Seidel, C. Wittrock, and H.H. Kohler. *Langmuir*, 12:5557, 1996.
- [105] D.M. Cyr, B. Venkataraman, and G.W. Flynn. *Chem. Mater.*, 8:1600, 1996.
- [106] Ducker W.A. and Grant L.M. *J. Phys. Chem.*, 100, 1996.
- [107] E.J. Wanless and W.A. Ducker. *J. Phys. Chem.*, 100:3207, 1996.
- [108] B.W. Barry and R. Wilson. *Coll. Polym. Sci.*, 256:251, 1978.
- [109] W.A. Ducker and L.M. Grant. *J. Phys. Chem.*, 100:11507, 1996.
- [110] G.C. Mc Gonial, R.H. Bernhardt, and D.J. Thomson. *J. Appl. Phys. Lett.*, 57:28, 1990.
- [111] K. Iwamoto, Y. Ohnuki, K. Sawada, and M. Seno. *Mol. Cryst. Liq. Cryst.*, 73:95, 1981.
- [112] M. Liphard, P. Glanz, G. Pilarski, and G.H. Findenegg. *Prog. Colloid Polym. Sci.*, 67:131, 1980.
- [113] S. Manne, J.P. Cleveland, H.E. Gaub, G.D. Stucky, and P.K. Hansma. *Langmuir*, 10:4409, 1994.
- [114] S. Manne and H.E. Gaub. *Science*, 270:1480, 1995.
- [115] E.J. Wanless, T.W. Davey, and W.A. Ducker. *Langmuir*, 13:4223, 1997.
- [116] F.G. Greenwood; G.D. Parfitt; N.H. Picton; D.D. Wharton. *In Adsorption from Aqueous Solutions*. W.J. Weber and E. Matijevic, 1968; p135.
- [117] A.C. Zettlemoyer, J.D. Skewis, and J.J. Chessick. *Am. Oil Chem. Soc.*, 39:280, 1962.

- [118] R.M.A. Azzam and N.M. Bashara. Ellipsometry and polarised light; amsterdam. 1989.

List of Figures

1.1	Schematic representation of a low-mass surfactant [4]	21
1.2	Schematic representation of the adsorption of surfactants at the solid/liquid interface [1]	23
1.3	Calorimetric determination of CMC and ΔH_{demic} for Octyl Glucoside according to Paula et al [13]	30
1.4	Schematic diagram of a scanning tunneling microscope	32
1.5	Schematic diagram of an atomic force microscope	33
1.6	AFM cantilever tip	35
1.7	Contact mode image (240x240 nm) of the adsorbate structure of 0.8 mol/m ³ C ₁₆ TAB on graphite [23]	37
2.1	SEM micrograph of the carbon black dispersion (20kV x 100)	43
2.2	SEM micrograph of the carbon black dispersion (20kV x 5000)	43
2.3	HOPG plates	44
2.4	HOPG crystallographic structure [41]	44
2.5	TAM 2277	48
2.6	Plot of the heat flow as a function of time	49
2.7	Used AFM set-up	50
2.8	AFM force curve [44]	51
3.1	Adsorption isotherm for the anionic surfactant SDS at the carbon black-water interface	53
3.2	Adsorption isotherms for the single surfactants at the carbon black-water interface	53
3.3	Surface tension curves and CMC for the single surfactants	54
3.4	CMC values (\downarrow) and adsorption isotherms for the single surfactants at the carbon black/water interface at T= 298 K, pH =10	55
3.5	Schematic presentation of a vertical and a horizontal orientation of the alkyl chain on hydrophobic surfaces	57
3.6	Adsorption isotherms for the single anionic surfactants	58
3.7	Adsorption isotherms for the anionic surfactants in the 1:1 mixture with the nonionic surfactant	59

3.8	Surface tension concentration curves and CMC values for the single anionic surfactants and their mixtures with the nonionic surfactant as function of the total surfactant concentration . . .	60
3.9	Adsorption isotherms of the nonionic surfactant in mixture with the anionic surfactants	61
3.10	Cumulative enthalpy of adsorption on carbon black for SDS . .	66
3.11	Differential molar enthalpy of adsorption on carbon black for SDS	66
3.12	Cumulative enthalpies of adsorption on carbon black for SDS, SDBS, SAS and $C_{12-14}E_7$	67
3.13	Differential molar enthalpies of adsorption on carbon black for SDS, SDBS, SAS and $C_{12-14}E_7$	67
3.14	Cumulative enthalpies of adsorption of SDS, $C_{12-14}E_7$ and their 1:1 mixture as function of the total adsorbed amounts (Γ_{total}) .	69
3.15	Molar enthalpies of adsorption of SDS, $C_{12-14}E_7$ and their 1:1 mixture as function of the total adsorbed amounts (Γ_{total}) . . .	70
3.16	Cumulative enthalpies of displacement of SDBS, $C_{12-14}E_7$ and their 1:1 mixture as function of the total adsorbed amounts (Γ_{total})	71
3.17	Molar enthalpies of adsorption of SDBS, $C_{12-14}E_7$ and their 1:1 mixture as function of the total adsorbed amounts (Γ_{total})	71
3.18	Cumulative enthalpies of adsorption of SAS, $C_{12-14}E_7$ and their 1:1 mixture as function of the total adsorbed amounts (Γ_{total}) .	72
3.19	Molar enthalpies of adsorption of SAS, $C_{12-14}E_7$ and their 1:1 mixture as function of the total adsorbed amounts (Γ_{total}) . . .	73
3.20	4 μ m x 4 μ m atomic force micrograph of a 50 mol/m ³ SDS solution at the graphite-water interface	76
3.21	300 x 300 nm atomic force micrograph of a 50 mol/m ³ SDS solution at the graphite-water interface	77
3.22	Height profile of the selected area in figure 3.21	77
3.23	Destruction of the structure of the adsorbed SDS layer when using higher imaging forces	78
3.24	600 x 600 nm atomic force micrograph of a 50 mol/m ³ SDBS solution at the graphite-water interface	80

3.25	SDBS/water phase diagramm [56]	81
3.26	300 x 300 nm atomic force micrograph of a 50 mol/m ³ SAS solution at the graphite-water interface	82
3.27	Height profile for the 50 mol/m ³ SAS solution given in figure 3.26	82
3.28	500 x 500 nm atomic force micrographs of a 50 mol/m ³ C ₁₂₋₁₄ E ₇ at the graphite-water interface	84
3.29	Height profile for the third domain in figure 3.28	84
3.30	300 x 300 nm atomic force micrographs of a 50 mol/m ³ C ₁₂₋₁₄ E ₇ at the graphite-water interface	85
3.31	Height profile for the indicated area in figure 3.30	85
3.32	300 x 300 nm micrograph of a 50 mol/m ³ SDS/C ₁₂₋₁₄ E ₇ 1:1 mixture at the graphite-water interface	87
3.33	Height profile for the indicated area in figure 3.32	87
3.34	300 x 300 nm micrograph of a 50 mol/m ³ SDBS/C ₁₂₋₁₄ E ₇ 1: 9 mixture at the graphite-water interface	89
3.35	300 x 300 nm micrograph of a 50 mol/m ³ SDBS/C ₁₂₋₁₄ E ₇ 2:8 mixture at the graphite-water interface	89
3.36	400 x 400 nm micrograph of a 50 mol/m ³ SDBS/C ₁₂₋₁₄ E ₇ 1:1 mixture at the graphite-water interface	90
3.37	300 x 300 nm micrograph of a 50 mol/m ³ SAS/C ₁₂₋₁₄ E ₇ 1:1 mixture at the graphite-water interface	92
3.38	Height profile for the indicated area in figure 3.37	92
4.1	Adsorption isotherm at T = 25°C and pH = 10 for C ₁₂₋₁₄ E ₇	98
4.2	Experimental results and adsorption isotherms obtained using the Langmuir model for SDS (experimental data from figure 3.2)	100
4.3	Experimental results and adsorption isotherms obtained using the Langmuir model for SDBS (experimental data from figure 3.2)	100
4.4	Experimental results and adsorption isotherms obtained using the Langmuir model for SAS (experimental data from figure 3.2)	101
4.5	Experimental results and adsorption isotherms obtained using the Langmuir model for C ₁₂₋₁₄ E ₇ (experimental data from figure 3.2)	102

4.6	Concentration of the adsorbed $C_{12-14}E_7$ at the surface (c_{ads}) as a function of the bulk solution concentration (c_{sol}) for $n=3$. . .	104
4.7	Concentration of the adsorbed SDS at the surface (c_{ads}) as a function of the bulk solution concentration (c_{sol}) for $n=3$	105
4.8	Concentration of the adsorbed SDBS at the surface (c_{ads}) as a function of the bulk solution concentration (c_{sol}) for $n=3$	105
4.9	Concentration of the adsorbed SAS at the surface (c_{ads}) as a function of the bulk solution concentration (c_{sol}) for $n=3$	106
4.10	Variation of the constants n , K_1 and K_2 in the Zhu equation for $C_{12-14}E_7$	108
4.11	Variation of the constants n , K_1 and K_2 in the Zhu equation for SDS	109
4.12	Variation of the constants n , K_1 and K_2 in the Zhu equation for SDBS	109
4.13	Variation of the constants n , K_1 and K_2 in the Zhu equation for SAS	110
4.14	Adsorption isotherms for surfactant mixtures at the carbon black-water interface	111
4.15	Adsorption isotherms for the anionic surfactants in the mixture at the carbon black-water interface	112
4.16	Adsorption isotherms for the nonionic surfactant in the mixture at the carbon black-water interface	113
4.17	Differential molar enthalpies of adsorption of the single surfactants at the carbon black-water interface (corresponds to figure 3.13)	116
4.18	Effect of the surfactant head group	117
4.19	Correlation between the enthalpies of adsorption and the ratio of the adsorbed amounts (corresponds to figure 3.15)	119
4.20	Space occupied by the cross sectional area of the head group according to the Langmuir film measurements	122
4.21	Structure of the adsorbed layer: (a) bilayer and (b) hemimicelle	123
4.22	Number of molecules per aggregate	123
4.23	Aggregate structure at the graphite surface for surfactant mixtures	127
5.1	Dispersion stabilization	130

5.2	Mechanisms involved during the washing process	131
5.3	Light transmission measurements of carbon black dispersions for the single surfactants	133
5.4	Light transmission measurements for the surfactant mixtures . .	134

List of Tables

1.1	Classification of surfactants based on the charge of the head-group	22
2.1	Used surfactants	41
2.2	AFM Cantilever specification	50
3.1	CMC values at T= 298 K, pH=10 for the single surfactants	54
3.2	Limiting areas per molecule for the single surfactants	57
3.3	Limiting area per molecule for the mixture	61
3.4	Ratios of the adsorbed amounts for the C ₁₂₋₁₄ E ₇ /SDS mixture (0.72/1)	62
3.5	Ratios of the adsorbed amounts for the C ₁₂₋₁₄ E ₇ /SDBS mixture (0.87/1)	63
3.6	Ratios of the adsorbed amounts for the C ₁₂₋₁₄ E ₇ /SAS mixture (0.75/1)	63
3.7	Comparison of the differential molar enthalpies of adsorption on carbon black for the single surfactants	68
3.8	Comparison of the differential molar enthalpies of displacement at the carbon black/water interface for surfactant mixtures	73
3.9	Comparison between the results of this study and the results of Király et al [54]	74
3.10	Calculation of the period for 50 mol/m ³ SDS at the graphite-water interface	79
3.11	Calculation of the period for 50 mol/m ³ SAS at the graphite-water interface	83
3.12	Calculation of the period for 50 mol/m ³ C ₁₂₋₁₄ E ₇ at the graphite-water interface	86
3.13	Comparison between the values of the periods measured using AFM for different C ₁₂ E _n at the graphite surface	86
3.14	Calculation of the period for 50 mol/m ³ SDS/C ₁₂₋₁₄ E ₇ mixture at the graphite-water interface	88
3.15	Calculation of the periods for 50 mol/m ³ SDBS/C ₁₂₋₁₄ E ₇ mixtures at the graphite-water interface	91
3.16	Periods of the structures observed for the studied systems	93
4.1	Values of K using the Langmuir model	101

4.2	Values of K_1 and K_2 for $n=3$ for the single surfactants using the Zhu equation	107
4.3	Ratios of the adsorbed amounts in the mixtures	114
4.4	Headgroup and chain length effects on the adsorption enthalpies	117
4.5	Comparison between the differential molar enthalpies of adsorp- tion at the carbon black surface	118
4.6	Periods registered for the single surfactants using AFM	120
4.7	Comparison between the number of molecules in micelles	124
5.1	Ratios of the adsorbed amounts for the $C_{12-14}E_7$ /SDS mixture .	135
5.2	Ratios of the adsorbed amounts for the $C_{12-14}E_7$ /SDBS mixture	135
5.3	Ratios of the adsorbed amounts for the $C_{12-14}E_7$ /SAS mixture .	136

Eklärung

Hiermit versichere ich, dass ich diese Arbeit selbstständig verfasst und keine anderen als die angegebenen Quellen und Hilfsmittel benutzt sowie Zitate kenntlich gemacht habe. Ich bin damit einverstanden, dass die Arbeit durch Dritte eingesehen werden darf.

Datum

Meriem Jabnoun

